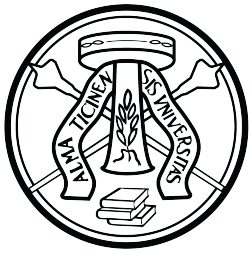

UNIVERSITÀ
DI PAVIA

University of Pavia

FACULTY OF ENGINEERING
Department of Electrical, Computer and Biomedical Engineering

Ph.D. Dissertation

Macroscopic Traffic Control via Connected and Automated Vehicles in Freeway Systems

Supervisor
Prof. Antonella Ferrara, Ph.D.

Candidate
Giulia Piacentini, M.Eng.

A.A. 2019/20

Ph.D. Dissertation

A.Y. 2019/20

Colophon

This thesis was typeset using the typographical language LaTeX.

A Chiara

Abstract

In the last decades traffic congestion in freeway systems has become a major problem, seriously affecting productivity, thus leading to a great social-economic cost. Congestion results in increased travel times for drivers, reduced safety and pollutant emissions. Variable speed limits and ramp metering are some of the most spread techniques for controlling traffic. Recent studies on the future of mobility have highlighted that the automotive world is changing fast, thanks to the newly available technology, and the future of vehicles is expected to move towards connectivity and automation. This introduces the possibility of evaluating new traffic control actions, adopting Connected and Automated Vehicles (CAVs) both as sensors and actuators. In this perspective, conventional traffic models need to be revised in order to capture the impact of smart vehicles on the traffic flow, and specific control actions can be introduced. This research mainly focuses on revising conventional macroscopic traffic models, suitable for traffic control purposes due to their lower computational complexity, in order to capture the presence of smart vehicles. Different modelling approaches are investigated. A first approach consists in modelling each single CAV as it was a moving bottleneck, impacting on the surrounding traffic. A second explored approach considers multi-class mixed human-driven and automated vehicles traffic flows.

The great spread of CAVs expected in next years suggests that high penetration rates are likely to appear in traffic systems. In this context, in addition to control each single smart vehicle, the possibility of controlling platooning of CAVs can be envisaged to increase the effectiveness of the traffic control action. Macroscopic models incorporating platoons, belonging to the class of moving bottlenecks models, are then discussed. Once obtained reliable modeling of CAVs moving in the traffic flow, specific control actions are designed. The speed, the number of occupied lanes and the length of platoons can be controlled in cooperative variable speed limits framework, where CAVs act as actuators for the traffic control laws. Adopting macroscopic first-order traffic flow models, although it is a good choice for traffic

control applications, introduces the problem of not being able to capture the capacity drop phenomenon. This has also been field of study and a model to describe the capacity drop in first-order models is presented.
As last point covered in this thesis, the conventional ramp metering control, already successfully applied worldwide, is revised by applying a sliding mode algorithm. A multi-level hierarchical more complex architecture is also developed to guarantee robustness of the control action in front of disturbances, thanks to the application of the sliding mode algorithms as decentralized controllers, supervised by an higher level model predictive control generating the optimal reference.

Acknowledgements

First and foremost, I would like to thank my supervisor Antonella Ferrara for all the support and the motivation, as well as all the opportunity that she provided me during my PhD.
I would also like to express my deep gratitude to Paola Goatin for her invaluable guidance and inspiration, starting since my first visit at INRIA.
I would like to thank Karl Henrik Johansson for hosting me at the KTH and Mladen Cicic for the fruitful collaboration and the useful discussions.
My sincere thanks also go to Markos Papageorgiou and Ioannis Papamichail for hosting me at the Technical University of Crete, and for sharing their immense knowledge in the traffic control field.
Special thanks to my co-authors, Cecilia Pasquale, Silvia Siri, Simona Sacone for the fruitful collaboration.
I am deeply grateful to all my lab mates from the Lab SISDIN, for the special atmosphere and the lunch discussions.
I also want to especially thanks Andrea, Bianca and Massimo for sharing with me this experience and for the continuous encouragement.
I would like to express my gratitude to my family and to my cousin Silvia for the support.
A special thanks to my boyfriend Daniele, for being by my side during this path.
Finally, a heartfelt thanks goes to my friends, Alessandra, Alessandro, Benedetta, Caterina, Clelia, Eleni, Federico, Gemma, Greta, Linda, Lucrezia, Valentina and Vittoria, that, year after year, always support me.

Contents

List of Figures

List of Tables

Introduction

Figure 1: Recurrent and non-recurrent congestion in freeway systems is a major problem. Example of congestion on a Chinese highway. *(Photo from Pixabay)*

Nowadays traffic congestion, both in urban and extra-urban areas, is a major problem. Traffic congestion appears every time that too many vehicles attempt to use a common transportation infrastructure with limited capacity at the same time. Highways, that were originally designed to have a sufficient capacity for virtually unlimited mobility, due to the increasing volumes of traffic, are now affected by recurrent and non-recurrent congestion, that leads to a degradation of the infrastructure. Congestion has a strong socio-economical impact, since it results in excess delays, reduced safety, and increased environmental pollution. The cost of congestion is partially related to the waste of time due to the increasing travel time that drivers spend on the roads. In addition to the travel times increase, the fuel consumption and the associated emissions of CO2, hydro-carbons, or particulated matter, are crucial factors when estimating the costs associated with vehicular

traffic. The fuel consumption of vehicular traffic is strongly correlated with the velocity profiles of the vehicles. Congestion introduces the need for an increased number of slow-downs and speed-ups that lead to an increased fuel consumption. In [139], [58] the effect of traffic congestion on the fuel consumption is investigated, showing that the increase in consumption can be really high, around 80%. In [8] the impact of traffic congestion on CO_2 and greenhouse gases emissions, and their impact on global warming is studied. Authors have highlighted how congestion mitigation, traffic smoothing and speed management strategies could reduce CO_2 approximately by the 30%. Traffic related pollution has also a consequent impact on people safety. For example, in the study carried out in [93], an evaluation of the public health impacts of ambient exposures to fine particulate matter (PM2.5) is done, leading to very negative cost estimations. An estimate of the economic cost of traffic congestion in U.K. has also been done in [56], resulting in a really high predicted cost for the society. Lastly, traffic congestion has a strong influence on drivers and passengers well-being since, as highlighted in the study carried out in [69], [68], drivers traveling in rush hours experience high levels of stress.

For all these reasons, an efficient management of freeways traffic networks has become of paramount importance. Advanced technologies and methodologies have been recently designed and are still under development with the aim to provide users with a safe, sustainable and smart traffic system.

This Thesis aims at revising traditional traffic control technologies, in the new recent context of autonomy, connectivity and automation that are spreading in road systems. Traditional control systems will be also adapted to this new context, introducing new algorithms that incorporates smart vehicles in traffic control systems in a cooperative way.

Outlines and Contribution of the Thesis

In this section, an overview of the thesis is provided, by describing the content of each chapter, the relative contribution and the publications on which each work is based.

Chapter 1: Background

In this chapter, a background is given to the research, firstly reporting a summary of traditional traffic models and control strategies. Then, an overview of Intelligent Transportation Systems (ITS) is reported, focusing on new technologies that are becoming available and that can be exploited in the traffic control domain. Possible models for capturing smart vehicles moving in a human-driven traffic flow are also discussed. In additional to this, advantages deriving from the use of platoons, both for vehicles traveling in the platoon itself and for the rest of the traffic flow, are described.

Chapter 2: Preliminaries

In this chapter, basic topics that are needed for the thesis comprehension are detailed. Specifically, the equations of the basic traffic models that are adopted along the discussion are introduced. Moreover, the chapter introduces the problem of the capacity drop, an important phenomenon that affects highways in presence of bottlenecks. Macroscopic first order models do not capture this important phenomenon, then several extensions have been proposed in the literature. This thesis contributes to the modeling of the capacity drop in first-order models with the proposal of a new extension to the Cell Transmission Model (CTM), that is consistent with empirical observations. This extension has the advantage to be a simple model and of being able to model different aspects of the capacity drop

phenomenon, as the congestion forming also in the bottleneck cell, in addition to the reduced discharge flow. The capacity drop model was proposed in

- G. Piacentini, A. Ferrara, I. Papamichail, and M. Papageorgiou. "Highway Traffic Control with Moving Bottlenecks of Connected and Automated Vehicles for Travel Time Reduction". In: *Proceedings of the 58th Conference on Decision and Control (CDC)*. 2019, pp. 3140–3145

The chapter ends with a list of performance indexes that will be used to evaluate the performance of the proposed control actions throughout the dissetation.

Chapter 3: Macroscopic Traffic Models Incorporating Intelligent Vehicles

In this chapter, models contributed by the author to describe the interaction between normal vehicles and smart vehicles are presented. Indeed, the main contribution of this thesis in the traffic control context is the idea of exploiting moving bottlenecks, large slow moving vehicles, in an innovative way. Moving bottlenecks, usually considered detrimental for the traffic flow, are here controlled and adopted as actuators to regulate the surrounding traffic. To do this, specific models are needed. While several microscopic modeling approaches are present in the literature, not many research have faced this problem from a macroscopic point of view. This thesis presents several models to capture moving bottlenecks in the traffic flow. A moving bottleneck model and its speed control have been developed, showing to be effective to dissipate traffic congestion and to reduce fuel consumption of the overall traffic flow. This has been presented in the following publication:

- Giulia Piacentini, Paola Goatin, and Antonella Ferrara. "Traffic control via moving bottleneck of coordinated vehicles". In: *Proceedings of the 15th IFAC Symposium on Control in Transportation Systems (CTS)* 51.9 (Jan. 2018), pp. 13–18

A second contribution in modelling smart vehicles in a macroscopic way has been developed by adopting a different approach that considers a flow divided in several classes of vehicles. Specifically, a new multi-class flow model has been developed by extending the traditional CTM. Unlike the majority of multi-class models present in the literature, this model distinguishes classes on the basis of

both their headway and their speed. Then, the speed of the automated cars class has been assumed as control variable in an optimal control design, showing good results in terms of travel times reduction for the overall traffic flow. This is based on the work published as:

- Giulia Piacentini, Mladen Cicic, Antonella Ferrara, and Karl Henrik Johansson. "VACS equipped vehicles for congestion dissipation in multi-class CTM framework". In: *Proceedings of the 18th European Control Conference (ECC)*. 2019, pp. 2203–2208

Chapter 4: Traffic Models Incorporating Platoons of Intelligent Vehicles

In this chapter, the concept of traffic control via smart vehicles is further extended considering platoons of CAVs as actuators. Although in the literature there are several studies about platooning and its benefits for vehicles traveling in it, the impact of platoon on traffic is not yet well understood and few results are available. Two different macroscopic models for platooning, from the point of view of traffic, are contributed by the author. Moreover, platoons are also exploited as actuators to mitigate congestion. The speed and the length of the platoon are indeed assumed as control variables with the aim of reducing travel times and fuel consumption on highway. This approach showed good results in simulations. The chapter is based on the following publications:

- Giulia Piacentini, Cecilia Pasquale, Simona Sacone, Silvia Siri, and Antonella Ferrara. "Multiple Moving Bottlenecks for Traffic Control in Freeway Systems". In: *Proceedings of the 18th European Control Conference (ECC)*. Napoli, Italy, 2019

- Giulia Piacentini, Paola Goatin, and Antonella Ferrara. "A Macroscopic Model for Platooning in Highway Traffic". In: *SIAM Journal on Applied Mathematics* 80.1 (Jan. 2020), pp. 639–656

- G. Piacentini, P. Goatin, and A. Ferrara. "Traffic Control Via Platoons of Intelligent Vehicles for Saving Fuel Consumption in Freeway Systems". In: *IEEE Control Systems Letters* 5.2 (2021), pp. 593–598

Chapter 5: An application of a Second Order Sliding Mode Algorithm to the Ramp Metering Problem

In this chapter, a different traffic control approach is adopted, focusing in the traditional ramp metering control. A sub-optimal second-order sliding mode algorithm is developed to solve a decentralized ramp metering problem. A more sophisticated control scheme, based on a two level model predictive control and sliding mode control, is also presented to improve robustness in front of uncertainties acting on the system. The work is based on:

- Giulia Piacentini, Gian Paolo Incremona, and Antonella Ferrara. "Freeway Traffic Control via Second-Order Sliding Modes Generation". In: *Proc. European Control Conference*. Saint Pittsburgh, Russia, May 2020, pp. 1–6

- Antonella Ferrara, Gian Paolo Incremona, and Giulia Piacentini. "A Hierarchical MPC and Sliding Mode Based Two-Level Control for Freeway Traffic Systems with Partial Demand Information". In: *Provisionally accepted to the European Control Journal*. 2021

Conclusion and Future Work

Finally, in this chapter the thesis is concluded, by summarizing the most important obtained results.Some possible future developments are also outlined.

Chapter 1

Background

The present chapter provides some background on a number of topics relevant to the rest of the thesis. First, a review of traditional traffic control actions is provided. Then, since one of the main objective of the thesis is the use of smart vehicles for traffic control actions, Intelligent Transportation Systems (ITS) and new technologies that have recently become available to drivers are reviewed. Possibilities introduced by the presence of smart vehicles for traffic control are investigated, and the most popular models developed to describe smart vehicles are resumed. Platooning and related traffic aspects are also discussed.

1.1 Traditional Control Methods for Highway Traffic Systems

In the last decades several traffic control actions have been studied and, often, successfully applied. In the following, two of the most common traffic control methods are reviewed.

1.1.1 Ramp Metering Control

Ramp metering (RM) is a well-known traffic control strategy that acts by regulating the number of vehicles that can access the mainstream from on-ramps, based on the current traffic situation and it is implemented via traffic lights [115]. RM represents the most direct action to control the highway traffic in the mainstream since it regulates the flow accessing it. This makes ramp metering one of the most effective traffic control strategy.
RM control can be local or coordinated. The local one is implemented in the vicinity

of each single ramp and takes into account only the local value of the density to compute the controlled metering rate. On the other hand, a coordinated ramp-metering controller collects information about the values of all the densities along the controlled stretch and then establishes the proper control input for each ramp. Once the amount of inflow allowed to access the mainstream is set by the controller, the actuation is done by means of traffic lights. It can be implemented both via traffic-cycle realization by converting the input information into a green-phase duration, or via an one-car-per-green realization, where only one car is allowed to pass for each green phase [117]. In addition to the direct control of the flow accessing the mainstream, RM has several side effects that have proven to be beneficial for the traffic flow. One of them is that RM can avoid the blocking of off-ramps due to queues forming in their proximity. Moreover, the RM approach influences routing decisions of drivers and can help to distribute them on different paths [112]. In terms of safety, ramps metering improves road merging, reducing the occurrence of car accidents [90].

The implementation of RM is traditionally done by adopting the well-known ALINEA [113], that has a simple local feedback control structure. ALINEA has been successfully applied worldwide and several field results are also available [114]. A proportional integral version has been also implemented, the so called PI-ALINEA [150], showing better performances in the case of bottlenecks located downstream of the metered ramp. The RM problem is also often solved by means of more sophisticated methods, based on optimal control approaches (see, among others, [49, 85]). In [84] a coordinated ramp metering problem is formulated as a constrained discrete-time nonlinear optimal control problem. A distributed model predictive control (MPC) scheme for freeway systems is applied in [47]. The drawback of optimal control strategies is the computational complexity that derives from the solution of large and often nonlinear optimization problems. This issue was successfully faced in [43] in which instead of computing the control law at each time step, an event-triggered MPC scheme is proposed. The control law is updated only when a given set of conditions is verified, thus strongly reducing the computational complexity. Another solution was proposed in [48], where a first-order model is formulated in a switched version and a switched controller is designed by adopting different control laws, depending on the current mode of the system.

A traffic system, due to its nature, is affected by several uncertainties which are often not manageable by adopting traditional control schemes. A solution that can face this issue is the application of Sliding Mode (SM)[144, 44] algorithms, that

have the advantage to be robust in front of disturbances acting on the system. In Chapter 5, a sliding mode algorithm will be presented to solve the ramp metering problem in an innovative way.

1.1.2 Variable Speed Limits Control

Variable Speed Limit (VSL) control systems consist in dynamic changing speed limits in response to traffic and weather conditions. Speed, volume detection, and road weather information are used to select the proper speeds which is communicated to drivers via variable posted signs [82]. VSLC has several positive effects on traffic. First of all, traffic breakdowns are easily resolved and sometimes avoided, for example by slowing down vehicles upstream of bottlenecks. In [61], [28], [27] the effectiveness of VSLC in reducing delays and queues at active bottlenecks locations are studied. In [26] the challenging problem of recurrent congestion on commuting corridors is faced by means of an innovative system that integrates variable speed control and travel time information for alleviating day-to-day recurrent congestion, obtaining higher throughput, stable traffic conditions, and shorter travel times. A MPC-based optimal coordination of variable speed limits to suppress shock waves in freeway systems is reported in [64], achieving a safer traffic flow by homogenizing the speeds. An empirical study focusing on identification and examination of several recurring freeway bottlenecks based on traffic data from a German highway is reported in [15], showing the influence of VSL on the congestion forming at bottlenecks. By reducing the speed of vehicles, also fuel consumption and related emissions are reduced.
A design of VSLC specifically oriented to reduce pollutant emissions is done in [99]. Minimizing the fuel consumption of a single vehicle, authors obtain the optimal trajectory, then a consequent carbon-footprint/fuel-consumption-aware variable-speed limit traffic control designed based on the optimal trajectory is applied. The homogenization of speeds consequent to the employment of VSLC leads to improvements in safety. In [1] the potential benefits of VSL implementation for reducing the crash risk on highways at different loading scenarios was studied, by proving that VSL is an effective crash prevention strategy, especially when the freeway is operating in uncongested conditions. In [94], a VSL control strategy to reduce the risks of secondary collisions during inclement weathers is developed. Indeed, bad weather conditions reduce travelers sight distance and increases vehicles stopping distance, resulting in increased risk of collisions. By selecting the speed

limit depending on traffic and weather condition, collisions are strongly reduced. Another potential benefit of VSLC is in presence of work zones. In [98] results of the conducted analyses have confirmed that VSL algorithms can yield a substantial increase in both work-zone throughput and a reduction in delays of users. A practical methodology to reduce traffic conflicts at work zones based on VSLC was proposed in [86] and evaluated in the field on a highway in Minnesota. VSLC control has been often applied in combination with ramp metering to obtain more effective combined actions, some examples are present in [118], [101], [22] and [65].

Although the list of VSL positive aspects is long, two main drawbacks characterize the traditional VSLC. First, traditional VSLs require ad hoc infrastructure, as stationary detectors to estimate the current traffic state and variable message signs to communicate the speed limit. Moreover, the impact of VSLs is very sensitive to the level of driver's compliance to the posted speed limits. The compliance rate has been proved to be very low, especially when dealing with familiar routes. For instance, an experimental study was reported in [63], where participants were familiarised with a particular route and then the displayed speed limit was changed. The experiments showed that most of the driver, after passing all signs, were still unaware that the speed limit had changed. In [67], a simulation model to evaluate the sensitivity of the safety and operational impacts of VSL to driver compliance is developed, finding out that VSL impacts are very sensitive to the level of drivers compliance.
A solution to all these drawbacks can be found looking at new technologies that are now being implemented on vehicles, leading to an Intelligent Transportation System (ITS), where connected and automated vehicles can cooperatively contribute to actuate traffic control methodologies.

1.2 Intelligent Transportation Systems

Recent studies on the future of mobility have highlighted that the automotive world is changing fast, due to the new technologies that have become available and in few years the automotive industry is expected to look radically changed. The future of vehicles is expected to move towards four major trends: shared/diverse mobility, electrification, connectivity and autonomous driving [147]. This renovated mobility scenario is expected to increase customer convenience and safety, but also to have a strong impact on the whole freeway system.

Figure 1.1: Advanced traffic control technologies and modern highway infrastructure represent a key point in the development of smart cities. *(Photo from Pexels)*

Focusing on vehicles automation, it is necessary to consider that there are several intermediate stages that need to be traversed in order to enter into the fully connected and automated mobility, but car connectivity is already a fact. A considerable number of new functionalities are offered to drivers and passengers by automated systems, which aim at making the driving experience safer and less demanding. Some of the offered technologies are the possibility of enabling autonomous driving on highways and temporary platooning of multiple cars, adaptive cruise control with consumption optimization and overtaking assistance systems. In urban context, intersections and parking assistance have encounter increasing popularity [78].
Autonomy allows vehicles to accomplish tasks without the driver being alert, awake or even present. Six consequent levels of automation are identified by the international standard [77], starting from level 0, with no automation present, to level 5, where the vehicle is fully autonomous and the human presence is no longer necessary or, in some cases, possible.

On the other hand, new functionalities and features are provided to users in term of connectivity, but also the whole traffic management system can benefit of connectivity, especially aiming at exploiting connected vehicles both as sensor, to gather information from the highway, and as actuators, to apply traffic control actions

Indeed, a connected car is able to exchange information in real time with its surroundings. Among all the existing VACS (Vehicle Automation and Communication Systems) categories, Vehicle-to-Environment (V2E) communication and,

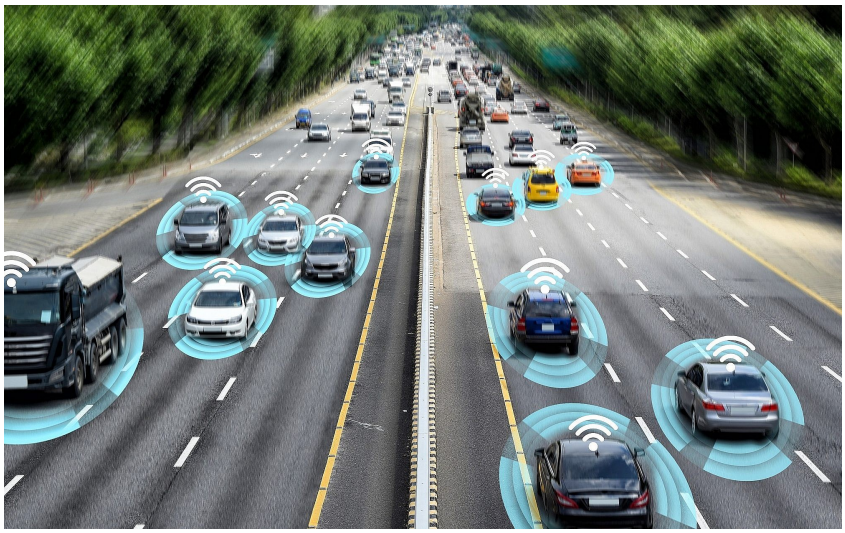

Figure 1.2: New communication features enable several levels of cooperation among vehicles and/or vehicles and the infrastructure. *(Photo from Getty Images)*

specifically, Vehicle-to-Vehicle (V2V) and Vehicle-to-Infrastructure (V2I) systems, depicted in the scheme of Fig. 1.3, can be efficiently used for traffic control purposes [39].
This kind of connection technologies enables data-enhanced driving functionalities, as for example the automatic vehicle speed adjustment depending on the traffic flow condition and the actual speed limits, based on Intelligent Speed Adaptation (ISA) systems [23], [145].

Several additional technologies are becoming available for drivers. The primary functionality of the so called Cruise Control (CC) is to maintain a desired speed set by a driver. The Adaptive Cruise Control (ACC) represents an advanced version of the earlier CC system, introducing the control of the acceleration based on a distance gap and a speed difference between preceding and current vehicles. ACC systems can indeed accelerate or decelerate if the preceding vehicle speed changes. The Cooperative Adaptive Cruise Control (CACC) represents a further extension to the adaptive cruise control concept. CACC system includes communication functions, compared to ACC, through V2V communications [41]. Communication allows the CACC vehicles to have shorter time headway (i.e., 0.5 seconds) compared to the ACC (i.e., 1.4 seconds). This also improves traffic flow conditions, increasing the capacity of a road.

It is interesting to glance an analysis of customer demand about connectivity and automation, as the market research done in [147]. The 55 % of customers appears

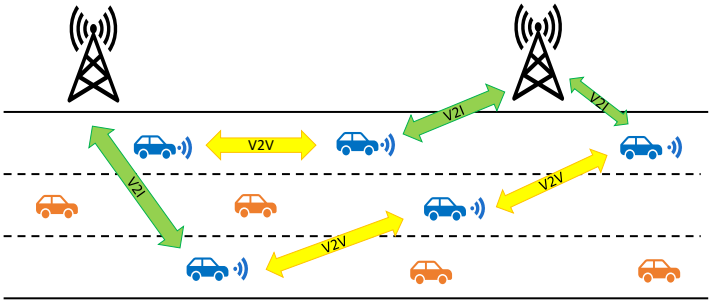

Figure 1.3: Scheme of smart vehicles connected via V2V and V2I communication systems.

interested in driving-relating connectivity functionalities. In [105], the survey highlights the 28 % of people buying a new car prioritizes vehicles connectivity features over the traditional engine power or fuel efficiency that was preferred in the past, and 13 % would not even buy an unconnected car. On the other side, promising business models are expected to be created by the 85 % of the automotive executives with new technologies in the field of connectivity and automation. The totality of new cars is then expected to be connected by 2025 [7]. In [66], future scenarios about the spread of autonomous cars are envisaged. The report claims that before 2030 fully autonomous vehicles are unlikely to be commercially available. On the other hand, the number of cars equipped with advanced driver-assistance systems (ADAS) is growing by 23% annually. A more aggressive scenario is envisioned in [66], claiming that around the 50% of cars that will be sold in 2030 will be highly autonomous, while an additional 15% will be fully autonomous.

Given this scenario, the great availability of Connected and Automated Vehicles (CAVs) could be exploited to apply innovative traffic control management and control techniques. Information about traffic conditions can be gathered via in-car sensors, in addition to traditional sensors placed along roads. On the other hand, CAVs are also suitable to be used as actuators, since control actions computed by centralized decision makers, aware of the conditions along the whole road, could be communicated to CAVs drivers, or even directly actuated as in-driven commands.

1.2.1 Traffic Control Actuation via CAVs and Cooperative Variable Speed Limits

In the literature several examples of cooperative variable speed limits, where CAVs are exploited both as sensors and actuators are present.

In [146] traditional road-side systems are replaced with intelligent vehicles actuation. A link-level traffic controller regulates traffic speeds through VSL gantries while intelligent vehicles control accelerations through vehicle propulsion to optimize their local situations. In [133] vehicles equipped with VACS are exploited both as sensor, gathering traffic data from on-board sensors, and as actuators for control systems. Three control actions, ramp metering, variable speed limit and lane changing control, are implemented and the control inputs are directly sent to automated vehicles, avoiding the need for special infrastructures. In [12] connected vehicles are instead used as sensors in a "mixed" traffic scenario with both connected and normal vehicles. Based on the average speed measurements reported by connected vehicles and from only few spot-sensor-based total flow measurements, the total density and flow are estimated. A motorway traffic flow with a sufficient penetration rate of VACS equipped vehicles is considered in [133] and their presence is exploited to actuate the control action. As the traffic situation evolves, a Decision Maker (DM) computes the solution of a specific optimization problem and assigns the control task to the proper equipped vehicle. In [106] a cooperative mainstream control that uses VSL is a context of presence of automated vehicles is applied. Since the automated vehicles can be designed to be much more strict in complying with VSL, the performances of the control are increased. In [59] communications between the infrastructure and the vehicles are used to transmit variable speed limits to upstream vehicles before the variable message signs become visible to the drivers, thus increasing the effectiveness of the control.

These mentioned works have been done in a microscopic context but a macroscopic approach should be preferred, because of the less computational effort required. To this aim, conventional models need to be revised in order to capture the presence of CAVs.

In this thesis, two main approaches will be followed. The first one relies on the concept of "moving bottleneck", that is usually studied with the aim to understanding the influence of slow moving vehicles, as buses or trucks, on the traffic. In the models presented in the following, moving bottlenecks will represent CAVs, whose speed will be assumed as control variable. A second approach to macroscopically

model CAVs, is the use of multi-class models, with mixed human-driven and normal cars flow.

1.2.2 Macroscopic multi-class models for traffic flow

One possible modelling approach is to consider multi-class flows of vehicles. While this is easy when dealing with microscopic models, it can be tricky when using macroscopic ones. Microscopic models of traffic are characterized by the fact that vehicles are considered as individual entities that globally form the traffic flow. They describe the longitudinal (car-following) and lateral (lane-changing) behavior of individual vehicles. Each single vehicle-driver units is described by its dynamical variables: position, speed and acceleration, therefore describing the reaction of each driver depending on the surrounding traffic. Among all the microscopic approaches, car-following models describe the interaction between adjacent vehicles in the same lane. Some of the most well-known car-following models are the Gazis-Herman-Rothery (GHR) model [53],the Gipps model [54] and the Intelligent Driver Model (IDM) [140]. A positive aspect of microscopic models is that since each vehicle is individually considered, it is easy to consider in the same models vehicles of different types and different mobility characteristics. A review of simulation microscopic models incorporating CAVs is done in [57]. Among others, in [136], a microscopic framework for simulations in presence of CAVs is studied, also showing the capability of CAVs in improving stability and in preventing shockwaves formation. Microscopic modelling considerations for smart vehicles and CACC systems are present in [108] and [131].
On the other hand, by adopting macroscopic approaches, the description of multi-class flows can be challenging. Some examples are present in the literature, most of them initially developed to account for the presence of trucks in the flow. An example of multi-class gas-kinetic model is presented in [71]. In [133], [132] a first-order multi-lane macroscopic traffic flow model for motorways with VACS-equipped vehicles is presented. A micro-macro extension to the second-order METANET model is studied in [119] to describe the behaviour of trucks in traffic flow. In [13] an n-population generalization of the Lighthill–Whitham and Richards (LWR) traffic flow model is presented. An extension of the LWR model with heterogeneous drivers is also formulated in [148], where the distribution of heterogeneous drivers is characterized by their choice of speeds in a traffic stream. A similar multi-class CTM able to model shared human and autonomous vehicle roads, considering multiple

vehicle classes with different reaction times, is studied in [92]. In Section 3.2, a new multi-class CTM model, that has been published in [127] will be presented.

1.2.3 Macroscopic traffic models incorporating moving bottlenecks

Moving bottlenecks are usually represented by large slow moving vehicles, as bus or trucks, that, due to their different motion, influence the surrounding traffic. Moving bottlenecks are normally considered detrimental for the traffic flow but, in the last years, an increasing attention has been paid to their possible exploitation to positively influence the traffic, via proper control actions. A first work in this direction has been published in [125], where a smart vehicle, modeled as a moving bottleneck, has been used to control the traffic.
Several experimental results are also available indicating that the control of a small number of autonomous or automated vehicles can crate benefits for the whole traffic flow. In [135], experiments on a circular track with several cars have been done. By controlling a single autonomous vehicle, stop-and-go waves result in being dampened and also the fuel consumption is reduced. A study about traffic flow control via very few AVs serving as mobile actuators is also carried out in [35].
Several models describing the interaction between moving bottlenecks and the traffic flow have been developed in the literature. In [107], moving bottlenecks are considered in an experimental way. The model given in [31] is an extension of the cell transmission model that includes the influence of moving bottlenecks and a control strategy is also derived for traffic jam resolution. A macroscopic model with moving bottlenecks is also proposed in [109], to study the impact of moving bottlenecks on the traffic flow, while a theory regarding congested patterns at moving bottlenecks location is developed in [81]. One of the models adopted in this thesis for moving bottlenecks is a coupled PDE-ODE model. Introduced in [89], it consists in a simple model of the interaction between buses and the surrounding traffic flow. This latter is described by the LWR model, while buses are moving capacity restrictions from the point of view of other drivers. A rigorous mathematical framework for that model was then proposed in [37], and a first numerical strategy to compute approximate solutions was proposed in [38], developing a finite volume algorithm using a locally non-uniform moving mesh which tracks the bus position. Finally, in [25], a numerical scheme conservative on fixed meshes and able to compute non-classical solutions was proposed, leading to the model that will be here adopted.

Figure 1.4: Heavy-duty vehicles driving close behind each other, forming a platoon, experience a reduced aerodynamic drag, and a consequent fuel consumption reduction. *(Photo from Pinterest)*

Another approach, that will be further detailed in the following of this thesis, is an extension of the CTM for moving bottlenecks, modeled as restriction on the free-flow speed [127].

1.3 Platooning on highways: effects on the traffic flow

Considering the high penetration rate of smart vehicles that is expected to appear in next years, and the consequent increased availability of vehicles that can be used to actuate traffic control actions, also their formations, as platooning, may be taken into account. A platoon is a formation of vehicles in one dimension constituted by a set of virtually linked vehicles driving at short distances. Platooning was first introduced for trucks since driving close together strongly improves the aerodynamics of all trucks in the platoon, as studied in [120]. Thanks to the recent semi-automated driving technologies, as CACC, trucks are easily enabled to drive very close. Moreover, new technologies also allow communication between vehicles joining the platoon, empowering cooperation between vehicles. Obtained benefits are significant, in terms of decrease in fuel and energy consumption, reduced greenhouse gas emissions and operating costs. A lot of works are present in the literature and experimental results are also available. The problem of Heavy-Duty

Vehicle (HDV) platooning to improve freight transportation sustainability is faced in [2]. A cooperative approach between HDVs to form platooning and reducing the fuel consumption while enhancing safety operations is presented, leading to significant improvements. In [70] the problem of how to coordinate a large fleet of trucks with a given itinerary to enable fuel-efficient platooning is considered, in order to elaborate fuel-efficient plans guaranteeing trucks to arrive at their destination within the given deadline. Experiments on platoon formation when trucks are moving in the traffic have been also conducted in [95]. An experiment conducted with two electronically coupled trucks at close spacing in [17] showed that both trucks experienced a considerable fuel consumption reduction compared to drive in isolation. In [142], an automated truck platoon and its configuration, sensing and control systems are studied. Experimental results confirm the effectiveness on the energy saving due to the formation of the automated platoon, leading to a fuel consumption reduction of the 14 % when considering only three trucks. While benefits introduced by platooning on fuel consumption reduction for the platoon vehicles are clear, and there has also been much work done on controlling the vehicles inside a platoon (see, among others, [143] [151]), the effect of platoons on the traffic flow is not yet well understood. Only recently vehicle platooning has been attracting attention because of its ability to improve road capacity, safety and fuel efficiency. Assuming that platoons can be controlled by communicating via V2I communications, they can be used as controlled moving bottlenecks in order to actuate traffic control actions [30]. This possibility has been recently investigated in the literature. A fluid queuing model to study the interaction between randomly arriving vehicle platoons and the background traffic at highway bottlenecks in a macroscopic way is proposed in [79]. An advanced control algorithm for the platoon control, which includes additional information about the downstream traffic conditions, has been developed in [72], with aim of detecting and identifying shock waves, and adapt the speed of platooned vehicles accordingly.

With the aim of developing a reliable model to capture the effect of platoons in the surrounding traffic, a new PDE-ODE model, published in [124], is discussed in Chapter 4.2.1. A control action aiming at reducing congestion and fuel consumption by controlling the speed and the length of the platoon is also developed in [122].

Chapter 2

Preliminaries

This chapter provides an overview on a number of topics relevant to the rest of the thesis. Specifically, the traditional macroscopic traffic models that will be adopted in the following are here detailed. A brief introduction to the capacity drop, a crucial phenomenon in the traffic flow theory, is reported, together with a model developed for its description. Traditional performance indexes used to evaluate the effectiveness of applied traffic control actions are listed.

2.1 An overview of macroscopic traffic models

In order to study the traffic system and to apply traffic control management techniques, reliable models are needed. The traffic flow theory and modelling has started to be taken into account in 1930s, pioneered by Greenshields that began to study the traffic by measuring traffic flow, density and speed by means of photographic measurement methods. Nowadays several traffic models exist and a classification can be done based on the level of aggregation.

Macroscopic models, in particular, also called hydrodynamic models, describe the traffic flow as if it was a fluid, as a liquid or a gas. Dynamical variables are locally aggregated quantities: the density of the traffic, the flow and its speed. The basis on which the macroscopic models are founded are hyperbolic systems of conservation laws, which are time-dependent systems of partial differential equations. The main advantage of macroscopic models over microscopic and mesoscopic models is the lower complexity, still keeping a good description of traffic. Due to the lower number of parameters needed in the macroscopic models, also the calibration is less demanding. Macroscopic models are then preferred for traffic control purposes, especially if the applied control law must be computed in real time. For all these

reasons, in the following only macroscopic models will be taken into consideration. Macroscopic models can be classified in continuous models, in which time and space are defined as continuous variables, and discrete models, in which time and space are discretised. A further distinction is made based on the order of the model. First-order models describe the dynamics of the density, that is the only state, while second-order models include the dynamics of the speed. Throughout the dissertation, the macroscopic aggregated variables used to describe the traffic are denoted as:

- ρ, the traffic density, defined as the number of vehicles per unit of length of the road.
- v, the mean speed of the flow.
- f, the flow.

In the following, some of the main macroscopic models, both first and second order, that will be used in the thesis, are described.

The Lighthill-Whitham-Richards model

The Lighthill-Whitham-Richards (LWR) model [97], [130] is a macroscopic first-order scalar model based on the principle of conservation of cars.

The conservation law is given by

$$\frac{\partial \rho}{\partial t} + \frac{\partial f(\rho)}{\partial x} = 0. \tag{2.1}$$

The corresponding law $f = f(\rho) = \rho v(\rho)$ that expresses the flux as a function of the density is called fundamental diagram. Several fundamental diagrams have been proposed in the literature to capture the relation between flow and density, based on data collected via empirical observation. In the following, when adopting the LWR model, the fundamental diagram proposed by Greenshield in 1934, that assumes a linear dependence of the speed on the traffic density, is adopted. Specifically,

$$v(\rho) = V\left(1 - \frac{\rho}{R}\right), \tag{2.2}$$

where V denotes the maximal speed of the flow and R the maximal (bump-to-bump) density. As a result, the fundamental diagram is a quadratic function.

$$f(\rho) = V\rho\left(1 - \frac{\rho}{R}\right). \tag{2.3}$$

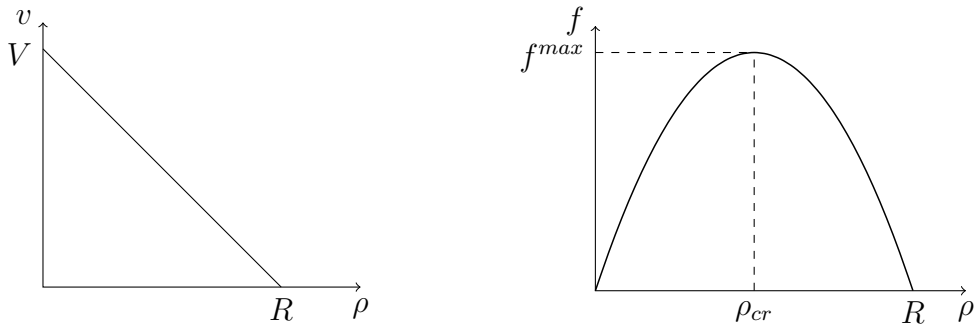

Figure 2.1: Linear speed density relationship and quadratic fundamental diagram.

The linear speed-density relationship and the consequent quadratic fundamental diagram are depicted in Fig. 2.1. This approach could be extended to any fundamental diagram $f : [0, R] \to \mathbb{R}_+$ with $f(0) = f(R) = 0$, eventually changing convexity in the congested region.

The conservation law of the LWR model needs to be discretized to be solved. This can be done by applying the standard Godunov's method [55]. For concave flux functions, this is equivalent to the supply-demand method that is typically used by the transportation engineers [36, 52, 88]. This latter will be here detailed and adopted along the thesis. To solve the conservation law, a discretization in both time and space is done, dividing the time in K time steps of duration T and the space in N cells of length L. In order to ensure numerical stability, the Courant-Friedrichs-Lewy (CFL) condition [34] must be fullfilled, specifically

$$T \leq \frac{L}{V}$$

For each cell $i = 1, \ldots, N$ a *demand* and a *supply* functions are defined. The demand of the ith cell at time step k represents the amount of cars that would leave the cell, while the supply of the ith cell represents the amount of cars that cell i can accommodate. They are respectively given by

$$D_i(k) = \begin{cases} f(\rho_i(k)) & \text{if } \rho_i(k) < \rho_{cr}, \\ f^{max} & \text{if } \rho_i(k) \geq \rho_{cr}, \end{cases}$$

$$S_i(k) = \begin{cases} f^{max} & \text{if } \rho_i(k) < \rho_{cr}, \\ f(\rho_i(k)) & \text{if } \rho_i(k) \geq \rho_{cr}, \end{cases}$$

Above, ρ_{cr} denotes the critical density while $f^{max} = f(R)$ is the maximal flux, the capacity, of the road. The demand and supply function of a generic cell i are depicted in Fig. 2.2.

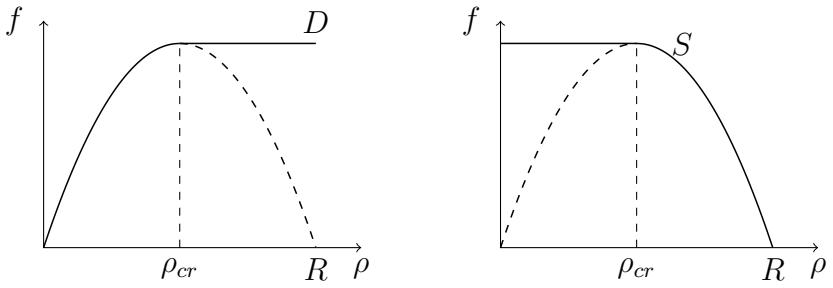

Figure 2.2: Demand and supply functions.

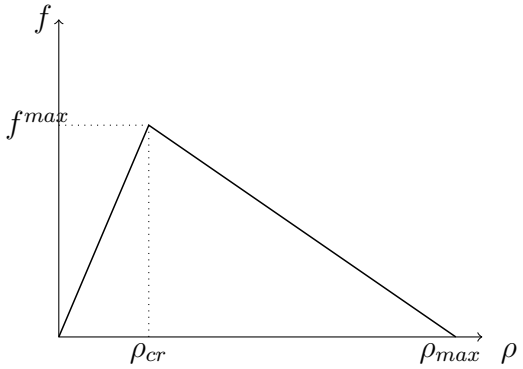

Figure 2.3: Triangular fundamental diagram.

The flux between two cells $i-1$ and i is then computed as

$$f_i(k) = \min\left\{D_{i-1}(k), S_i(k)\right\} \tag{2.4}$$

and the density of each cell i is updated as

$$\rho_i(k+1) = \rho_i(k) + \frac{T}{L}\left[f_i(k) - f_{i+1}(k)\right]. \tag{2.5}$$

The Cell Transmission Model

The Cell Transmission Model (CTM) [36] is the discretized version of the *LWR* model. The space is discretized in N cells of length L and the simulation time is composed by K time steps of T seconds. In order to ensure numerical stability the CFL condition $T \leq L/v^{free}$ must be satisfied, where v^{free} is the free flow speed of the traffic.

Unlike the quadratic fundamental diagram adopted for the LWR model, here the behavior of each cell is described by a triangular fundamental diagram, defined by some parameters:

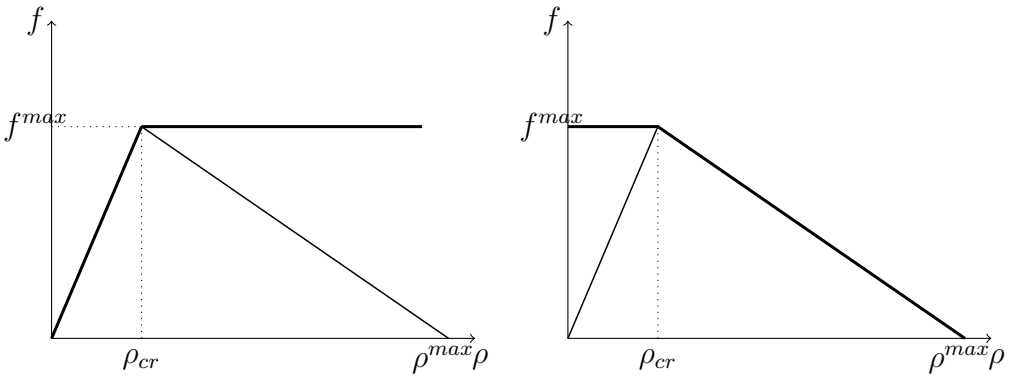

(a) Demand (b) Supply

Figure 2.4: Demand and supply functions for the CTM model.

- ρ_i^{max} is the maximum density of cell i.
- ρ_i^{cr} is the critical density of cell i.
- f_i^{max} is the free-flow capacity of cell i.
- v_i is the free-flow speed of cell i.
- w_i is the congestion wave speed of cell i.

The triangular fundamental diagram is depicted in Fig. 2.3.

The state variables are the traffic densities $\rho_i(k)$ of cell i at time step k, $f_i(k)$ is the flow entering cell i from cell $i-1$ during interval of time $[kT, (k+1)T)$. The evolution of the state is described by

$$\rho_i(k+1) = \rho_i(k) + \frac{T}{L}\left[f_i(k) - f_{i+1}(k)\right] \tag{2.6}$$

Again, for each cell i, a *demand* and a *supply* functions are defined as

$$D_{i-1}(k) = \min\left\{v_{i-1}(k)\rho_{i-1}(k), q_{i-1}^{\max}\right\} \tag{2.7}$$

$$S_i(k) = \min\left\{w_i(\rho_i^{jam} - \rho_i(k)), q_i^{\max}\right\} \tag{2.8}$$

The demand and supply function are depicted in Fig. 2.4. The flow between the two cells is given by

$$f_i(k) = min\left\{D_{i-1}(k), S_i(k)\right\} \tag{2.9}$$

The Metanet model

The METANET model [116] is a macroscopic discrete second-order model that was firstly applied to the Boulevard Périphérique in Paris. The name METANET, acronym for "Modèle d'Écoulement de Trafic sur Autoroute NETworks", was firstly associated with the simulation tool for the freeway network, but it is now adopted to generically indicate the second-order traffic flow model.

The traffic dynamics in a freeway link, with a number of on-ramps divided in N cells of equal length L_i, $i = 1, \ldots, N$, is described. Each cell has a number λ_i of lanes. In each cell, the aggregate quantities adopted to describe the dynamics of the traffic flow are the same of the LWR and the CTM models, the density ρ, the flow f and the flow speed v, while the dynamic equations of the METANET model are:

$$\rho_i(k+1) = \rho_i(k) + \frac{T}{L_i \lambda_i} \left(f_{i-1}(k) - f_i(k) \right) \tag{2.10}$$

$$\begin{aligned} v_i(k+1) = v_i(k) + \frac{T}{\tau} \left(V(\rho_i(k) - v_i(k) \right) + \frac{T}{L_i} v_i(k) \left(v_{i-1}(k) - v_i(k) \right) - \\ - \frac{\nu T}{\tau L_i} \frac{\rho_{i+1}(k) - \rho_i(k)}{\rho_i(k) + \kappa} \end{aligned} \tag{2.11}$$

for $i = 1, ..., N$. The traffic flow is given by

$$f_i(k) = v_i(k) \rho_i(k) \tag{2.12}$$

and the steady-state speed $V(\rho_i(k))$ is expressed as a function of the free-flow speed v_f, and of the critical density ρ_cr, i.e.,

$$V(\rho_i(k)) = v_\mathrm{f} \exp \left(-\frac{1}{p} \left(\frac{\rho_i(k)}{\rho_\mathrm{cr}} \right)^p \right) \tag{2.13}$$

above, τ is the time constant, ν is the anticipation constant and κ is a correction factor expressed in vehicles per kilometer per lane. p is an empirical correction factor to take into account the maximum flow, given the features of the considered cell. The trend of the steady-state speed is depicted in Fig. 2.5.

The first equation represents the conservation of cars in a cell, while the second equation describes the evolution of the speed. Specifically, the first term of (2.11) is called relaxation term and aims to model the tendency of drivers to reach their steady-state speed depending on the actual density $\rho_i(k)$, according to the time constant τ which represents the swiftness of drivers. The second term of the right

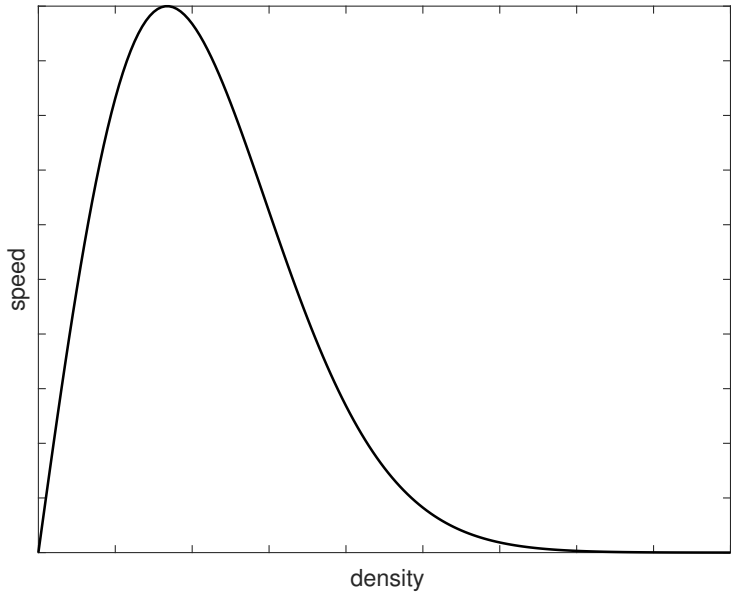

Figure 2.5: Trend of the steady-state speed in the METANET model.

side of (2.11), called convection term, models the delay of vehicles in adapting their speed to the one of cell i when arriving from cell $i-1$. The third term, the anticipation term, takes into account the behaviours of drivers that, looking at the situation downstream their position, adjust the speed.

2.2 The Capacity Drop Phenomenon

A phenomenon of great interest in the traffic flow modelling, that has an important impact on congestion on highway, is the so called capacity drop. First-order traffic models have the advantage of being simple and computational efficient and this makes them suitable to be used for traffic control application. However, they have the drawback of not being able to capture the capacity drop. On highways, the capacity is defined as the maximum throughput and it represents an essential concept for the design and the analysis of a freeway system. However, most of the time highways results to be underutilized due to the presence of recurrent and non-recurrent congestion and this is also due to the capacity drop phenomenon. Indeed, congestion usually forms in correspondence of bottlenecks along the highways. A bottleneck may be any location with particular characteristics, such as lane-drops, merge areas, tunnels, strong curvatures, but also traffic accidents or work-zones. In all these cases, whenever the incoming traffic demand overcomes the capacity of

the bottleneck, a jam forms and propagates. It has been observed that in all these situations, the discharge flow from the bottleneck, i.e. the outflow from its location, appears to be lower than the capacity. Empirical observations have indeed shown that the discharge flow is from the 5% to the 25% lower than the nominal capacity in free-flow conditions. This phenomenon is probably due to microscopic phenomena, most of them related to the behavior of drivers, lane-changing and velocity changes [141]. First-order traffic flow models cannot describe such phenomenon. Since they still remain the best modelling option especially for traffic control applications, various extensions have been studied in the last years in order to make them able to model the capacity drop. A review of the main extensions of first-order models incorporating capacity drop has been done in [83], where several approaches are proposed and validated with real data. One of the most widespread approach is the modification of the CTM demand function at the bottleneck location, by reducing it. Some others approaches modify the capacity instead, as in [62].

2.2.1 A CTM extension for capacity drop

A simple model to capture the capacity drop in the CTM framework, published in [121], is here reported. To do this, a stretch of highway modeled by means of the CTM with a bottleneck located in a cell, denoted as $\bar{i}$, is considered. The bottleneck reduces the capacity of the cell. Specifically, when the bottleneck becomes active, i.e. when the inflow from upstream exceeds the capacity of the bottleneck cell, two phenomena are observed. First, cell $\bar{i}$ gets congested, and the jam spreads upstream for a number of cells. At the same time, the discharge flow from cell $\bar{i}$ is reduced and appear to be lower than its free-flow capacity. This difference between the free-flow capacity and the discharge flow is the so called capacity drop. The first question to answer is what happens in this situation when the traditional CTM is adopted. Let the bottleneck cell $\bar{i}$ have an initial situation in which its density is lower than the critical value and the incoming flow from the previous cell $\bar{i}-1$ is equal to its capacity $c_{\bar{i}-1}$, $c_{\bar{i}-1} > c_{\bar{i}}$, i.e. the bottleneck is active. Since the density in cell $\bar{i}$ is under-critical, its state is described by the left part of the fundamental diagram: the supply of cell $\bar{i}$ is equal to its capacity $c_{\bar{i}}$. The flow between $\bar{i}-1$ and $\bar{i}$ is consequently obtained as the minimum between the two values, that results in being the bottleneck cell capacity $c_{\bar{i}}$. On the other hand, the demand of cell $\bar{i}$ is represented again by the left part of the fundamental diagram,

and it is lower than $c_{\bar{i}}$. Then the outflow from cell $\bar{i}$ is surely lower than its inflow, and its density increases. At some point the density reaches the critical value. Now the incoming flow is still equal to $c_{\bar{i}}$, but also the demand function is equal to $c_{\bar{i}}$, i.e. inflow and outflow are the same and the density remains constant. Then, the only possible scenario is that the bottleneck cell $\bar{i}$ never gets congested and its density remains always equal to the critical one. This is totally in contrast with empirical observations. In addition to this, since the density of cell $\bar{i}$ remains constant at its critical value, its demand is equal to its capacity, again in contrast with empirical observations, that show a reduced outflow from a bottleneck location.
With the aim of solving these issues, a simple model for the capacity drop has been developed. It consists in two different modelling strategies that are simultaneously applied. The first one allows the bottleneck cell to get congested, instead of having a constant density equal to the critical one. To this aim, its supply is no more constrained by the capacity of the cell (Fig. 2.6(d)). In this way, the bottleneck cell receives more flow than its capacity, its density increases and overcomes the critical value. In order to model the reduction of the discharge flow from the cell in which there is the bottleneck, the second strategy is applied. It consists in modifying the demand of the cell by decreasing it linearly with the increasing value of the density, that thanks to the first mechanism can now be over-critical. This reduced capacity is denoted with $q_i^{\max}$ and it coincides with the free-flow capacity c_i when there is no congestion, while it is lower than c_i when the cell is congested. The new capacity, demand and supply functions are given by

$$q_i^{\max}(k) = \min\left\{c_i, c_i + (\eta - 1)c_i \frac{\rho_i(k) - \rho_i^{cr}}{\rho_i^{max}(k) - \rho_i^{cr}}\right\} \tag{2.14}$$

$$D_i(k) = \min\left\{v_i(k)\rho_i(k), q_i^{\max}\right\} \tag{2.15}$$

$$S_i(k) = w_i(\rho_i^{max} - \rho_i(k)) \tag{2.16}$$

Where $c_i(k)$ is the free-flow capacity of cell i and $q_i^{\max}(k)$ is the reduced capacity in presence of active bottlenecks.

The parameter $\eta \in]0, 1[$ indicates the amplitude of the reduction of the discharge flow and c_i is the free-flow capacity of cell i.

Eq. (2.14)-(2.16) are applied to every cell of the stretch but they have an effect only when a bottleneck is present and active in a cell. Fig. 2.6 shows all the modified demand and supply functions.

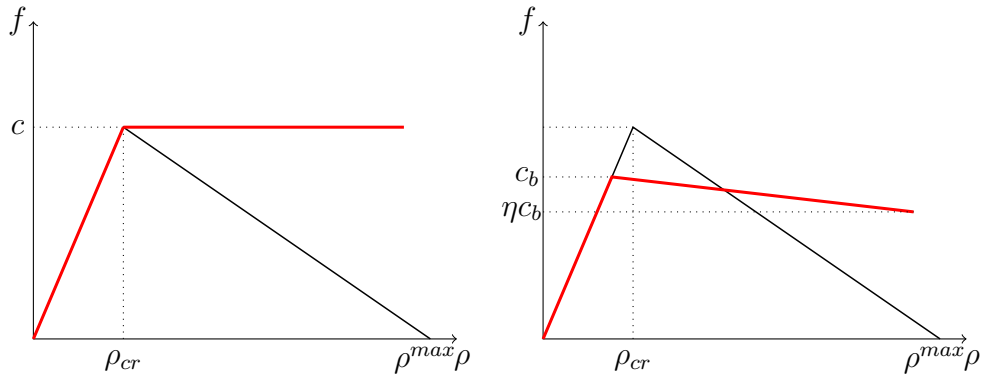

(a) Normal demand

(b) Reduced demand

(c) Normal supply

(d) Modified supply

Figure 2.6: Normal and modified demand and supply functions to model the capacity drop.

In [29] real data obtained from three bottlenecks, with different features, were analyzed. In the totality of the cases a strong relationship between the severity of the capacity drop and the traffic density was observed. In this perspective, control schemes aiming to maintain the density in the bottleneck area close to a reference value would then be beneficial for the reduction of the congestion. This will be taken into account in the formulation of the control strategies.

2.3 Model Predictive Control

In this section, a brief account of the Model Predictive Control (MPC) approach (see, among others, [102], [21]) is done, since it will be widely adopted along the dissertation. MPC era started in the late 70s, first applied in refineries and petrochemical plants and it has encountered increasing popularity, thanks to the advent of cheaper and faster microprocessors. MPC experienced an explosive growth due to its widespread adoption by the process industries where it proved to be highly successful in comparison with alternative methods for multi-variable control. Industrial control problems involve many interacting variables and various, potentially conflicting objectives, that were not manageable via traditional approaches.

MPC works by using a model of the system to make predictions about the system future behavior and performs on-line optimization for optimal control adjustments. Basically, there is no explicit form of control law, but just the plant model, an objective function, and constraints are specified.
At each time step, a prediction of the system trajectory is done over a finite time horizon and a chosen cost function is optimized along the horizon. The online optimization algorithm solves the problem to find the optimal control sequence optimizing the cost function. At this point, only the first sample of the control sequence is actually applied to the real system. At the following time step, based on the new available system information, the MPC repeats the prediction and the optimization to update the optimal input trajectory after the feedback update. A scheme for a generic MPC applied in the context of traffic control is depicted in Fig. 2.7.
MPC can handle multi-input multi-output systems that may have interactions between their inputs and outputs and also input and output constraints. Moreover, the MPC strategy has preview capability since it can incorporate future information into the control problem to improve the performance of the controller. In the

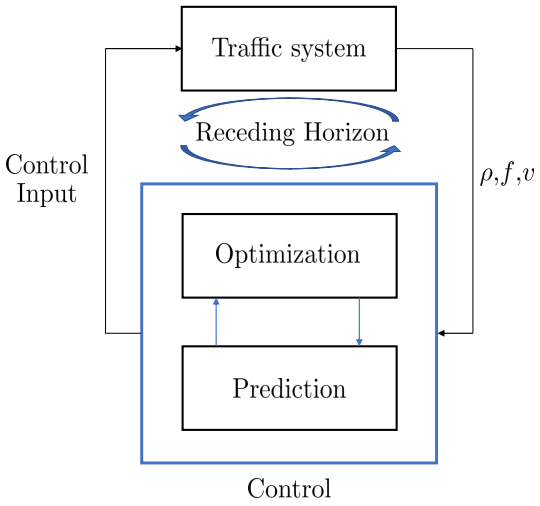

Figure 2.7: Scheme of a generic MPC strategy in the traffic control context.

following, many of the proposed control problem will be solved via the MPC approach.

2.4 Sliding Mode Control

Another control method that will be applied in the following to traffic control, especially in the ramp metering framework, is the so-called Sliding Mode Control (SMC). The SMC theory starts at the end of the 70s, with the first publications in English by Vadim I. Utkin (Ph.D. 1964, Institute for Control Sciences, Moscow, Russia). SMC is a nonlinear control technique consisting in a state-feedback control law that is discontinuous in time, since it can switch from a continuous structure to another one based on the current state. Then, sliding mode control belongs to the class of variable structure control methods. In its traditional version the SMC is then characterized by a bounded discontinuous input signal. This discontinuity has the drawback of being the main cause of the so-called chattering phenomenon [91], that can be disruptive for the system under control. To avoid such phenomenon, the discontinuity can be confined to the time derivative of the effective control input fed into the plant, giving rise to the so-called Higher-Order Sliding Mode (HOSM) control algorithms, which will be applied in the following.

In the context of modern control theory, any variable structure system, like a system under SMC, may be viewed as a special case of a hybrid dynamical system

as the system both flows through a continuous state space but also moves through different discrete control modes.

The great advantage of SMC is the capabilty of being a computationally light easy-to-implement solution capable to guarantee finite-time stabilization and robustness of the controlled system in front of a wide class of uncertainties, that is an important feature for traffic control systems.

2.5 Performance indexes

In all the situations in which macroscopic models are adopted, the characteristics about single vehicles, their trajectory, speed and travel times can not be individually tracked. On the other hand, there is the need for adopting performance indexes to be able to evaluate if the proposed control actions are useful and effective. The most common adopted indexes in the macroscopic traffic context are here listed.

The Total Travel Time (TTT) [veh· h] is defined as the total time spent by all the traveling vehicles in the mainstream. It is defined as

$$TTT = T \sum_{k=0}^{K} \sum_{i=1}^{N} L_i \rho_i(k) \tag{2.17}$$

The Total Travel Distance (TTD) is the total distance [veh km] covered by all the vehicles in the considered time horizon. It is given by

$$TTD = T \sum_{k=0}^{K} \sum_{i=1}^{N} L_i \phi_i(k) \tag{2.18}$$

The Mean Speed (MS)[km/h] of vehicles traveling in the considered system is then obtained as

$$MS = \frac{TTD}{TTT} \tag{2.19}$$

In case of the presence of ramps, specifically in the context of ramp metering control applications where on-ramps can be closed, also the time spent by drivers waiting at the on ramp must be considered.

Chapter 3

Macroscopic Traffic Models Incorporating Intelligent Vehicles

This chapter deals with models developed to describe situations in which both human-driven vehicles and smart vehicles share the same road. Two modelling approaches are studied in this dissertation. The first one describes each single intelligent vehicle as a moving bottleneck, having a motion law different from the rest of the traffic flow, and impacting its neighbourhood. A second investigated approach defines the traffic flow as a multi-class flow, distinguishing between classes of normal vehicles, CAVs, but also trucks and other vehicles that move following a their own motion law. The chapter first introduces a moving bottleneck model together with the speed control that has been designed to reduce congestion. The second part of the chapter is devoted to the description of a multi-class model, where the speed of the CAVs class is controlled to positively influence the rest of the traffic.

3.1 Intelligent Vehicles as Moving Bottlenecks

This section deals with the first modeling approach of considering intelligent vehicles as moving bottlenecks, leading to a coupled PDE-ODE model, presented in [125]. The innovative idea behind this work is to exploit moving bottlenecks, usually considered detrimental for the traffic flow, to get benefit for the overall traffic. In the following, equations constituting the model are described, followed by a description of the control law that has been applied to control the MB and simulation results are presented.

3.1.1 A coupled PDE-ODE model for Moving Bottlenecks in Traffic Flow

The adopted model consists in an existing model taken from [25], [87] that adapts the traditional LWR model [96, 129], described in Section 2.1, to model interactions between slow moving vehicles and the bulk traffic flow.
The standard LWR model with linear speed-density relation and quadratic fundamental diagram is then considered

$$v(\rho) = V\left(1 - \frac{\rho}{R}\right), \tag{3.1}$$

$$f(\rho) = V\rho\left(1 - \frac{\rho}{R}\right). \tag{3.2}$$

where V is the maximal speed of the traffic flow and R denotes the maximal (bump-to-bump) density.

Anyway, the same approach can be extended to different fundamental diagrams $f : [0, R] \to \mathbb{R}_+$ with $f(0) = f(R) = 0$, eventually changing convexity in the congested region.
Smart controllable vehicles are seen as slow moving large vehicles reducing the capacity of the highway, generating a moving bottleneck for the surrounding traffic flow. To do this, a Partial Differential Equation (PDE) is used to model the traffic flow, while an Ordinary Differential Equation (ODE) tracks the trajectory of the vehicle. The resulting coupled PDE-ODE model is given by:

$$\frac{\partial \rho}{\partial t} + \frac{\partial f(\rho)}{\partial x} = 0 \tag{3.3a}$$

$$\rho(0, x) = \rho_0(x) \tag{3.3b}$$

$$f(\rho(0, t)) = f_{in}(t) \tag{3.3c}$$

$$f(\rho(L, t)) = f_{out}(t) \tag{3.3d}$$

$$f(\rho(t, y(t))) - \dot{y}(t)\rho(t, y(t)) \leq \frac{\alpha R}{4V}(V - \dot{y}(t))^2 \tag{3.3e}$$

$$\dot{y}(t) = \omega(\rho(t, y(t)+)) \tag{3.3f}$$

$$y(0) = y_0 \tag{3.3g}$$

for $x \in [0, L]$, $L > 0$, and $t > 0$, being L the length of the road. The first equation of 3.3 is the conservation law, where $\rho = \rho(t, x) \in [0, R]$ and ρ_0 is the initial value for the density. Equations 3.3c, 3.3d are the boundary conditions,

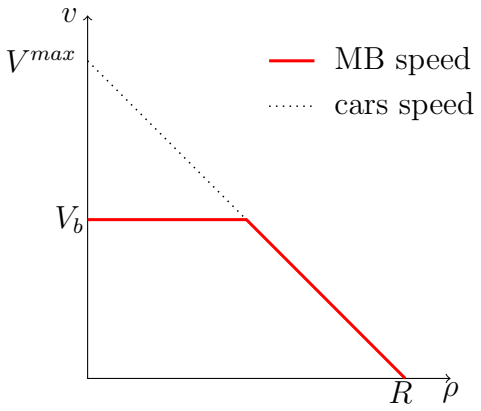

Figure 3.1: Speed of cars and of the MB.

i.e. the arriving inflow at the beginning of the stretch, denoted by f_{in} and the outflow at the end, f_{out}. The variable $y = y(t)$ denotes the position of the moving bottleneck and ω its motion law, that depends on the downstream traffic density $\rho(t, y(t)+) = \lim_{x \to y(t)+} \rho(t, x)$:

$$\omega(\rho) = \min(V_b, v(\rho)) \tag{3.4}$$

The slow vehicle has its own maximal speed V_b that can not be higher than the maximal speed of the traffic flow ($V_b \leq V$). Then, the moving bottleneck can assume its maximum speed if the surrounding traffic is not congested but it has to adapt its velocity when the average speed of the neighbouring flow decreases, as shown in Fig. 3.1. It is then not possible for the moving bottleneck to overtake cars.

The loss of highway capacity due to the presence of the moving bottleneck is expressed by the inequality constraint on the vehicles flow at the moving bottleneck position, see equation (3.3e). The coefficient $\alpha \in]0, 1[$ gives the reduction rate of the highway capacity due to the large vehicle occupying some lanes. The inequality (3.3e) was derived by studying the problem in the moving bottleneck reference frame, i.e., setting $X = x - y(t)$ and rewriting the conservation law as $\partial_t \rho - \partial_X F(\rho) = 0$, with $F(\rho) = f(\rho) - \dot{y}\rho$.

The rescaled flux function $f_\alpha : [0, \alpha R] \to R+$ describing the reduced flow at $x = y(t)$ is

$$f_\alpha(\rho) = V\rho\left(1 - \frac{\rho}{\alpha R}\right).$$

Moreover, $\rho_\alpha \in]0, \alpha R/2[$ is such that $F'_\alpha(\rho_\alpha) = 0 \iff f'_\alpha(\rho_\alpha) = \dot{y}$ with $F_\alpha(\rho) = f_\alpha(\rho_\alpha) - \dot{y}\rho$. Then

$$\rho_\alpha(\rho) = \frac{\alpha R}{2}\left(1 - \frac{\dot{y}}{V}\right).$$

At this point, by observing that $F_\alpha = F_\alpha(\rho_\alpha) = f_\alpha(\rho_\alpha) - \dot{y}\rho_\alpha = \frac{\alpha R}{4V}(V - \dot{y}(t))^2$, and imposing that in the moving bottleneck reference frame the flux function F should be less than the maximum value of the flux of the reduced flow, at the moving bottleneck position, the inequality of system 3.3 is obtained.

The numerical scheme able to compute approximate solutions of system (3.3) has been developed in [25]. Specifically, authors detail the construction of the solutions to the Riemann solver for (3.3a), (3.3b) for the Riemann type initial datum

$$\rho(0,x) = \rho_0(x) = \begin{cases} \rho_l & \text{if } x < y_0, \\ \rho_r & \text{if } x \geq y_0, \end{cases}$$

where y_0, the position of the MB, is the point in which the flux discontinuity arises. The solutions to the Riemann problem, namely $\hat{\rho}, \check{\rho}$, are the values expected to appear respectively upstream and downstream the moving bottleneck. Once detailed the Riemann solver, a reconstruction based numerical method able to numerically capture non-classical shocks for the coupled PDE-ODE problem with moving constraints is developed, see [25].

A simulation example of the model in open loop is here reported. For the simulation, a road stretch of 50 km, divided in 250 cells is considered, for half an hour of simulation. The maximum density is chosen $R = 400$ veh/km, the maximum speed is $V = 140$ km/h, the capacity restriction factor is $\alpha = 0.6$ and three lanes are considered. As initial density, a Riemann type datum is considered:

$$\rho_0(x) = \begin{cases} 150 & \text{if } x \leq y_0, \\ 100 & \text{if } 0.2 \leq x < y_0, \end{cases} \qquad y_0 = 25, \tag{3.5}$$

By computing the solutions to (3.3a), (3.3b), (3.5) by means of the Riemann solver developed in [25], the obtained solutions result to be $\hat{\rho} = 256$ veh/km and $\check{\rho} = 58$ veh/km. The reconstruction strategy gives rise at the solution reported in 3.2, in which the trend of the density in space at different time during the simulation is reported. In the first figure 3.2(a), the Riemann type initial density is shown. In

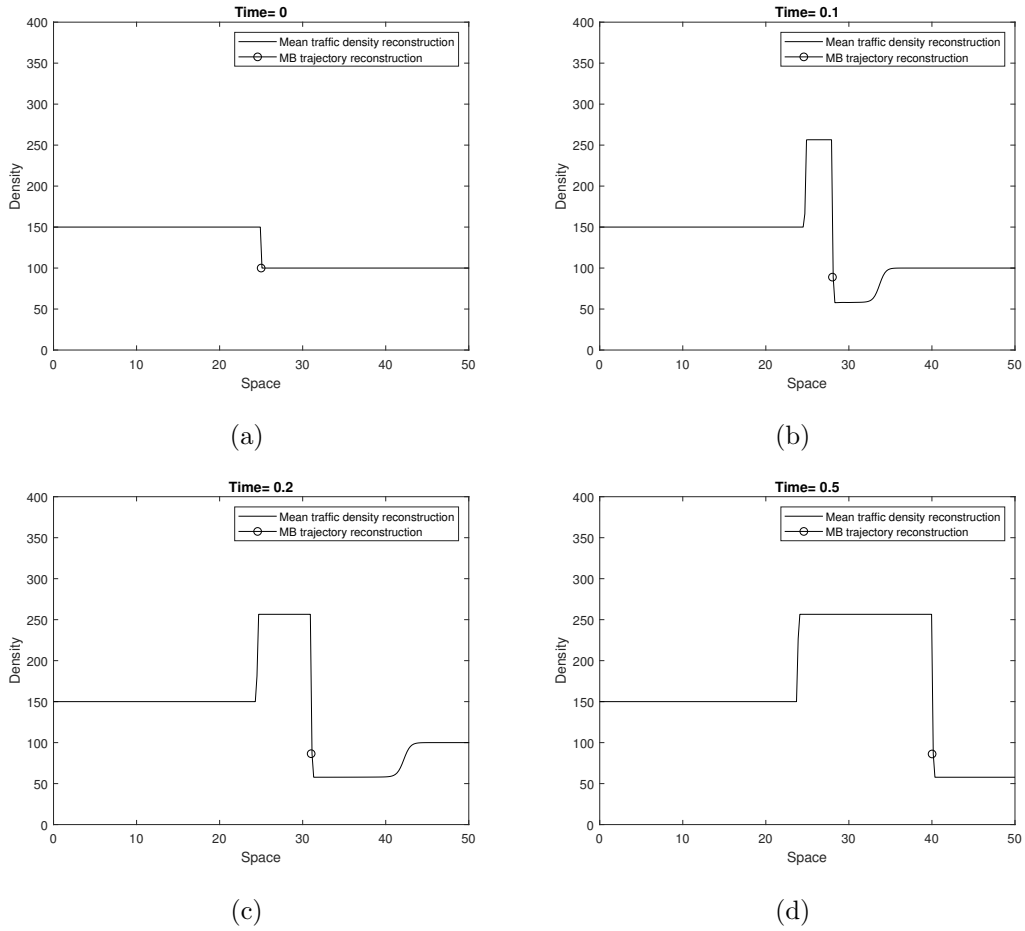

Figure 3.2: Example of density profile at different times for the initial density (3.5)

Fig. 3.2(b), the expected solution appears, with a rarefaction wave followed by a shock, and it evolves during time as shown in the last two figures.

3.1.2 Control of moving bottlenecks for congestion dissipation

In this section the control of the speed of the moving bottleneck, modelled as described in the previous section, is designed. The aim is to reduce congestion and pollution for the overall traffic flow. Specifically, a Model Predictive Control (MPC) approach is adopted, motivated by its capability to deal with nonlinear systems, multi-criteria optimization and constraints [100].

At each time step, the controller computes the optimal values of the control variable based on the evaluation of a selected cost functional, by predicting of the evolution of the system. Unlike for linear systems, where the prediction of the state along the chosen time horizon linearly depends on the future control moves and

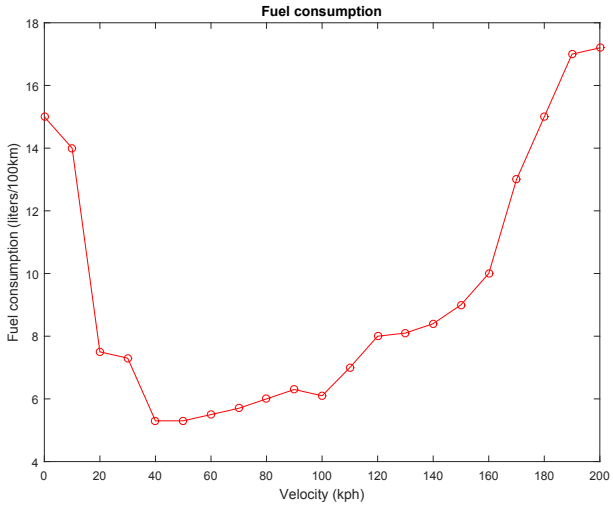

Figure 3.3: Approximated average trend of fuel consumption versus cruise speed for steady-speed driving

explicit formulæ exist, the problem here can only be solved numerically, by means of iterative optimization algorithms that require, at each iteration, a simulation run of system (3.3).

The control variable is then the maximum speed of the moving bottleneck $V_b(k)$. Since the road transport is one of the main source of air pollution, it is of paramount importance to reduce its impact. In this perspective, as cost function to be minimized, here the focus of the controller is on the fuel consumption of the overall traffic flow. A macroscopic fuel consumption model derived by [128] is considered to compute the cost function. The choice of the model has been done considering that since the model is first-order, the dynamics of acceleration is not detailed, and the fuel consumption model has to require as input only the average speed. In [14] the curves expressing the fuel consumption of vehicles depending on their cruise speed are considered. From these characteristics, it is possible to notice that vehicles consumes more when travelling at too low or too high speed. An approximated trend of a vehicle characteristics, taken from [125], is shown in Fig. 3.3.

The fuel consumption efficiency curve is multiplied by the vehicle speed in order to get the consumption rate, expressed in liters/hours. Then, the average of these curves is computed and approximated via a sixth order polynomial, denoted as $K(v)$. The resulting polynomial is

$$\begin{aligned} K(v) = 5.7 \cdot 10^{-12} \cdot v^6 - 3.6 \cdot 10^{-9} \cdot v^5 + 7.6 \cdot 10^{-7} \cdot v^4 - \\ - 6.1 \cdot 10^{-5} \cdot v^3 + 1.9 \cdot 10^{-3} \cdot v^2 + 1.6 \cdot 10^{-2} \cdot v + 0.99. \end{aligned} \tag{3.6}$$

above, $K(v)$ expresses the fuel consumption as a function of the speed.

Table 3.1: Simulation parameters

L	50 km
V	140 km/h
R	400 veh/km
T_f	1 h

Since in the LWR model the velocity is a function of the density, it is possible to derive the trend of the fuel consumption as a function of the traffic density, specifically here the linear relationship (3.1) is adopted. The polynomial (3.6) can be then re-parametrized in terms of the density ρ, to get the function $\mathcal{K}(\rho) = K(v(\rho))$, that is the consumption rate of one car as a function of the traffic density at the vehicle position. At this point, the Total Fuel Consumption (TFC), that will be denoted by $\mathcal{F}$, of the overall traffic flow as function of the density is obtained

$$\mathcal{F}(\rho) = \rho\mathcal{K}(\rho) \tag{3.7}$$

At the k-th iteration step, the optimal speed value $V_b(k)$, assuming the current density value $\rho(t_k, \cdot)$ as initial datum in (3.3), over the fixed time horizon $[t_k, t_k+\Delta T]$, is obtained as

$$V_b(k) = \arg\min \left\{ \int_{t_k}^{t_k+\Delta T} \int_0^L \mathcal{F}(\rho(t,x))dxdt \right\}. \tag{3.8}$$

subject to model dynamics (3.3) and to the following constraint

$$V_{min}(k) \leq V_b(k) \leq V_{max}(k) \tag{3.9}$$

Above, $V_{min}(k)$ and $V_{max}(k)$ are two values chosen to constrain the velocity. The upper limit prevents the MB to assume speeds higher than the maximum speed of the traffic flow. The lower limit is needed to avoid the MB from assuming too low speed, that would be not realistic on highways.

3.1.3 Simulation Results

In order to assess the validity of the approach a simulation case has been studied. Specifically, a section of highway of length $L = 50$ km with three lanes, no ramps and uniform road conditions, as depicted in 3.4, is considered.

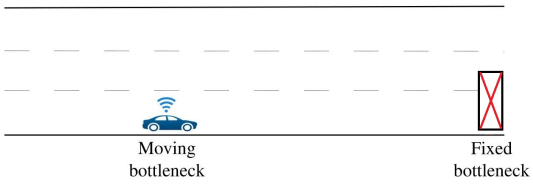

Figure 3.4: Simulation scenario.

The parameters used in the simulation are reported in Table 3.1, choices have been done considering 5 m of average vehicle length and a 50% of safety distance. The initial density is $\rho_0 = 0.3 \cdot R$, while the boundary conditions are given by the following inflow $f_{in}(t)$ and outflow $f_{out}(t)$:

$$f_{in} = \begin{cases} f_{max} & \text{if } t \leq 0.5T_f, \\ 0 & \text{if } t > 0.5T_f, \end{cases} \tag{3.10}$$

$$f_{out} = 0.5 f_{max} \quad \forall t \in [0, T_f], \tag{3.11}$$

where $f_{max} = \max_{\rho \in [0,R]} f(\rho) = f(R/2)$ is the maximum flow.

Concerning the MPC, the optimization time horizon is 15 minutes. To reduce the computational burden deriving from the non-linear problem minimization, the optimization is done every 5 minutes, instead of at each time step. At any computation time step, a constant speed V_k is computed and then applied to the controlled vehicle for the time interval $[t_k, t_k + \Delta\tau]$, with $\Delta\tau = 5$ min. The control speed is constrained to vary between $V_{min} = 30$ km/h and $V_{max} = 80$ km/h. This results in a piece-wise constant control speed, i.e.

$$V_b(t) = V_b(k) \quad \text{for } t \in]t_k, t_k + \Delta\tau] \tag{3.12}$$

The trend of the density with respect to time and space is depicted in Fig. 3.5. In the uncontrolled case, a jam starts forming due to the fixed bottleneck present at the end of the stretch, that strongly limits the inflow. Congestion propagates for several kilometers upstream. In this case, the moving bottleneck is no controlled and it travels at its maximum speed until it reaches the congested zone, where it has to adapt its speed to the surrounding traffic. In the control case, a congestion starts forming, but the control of the moving bottleneck reduces the congested zone. This is due to the fact that the controller properly slows down the MB and this creates a controlled congestion upstream the bottleneck. The control speed computed by the MPC and applied to the MB is reported in Fig 3.6. In Table 3.2, the TFC is compared for both the situations. This latter is reduced from $2.7413 \cdot 10^4$ liters in

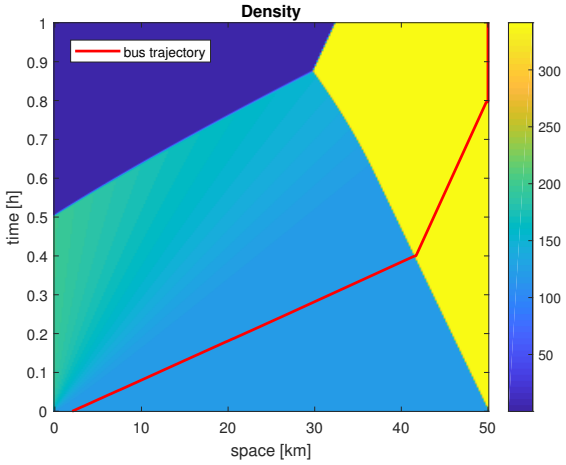

(a) Uncontrolled case.

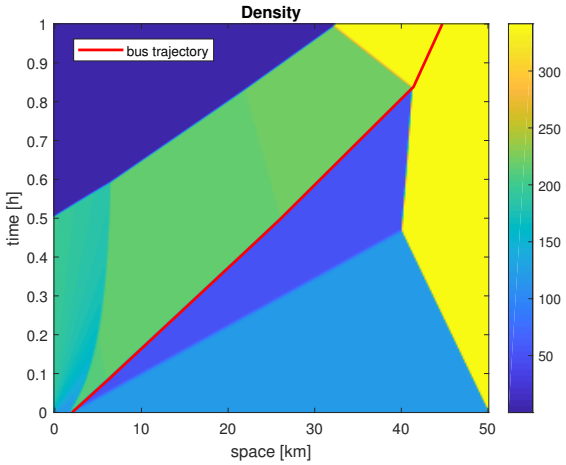

(b) Controlled case.

Figure 3.5: Density trend in the no control and controlled case

the uncontrolled case to $2.6852 \cdot 10^4$ liters in the MPC controlled simulation, thus resulting in 561 liters of fuel saving. This corresponds to a 2.05% reduction rate, that represents both an economical return for drivers and a reduction of pollutants emissions, beneficial for the environment.

Conclusion

To conclude, in this section a model describing the trajectory of each single smart vehicle as a moving bottleneck has been presented. The moving bottleneck has been adopted as actuator for a traffic control action aiming at reducing congestion. Specifically, the speed of the actuator has been computed via a MPC approach, minimizing the fuel consumption of the overall traffic flow. The approach has been

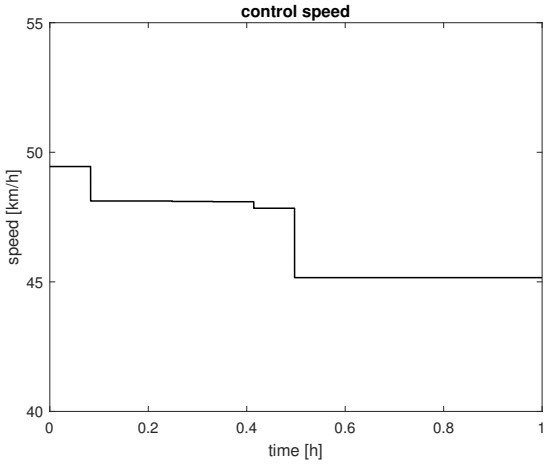

Figure 3.6: Control speed of the moving bottleneck.

Table 3.2: Comparison between cost functionals in the controlled and uncontrolled case.

	TFC [liters]	TFC reduction %
Uncontrolled	$2.7413 \cdot 10^4$	0
Controlled	$2.6852 \cdot 10^4$	2.05

assessed in simulation, showing good results. Further developments of this model will be addressed in Section 4.2.

3.2 A Multi-class Model for Mixed Automated and Human-Driven Traffic Flow

In this section a different modelling approach to capture the presence of CAVs on highways is presented. Unlike the previous models, in which each CAV was modeled as a moving bottleneck, here the multi-class modelling approach that was presented in [127] is reported. Instead of considering each single CAV, a mixed flow composed both by human-driven vehicles and CAVs is used. The model has been developed starting from the traditional CTM [36], described in Section 2.1, extending it in order to model a multi-class situation, taking inspiration from [149] and [79], where proportional priority is allocated to each class of vehicles. Let us consider different classes $c \in C$ of vehicles, distinguished on the basis of some features. Specifically, classes are here differentiated based on different headway, i.e the time distance between traveling vehicles, and their free-flow speed. The minimum headway that should be maintained in order to safely drive and to prevent collisions with the vehicle in front usually is two seconds. This comes from microscopic considerations taking into account the reaction times of human drivers [5]. Autonomous vehicles allow a shorter time headway since their reaction times are obviously smaller than human drivers' ones [51], [40].
In the following, the model will be detailed and the controller designed to regulate the speed of vehicles belonging to a specific class is presented.

3.2.1 The Multi-class Model

Although the model can support the deployment of multiple classes, only two of them are of interest in this context. Specifically, two classes a and b, where a represents the automated vehicles and b the class of "background" vehicles, i.e. human driven vehicles, are considered. The headway of the two classes is denoted by h_a, h_b while H is a chosen default headway adopted to derive the parameters of the fundamental diagrams of cells, as the critical density and the maximum density. Densities of class a and b in cell i at time step k are respectively indicated by $\rho_i^a(k)$ and $\rho_i^b(k)$. An "effective traffic density" $\bar{\rho}_i(k)$ is defined by summing the densities of individual classes weighed by their headway, specifically

$$\bar{\rho}_i(k) = \sum_{c \in C} \frac{h_c}{H} \rho_i^c(k) \tag{3.13}$$

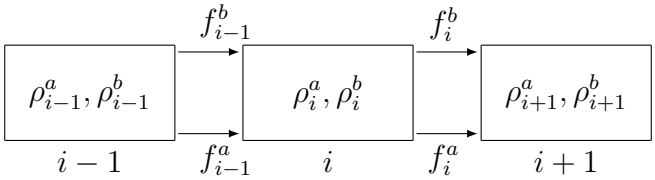

Figure 3.7: Sketch of the highway divided in cells.

and the share of aggregate flow is then given by

$$\bar{r}^c_i(k) = \frac{\rho^c_i(k)}{\bar{\rho}_i(k)} \tag{3.14}$$

For consistency, the conservation law of the class specific density ρ^c must be respected, then

$$\frac{\partial \rho^c(x,t)}{\partial t} + \frac{\partial f^c(x,t)}{\partial x} = 0 \tag{3.15}$$

$\forall c \in C$

To update the density of each class, a class-specific transition flow f^c is computed. This latter is proportional to r^c and by assuming that different classes have different free flow speed v_c, demand and supply functions specific for each class $c \in C$ are individuated

$$D^c_{i-1}(k) = \bar{r}^c_{i-1}(k) \min\left\{v^c_{i-1}(k)\bar{\rho}_{i-1}(k), q^{max}_{i-1}\right\} \tag{3.16}$$

$$S^c_i(k) = \bar{r}^c_{i-1}(k) \min\left\{(\rho^{max}_i - \bar{\rho}_i(k))w_i, q^{max}_i\right\} \tag{3.17}$$

and the class-specific flow is as usual computed as the minimum between the two functions

$$f^c_i(k) = \min\left\{D^c_{i-1}(k), S^c_i(k)\right\} \tag{3.18}$$

The state ρ^c of each class c is then updated according to

$$\rho^c_i(k+1) = \rho^c_i(k) + \frac{T}{L}\left[f^c_i(k) - f^c_{i+1}(k)\right] \tag{3.19}$$

The total transition flow can be obtained by summing

$$f_i(k) = \sum_{c \in C} f^c_i(k) \tag{3.20}$$

For each cell i the penetration rate $p(k)$ of CAVs at time instant k is defined as

$$p(k) = \frac{\rho^a_i(k)}{\rho^a_i(k) + \rho^b_i(k)} \tag{3.21}$$

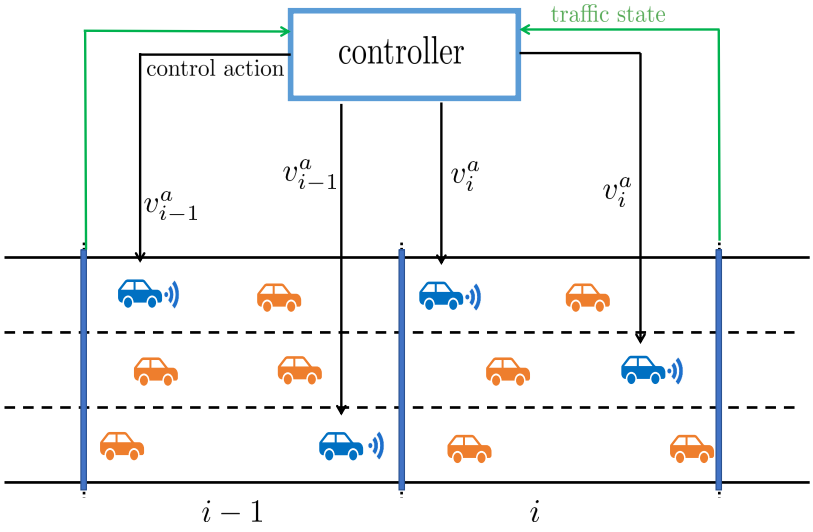

Figure 3.8: Scheme of the control applied to vehicles belonging to the automated vehicles class.

A sketch of the freeway with multiple classes of vehicles is depicted in Fig.3.7. It is worth noting that, unlike the majority of similar multi-class models, here the penetration rate is not an a priori imposed parameter but it dynamically varies depending on the system evolution.

As mentioned in Section 2.2, the CTM belongs to the class of first order models, then it does not include the capacity drop modeling. In order to overcome this issue and make the set-up more realistic, a term is added to the model to capture the capacity drop. Among the several extension proposed in literature, for this model the one proposed in [62] is applied. It computes the capacity of each cell as

$$q_i^{\max}(k) = \min\left\{c_i, c_i\left(1 - \alpha\frac{\rho_{i-1}(k) - \rho_{i-1}^{cr}}{\rho_{i-1}^{max}(k) - \rho_{i-1}^{cr}}\right)\right\} \tag{3.22}$$

Above, c_i is the free-flow capacity of cell i, i.e. the capacity that the cell have when no congestion is present. When the density in the cell increases, its capacity linearly decreases and the intensity of its reduction is given by the value of the parameter α.

3.2.2 Control of intelligent vehicles

The multi-class model described in the previous section is used to develop a traffic controller aiming at reducing congestion on highway. Specifically, situations in which bottlenecks are present along the highway creating congestion are considered. Bottlenecks are locations with particular characteristics, such as merge areas, lane drops, tunnels, strong curvatures, or locations interested by temporary events such as traffic accidents, work zones and so on, that reduce capacity, creating jams. In the following, an highway whose capacity is affected by a bottleneck is considered and a control action is applied to vehicles belonging to class a, the automated cars. Specifically, the free-flow speed v^a of the automated vehicles class is controlled with the aim of uniforming the traffic density and to reduce congestion. A scheme of the controller is depicted in Fig. 3.8.

Considering the traffic system, its states are the densities of the two classes $\rho(k) = [\rho_a(k)\, \rho_b(k)]$, while the control variable is the vector of the class a free-flow speed for each cell $i = 2, ..., N$. The optimization problem is formulated over the finite prediction horizon of K_p time steps as follows. At each time k, given the current initial state $\underline{\rho}(k) = [\underline{\rho}^a(k)\, \underline{\rho}^b(k)]$, find the optimal control sequence $\underline{u}(h) = [u_2(h)...u_N(h)], h = k, ..., k + K_p$ that minimizes the objective cost function J. $\underline{u}(h)$ is a matrix having as entries the optimal values of the free-flow speed of class a for each cell $i = 2, ..., N$. The optimization problem is given by

$$J = T \sum_{h=k}^{k+K_p} \sum_{i=1}^{N} L_i \bar{\rho}_i(h) - \beta \sum_{h=k}^{k+K_p} \phi_{i_b}(h) \tag{3.23}$$

subject to the model dynamics (3.13)-(3.22) and to

$$\underline{u}^{min} \leq \underline{u}(k) \leq \underline{u}^{max} \qquad \text{for } k = 1, ..., K \tag{3.24}$$

The cost function of Eq.(3.23) is given by Total Travel Time (TTT), see section 2.5, as first term, while the second term represents the discharge flow from the bottleneck cell i_b, to be maximized to reduce the capacity drop occurrence. The parameter β acts as weight in the cost function. This results in a non-linear multi-variable minimization problem that is solved by means of the interior-point algorithm implemented in the CasADI software tool [3].

3.2.3 Simulations Results

The MPC described in the previous paragraph is simulated to assess its validity. A stretch of highway of $N = 9$ cells of length $L_i = 0.7$ km for $i = 1, ..., N$ and three

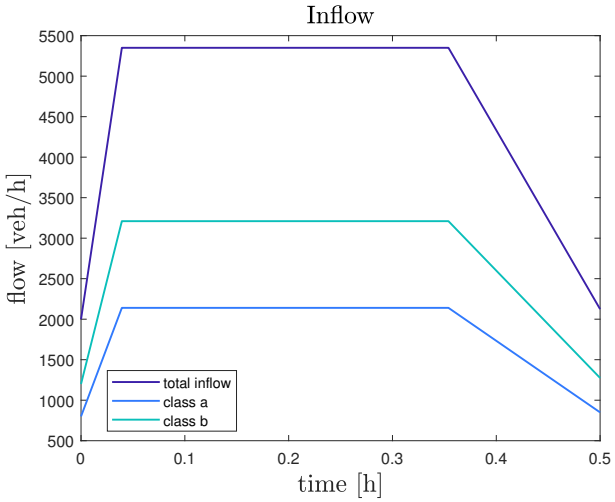

Figure 3.9: Demand of cell 0

lanes is taken into consideration. The free-flow capacity of each cell is $c = 6000$ veh/h, while q^{max} is given by Eq.(3.22), the critical density is $\rho^{cr} = 63.2$ veh/km and the jam density $\rho^{max} = 305.1$ veh/km. The human-driven vehicles class has a fixed free-flow speed $v^b = 95$ km/h, while the congestion wave speed is $w = 24.8$ [km/h]. The parameter expressing the capacity drop amplitude α in Eq. (3.22) is equal to 0.56. For both the classes the headway is set to 1 second. As incoming demand a trapezoidal shape is considered for both the classes, as depicted in Fig. 3.9. In this presented scenario, the 30% of the flow is composed by CAVs, the remaining flow by human-driven vehicles. As initial condition, the total density, sum of the initial density of the two classes, is equal to 30 veh/km.
A temporary bottleneck reduces the capacity of the highway for a part of the simulation. Specifically, in cell $i = 8$, the free-flow capacity is reduced to $c_8 = 5000$ veh/h from the beginning of the simulation and it lasts for the 60% of the simulation time. At the end of this period the capacity is restored to the value of 6000 veh/km. The controller detailed in Section 3.2.2 is applied with a prediction horizon of $K_p = 14$ time steps, thus the prediction time is around five minutes. The control speed v^a is constrained to vary between $v^{min} = 50$ km/h and $v^{max} = v^{free} = 95$ [km/h]. The speed control starts from cell $i = 2$, no control action is applied to the first cell, $v_1^a = v^{free}$.

Fig. 3.10 reports the trend of the traffic density when no control is applied, and so the speed of the two classes is equal to $v^{free} = 95$ km/h and the model behaves as the traditional *CTM*, with the capacity drop extension. Focusing on the incoming traffic demand depicted in Fig.3.9, at time instant $k = 7$ it exceeds

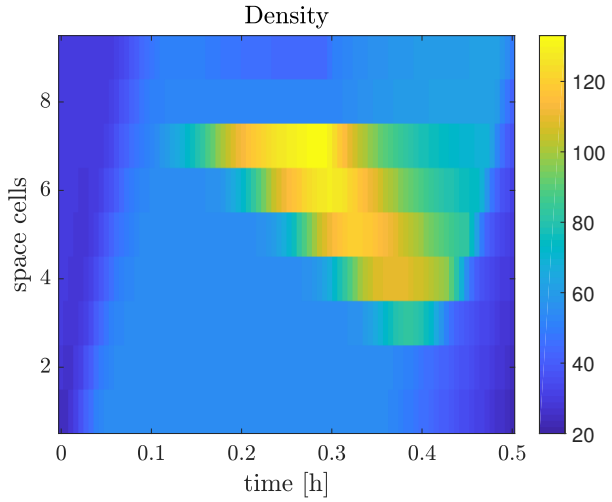

Figure 3.10: Density trend when no control is applied.

the capacity of the bottleneck, that activates and congestion starts forming. The congestion propagates upstream, pushed by the drop in the capacity that limits the discharge flow from the bottleneck. With the chosen value of $\alpha = 0.56$, the maximum capacity drop results into a reduction of the 16% of the discharge flow. When the temporary bottleneck is cleared and the capacity of cell $i = 8$ is restored to its maximum value, the congestion dissipates. The higher is the value that the density of cell $i = 7$ reaches, the higher will be the reduction of the discharge flow, and the higher the congestion. Therefore, an effective control has to avoid to reach too high congestion states in order to guarantee the maximum discharge rate, and a limited occurrence of the capacity drop.

The speed control designed in Section 3.2.2 is now applied. The control action is actuated via vehicles belonging to class a, then for different penetration rates, the control can be more or less aggressive. In this perspective, the control action has been simulated in different scenarios with different penetration rates. Fig. 3.11 shows the density in the controlled case for different penetration rates of CAVs. The penetration rate is determined by the share of class a vehicles in the inflow but its value is not kept constant and dynamically varies. It is possible to see that even when the penetration rate is low, ~ 0.1, as depicted in Fig. 3.11(a), there is a congestion mitigation that leads to a slight travel time reduction. Of course, the higher is the penetration rate, the more effective the control action is. With the highest simulated penetration rate, ~ 0.6 reported in Fig. 3.11(f), congestion appears almost totally dissipated.

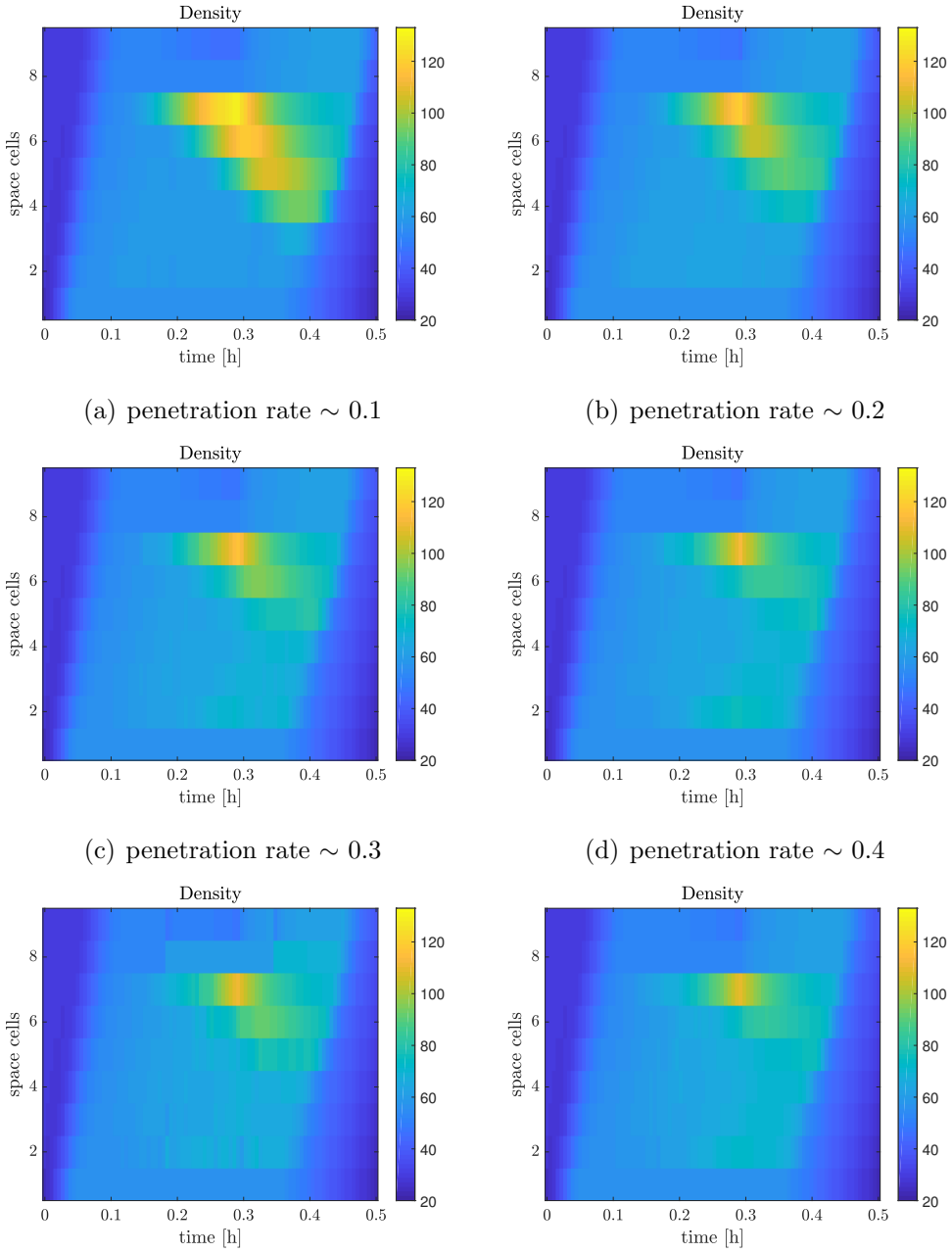

(a) penetration rate ~ 0.1

(b) penetration rate ~ 0.2

(c) penetration rate ~ 0.3

(d) penetration rate ~ 0.4

(e) penetration rate ~ 0.5

(f) penetration rate ~ 0.6

Figure 3.11: Comparison between control scenarios with different penetration rate of CAVs.

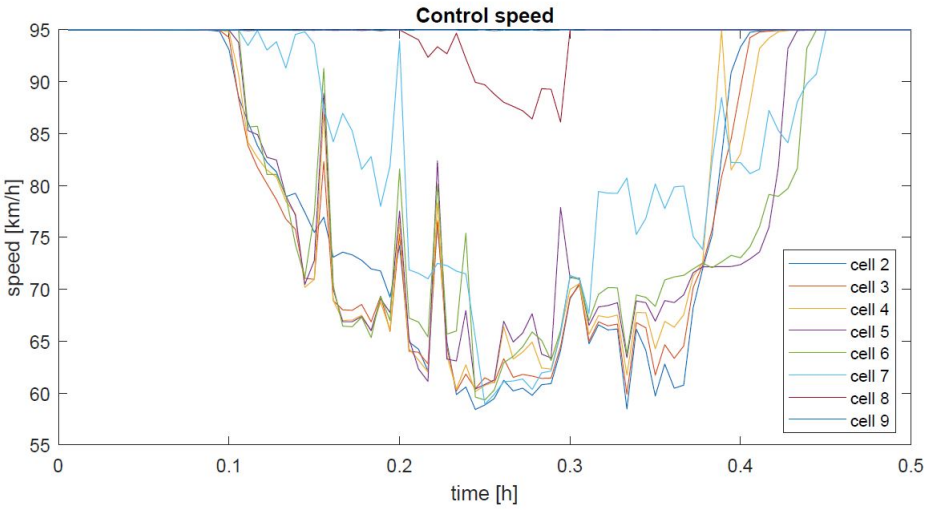

Figure 3.12: CAVs class control speed computed via the MPC.

In Table 3.3 an evaluation of the performance indexes introduced in Section 2.5 for each simulated penetration rate. The Total Travel Time (TTT) decreases more steeply with penetration rates increasing from the value of 0.1 to 0.3, going from the value of 188.79 to 175.22 veh h, then by further increasing its value, the decrease of the TTT tapers off. This is due to the fact that over a certain value of penetration rate there is some form of saturation in the applied control action. The Total Traveled Distance (TTD) increases from the value of 14893 to 14901 veh·km when $p = 0.3$, leading to a consequent increase of the mean speed. The scenario with penetration rate $p = 0.3$, i.e. the best compromise of lowest penetration rate with good control effectiveness, is here detailed as example. For this scenario, the incoming flow allocated to each class is indicated in Fig. 3.9, while Fig.3.11(c) reports the density trend. The control speeds computed by the MPC are depicted in Fig. 3.12.

The controller properly decreases the speed of class a in the cells located upstream the bottleneck. This is motivated by the need of delaying the traffic jam formation. The most aggressive control action appears to be applied to cell $i = 2$ that is the farthest from the bottleneck location. Cell $i = 9$, located downstream the bottleneck, does not have any modification in the free-flow speed imposed by the controller, as expected. Its value is kept fixed at 95 km/h to guarantee the maximum outflow. When the temporary bottleneck is cleared, the speed is restored by the controller to the normal maximum free-flow value of 95 km/h in all the cells.

Looking at the density distribution along the highway, in the control case it appears globally more uniform and the congestion propagates for only one cell and

Table 3.3: Comparison between performance indexes in the uncontrolled case and in the control case with different penetration rate.

	TTT	TTD	MS
No control	188.7947	14893	78.88
p=0.1	183.2409	14895	81.29
p=0.2	176.8308	14900	84.26
p=0.3	175.2191	14901	85.04
p=0.4	173.6013	14901	85.84
p=0.5	174.7722	14899	85.25
p=0.6	173.0361	14903	86.13

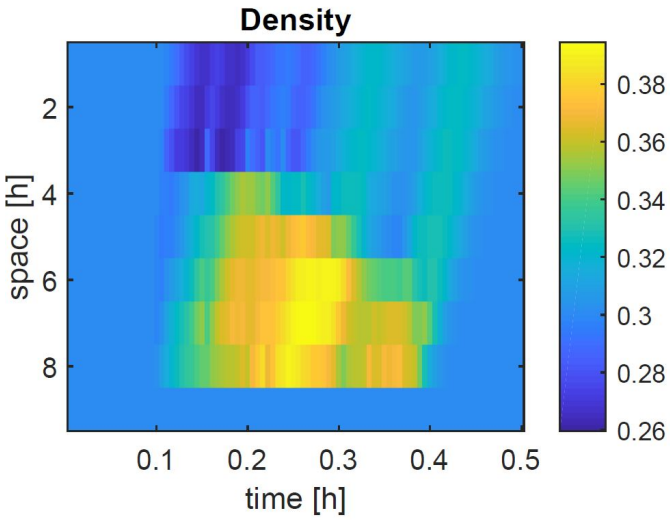

Figure 3.13: Distribution of the penetration rate of class a vehicles along then stretch of highway

too high value of density are reached only in the cell immediately upstream the bottleneck, and they last for a short span of time.
Fig. 3.13 depicts how the distribution of autonomous vehicles varies along the stretch, i.e. the dynamic evolution of the penetration rate. At the beginning of the simulation, the penetration rate is constant along the stretch and equal to 0.3 since it is determined only by the inflow of Fig. 3.9. When the control action is applied, the controller communicates the optimal speed to vehicles belonging to class a, thus slowing down the free-flow speed of the connected/automated vehicles class. The consequence is that they tend to accumulate in the first part of the stretch during the simulation. The accumulation dissolves when the bottleneck is cleared and the automated/connected vehicles class can flow again at the free-flow speed of 95 km/h.

Final Considerations

In this section of the thesis a multi-class model able to capture a mixed flow of human-driven cars and CAVs is presented. Since the model is still a macroscopic model, the computational burden is limited compared to microscopic approaches, but the model appears to be still able to describe the presence of CAVs. The proposed control action aiming at regulating the speed of the connected/automated class vehicles influences also the human-driven vehicles and obtains benefits for the overall traffic flow. The overall density experiences an homogenization and the congestion is strongly reduced. The control action is effective also with limited penetration rates, and it becomes more and more effective by increasing the share of CAVs.

Chapter 4

Traffic Models Incorporating Platoons of Intelligent Vehicles

In this chapter the concept of exploiting connected and automated vehicles as actuators for traffic control purposes is further developed. Specifically, instead of controlling single vehicles, platoons of cars are here taken into account. In this perspective, conventional traffic models need to be revised to be able to incorporate platoons of vehicles. While some researches has moved in the direction of modelling the interaction between platoon and traffic from a microscopic point of view, few results are available in the macroscopic context. This work aims at filling this gap by proposing a macroscopic approach for platooning in highway traffic.
Two different extensions to traditional macroscopic models are presented in the following, both of them exploiting the moving bottleneck concept already developed in Section 3.1.1 for a single vehicle. Specific traffic control actions using platoons as actuators are also designed.

4.1 A CTM extension to capture platoons of intelligent Vehicles

In this section, the traditional CTM model is extended to consider platoons of smart vehicles moving in the human-driven surrounding flow. Specifically, the state equation is properly augmented to take into account platoons, whose presence is captured by modifying the free-flow speed of the cells in which they are traveling. Platoons of CAVs are then assumed as actuators and their speed becomes the control variables to design different control schemes that aim at reducing congestion.

4.1.1 The Model

The Moving Bottleneck Cell Transmission Model (MB-CTM), presented in [127], is here described. The basic CTM and the relative adopted notation are reported in the preliminaries Section 2.1.

To the aim of this work, for each cell $i = 1, \dots, N$, and for each time step $k = 0, \dots, K-1$, the dynamic state equation (2.6) updating the traffic density is enhanced to capture the presence of J moving bottlenecks. Specifically, the equation describing the dynamic evolution of the traffic density is augmented, becoming

$$\rho_i(k+1) = \rho_i(k) + \frac{T}{L}\left[f_i(k) - f_{i+1}(k)\right] + \sum_{j=1}^{J}\left[\delta_i^j(k)\frac{o^j}{L} - \delta_{i+1}^j(k)\frac{o^j}{L}\right] \tag{4.1}$$

where o^j denotes the occupancy [veh] of the moving bottleneck $j = 1, \dots, J$, while $\delta_i^j(k)$ is a binary variable that is introduced in order to track the entrance (or the exiting) of moving bottlenecks in a cell. Specifically, $\delta_i^j(k)$ is defined as follows

$$\delta_i^j(k) = \begin{cases} 1 & \text{if the moving bottleneck } j \text{ enters} \\ & \text{cell } i \text{ at time step } k \\ 0 & \text{otherwise} \end{cases} \tag{4.2}$$

At each time step k, at most one moving bottleneck can be present in each cell i. Then, condition $\sum_{j=1}^{J} \delta_i^j(k) \leq 1$ must be fulfilled.

The traffic flow $f_i(k)$ entering the ith cell is obtained as the minimum between the so called demand function of cell $i-1$ and the supply function of cell i. As described in Section 2.1, these quantities are computed as

$$f_i(k) = \min\left\{D_{i-1}(k), S_i(k)\right\} \tag{4.3}$$

$$D_{i-1}(k) = \min\left\{v_{i-1}(k)\rho_{i-1}(k), q_{i-1}^{\max}\right\} \tag{4.4}$$

$$S_i(k) = \min\left\{w_i(\rho_i^{\max} - \rho_i(k)), q_i^{\max}\right\} \tag{4.5}$$

While in the standard CTM the speed $v_i(k)$, the free-flow speed, is a parameter, in this extension $v_i(k)$ in (4.4) is given by

$$v_i(k) = \begin{cases} f(\bar{v}^j(k)) & \text{if the moving bottleneck } j \text{ is in} \\ & \text{cell } i \text{ at time } k \\ v_i^{\text{free}} & \text{otherwise} \end{cases} \tag{4.6}$$

where $\bar{v}^j(k)$ represents the speed of the moving bottleneck j at time step k. According to (4.6), if the moving bottleneck j is in cell i, the speed $v_i(k)$ is a function of the moving bottleneck speed. Note that the speeds of the moving bottlenecks $\bar{v}^j(k)$, $j = 1, \ldots, J$, will represent the control variables.

As a first approximation, the moving bottleneck directly affects the speed of the cell, such that $f(\bar{v}^j(k)) = \bar{v}^j(k)$. Accordingly, equation (4.6) becomes

$$v_i(k) = \begin{cases} \bar{v}^j(k) & \text{if the moving bottleneck } j \text{ is in} \\ & \text{cell } i \text{ at time } k \\ v_i^{\text{free}} & \text{otherwise} \end{cases} \tag{4.7}$$

To the aim of tracking the trajectory of each moving bottleneck in this macroscopic modelling scenario, the covered distance $p^j(k)$ is introduced and updated as follows

$$p^j(k+1) = p^j(k) + \bar{v}^j(k) \cdot T \tag{4.8}$$

When the moving bottleneck j is in a location in which is close to cross the interface between two consecutive cells, namely $i-1$ and i, $p^j(k)$ is updated according to the amount of flow that the downstream cell accepts. Two different situations have then to be considered, corresponding to the *Free-Flow Case* and the *Congested Case*.

Free-Flow Case. In this first case, condition $D_{i-1}(k) \leq S_i(k)$ holds. The downstream cell i can receive the demand of cell $i-1$ and, consequently, also the moving bottleneck j in cell $i-1$. Hence, moving bottleneck j continues moving with speed $\bar{v}^j(k)$, its position $p^j(k)$ is updated by equation (4.8) and $\delta_i^j(k)$ is set equal to 1.

Congested Case. In this case, condition $D_{i-1}(k) > S_i(k)$ is satisfied. Then, cell i is too congested to receive the whole traffic demand arriving from cell $i-1$. It is therefore necessary to evaluate if the moving bottleneck j is involved in the part of flow that actually accesses the downstream cell.
To do this, $\bar{p}^j(k)$ is used to denote the position that the moving bottleneck would reach if it could enter cell i, which is computed as

$$\bar{p}^j(k+1) = L \cdot (i-1) + (T - \Delta T^j) \cdot \frac{f_i(k)}{\rho_i(k)} \tag{4.9}$$

Above,

$$\Delta T^j = \frac{L \cdot (i-1) - p^j(k)}{\bar{v}^j(k)} \tag{4.10}$$

Indicated with l^j the length of the j-th moving bottleneck, two further subcases of the congested case are possible.

- *Case 1* - If condition $(T - \Delta T^j) \cdot \frac{f_i(k)}{\rho_i(k)} \geq l^j$ is satisfied (i.e. the platoon can enter cell i), the moving bottleneck j enters cell i with probability $\frac{S_i(k)}{D_{i-1}(k)}$. This choice of adopting the probability is justified by the fact that having used a macroscopic model discrete in space, the precise location of the moving bottleneck inside the traffic flow can not be precisely known. Hence, the probability term models the uncertainty on its location. The higher is the supply of the receiving cell i, the higher the probability that the moving bottleneck can cross the cell interface.
  The position is then updated as follows:

  - if the moving bottleneck can access cell i, the corresponding binary variable $\delta_i^j(k)$ is set to 1 and the position becomes

    $$p^j(k+1) = \bar{p}^j(k+1) \tag{4.11}$$

    When moving bottleneck j enters the congested cell i, its speed is no longer controlled and it becomes

    $$\bar{v}^j(k) = \frac{f_i(k)}{\rho_i(k)} \tag{4.12}$$

  - if the j-th moving bottleneck cannot enter cell i, the binary variable $\delta_i^j(k)$ is set to 0 and the moving bottleneck stops in cell $i-1$, at the end of the cell:

    $$p^j(k+1) = L \cdot (i-1) \tag{4.13}$$

    and, accordingly, the moving bottleneck speed is

    $$\bar{v}^j(k) = \frac{L \cdot (i-1)}{T} \tag{4.14}$$

    Moreover, in this case, if at time step $k+1$ the downstream cell i can receive the moving bottleneck, i.e. $S_i(k+1) \geq S^{\min}$ (with $S^{\min}$ properly defined), the moving bottleneck that was in cell $i-1$ at time step k can access the cell i. Therefore, $\delta_i^j(k+1)$ is set to 1 and the position is updated according to (4.8). In this case the speed $\bar{v}^j$, at time step $k+1$, is defined by the controller if cell i is in free-flow condition, otherwise it is computed following (4.12). If $S_i(k+1) < S^{\min}$, the platoon remains in cell $i-1$ and the same condition is checked at $k+2$.

Case 2 - If $(T - \Delta T) \cdot \frac{f_i(k)}{\rho_i(k)} < l^j$, i.e. the platoon can not enter without dividing itself in two portions, the moving bottleneck stops at cell $i-1$. The position of the moving bottleneck at time step $k+1$ is then given by (4.13), while its speed is computed following (4.14) and $\delta_i^j(k)$ is set equal to 0.

Also in this case, if at time step $k+1$ the condition $S_i(k+1) \geq S^{\min}$ is satisfied, the moving bottleneck can access cell i, and its position is updated according to (4.8), setting $\delta_i^j(k+1)$ to 1. The speed of the moving bottleneck at time step $k+1$ is imposed by the state of the receiving cell. If $S_i(k+1) < S^{\min}$, the platoon still remains in cell $i-1$ and the same condition is checked at $k+2$.

4.1.2 Multiple Moving Bottlenecks Control via Platoons of Intelligent Vehicles

The model presented in Section 4.1.1 is here adopted to describe the traffic behavior and proper control actions are discussed. Control strategies for problems described by means of the MB-CTM model have been presented in [127], [121]. As before, the basic idea is to exploit the presence of intelligent, automated and connected vehicles to implement, by means of vehicles coordination, suitable control actions with the aim of positively affecting the overall traffic system. Several control schemes can be used. A possible classification between them can be done:

- centralised control schemes, as depicted in Fig. 4.1;
- decentralised control schemes, as shown in Fig. 4.2.

A centralised scheme involves the presence of a central controller having the full knowledge of the entire freeway, via traffic data collected both by means of traditional sensors and from all the data directly transmitted from connected vehicle via V2I communication systems. The central controller takes decision about the formation of the platoons specifying their size and speed, based on the collected information. In addition to this, communication and coordination between platoons is allowed by the presence of vehicles communication systems, with the aim to boost the effectiveness of the strategy.

On the other hand, a decentralized control scheme includes local controllers establishing the action for each platoon, as shown in Fig. 4.2. In this scheme, the size of the platoons is a priori known and the each controller indicates the speed that each platoon has to assume. Each decentralised controller decides the strategy on the basis of the information exchanged among the different (at least

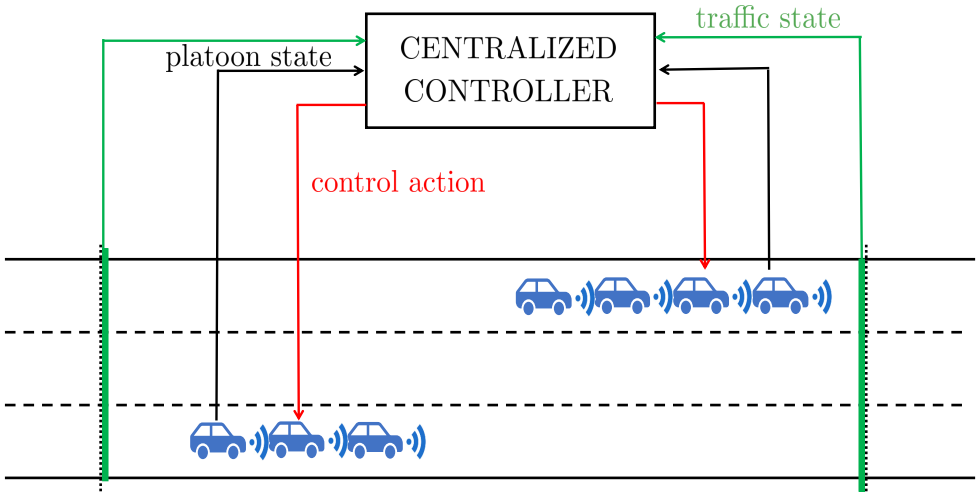

Figure 4.1: The centralized control scheme

close) controllers.
In the following, two different control schemes are applied. The first one is a decentralised control scheme where each controller is implemented by means of a PI-type feedback control law, while the second one involves a Model Predictive Control.

4.1.3 Proportional Integral Control Strategy

The presented control scheme aims at preventing congestion that would originate due to physical bottlenecks located further downstream. To do this, it regulates the upstream flow by exploiting controlled platoons. This action inevitably produce a controlled congestion, due to the presence of platoons travelling at lower controlled speeds.

As remarked in 4.1.1, platoons are modelled as J moving bottlenecks, whose speeds represent the control variables. At each time step k each speed is computed by a PI-type feedback regulator, according to the following

$$\bar{v}^j(k) = \bar{v}^j(k-1) + K_P \left[e^j(k) - e^j(k-1) \right] + K_I \cdot e^j(k) \tag{4.15}$$

where K_P and K_I respectively represent the proportional and the integral gain, while $e^j(k)$ is the density error. Specifically, as error, the difference between a density set-point $\hat{\rho}$ and a mean density value $\bar{\rho}^j(k)$, referred to the traffic densities

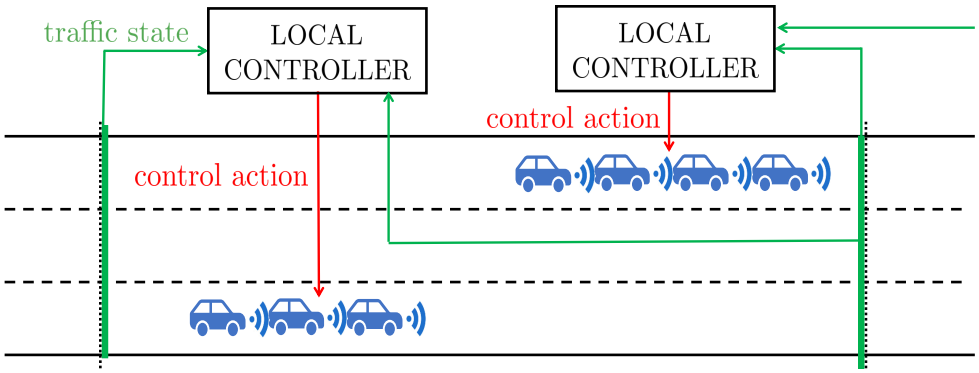

Figure 4.2: The decentralized control scheme

measured in a set of downstream cells is adopted. Specifically,

$$e^j(k) = \hat{\rho} - \bar{\rho}^j(k) \tag{4.16}$$

The set-point is set equal to the value of the critical density ρ_i^{cr} of the physical bottleneck. Moreover, with $i^j(k) \in \{1, \dots, N\}$ the cell corresponding to the position $p^j(k)$ of the moving bottleneck j at time step k is denoted, while $i^{\text{B}}(k) \in \{1, \dots, N\}$ indicates the cell related to the position of the physical bottleneck at time k. The average density is then computed on the subset of cells $I^j(k) \subseteq \left\{i^j(k), i^j(k)+1, \dots, i^{\text{B}}(k)\right\}$. Specifically, this set is defined so that $i \in I^j(k)$ if $\rho_i(k) \geq \varrho$, where ϱ is a density threshold properly defined. The average density $\bar{\rho}^j(k)$ to be used in (4.16) is computed as

$$\bar{\rho}^j(k) = \frac{\sum_{i \in I^j(k)} \rho_i(k)}{|I^j(k)|} \tag{4.17}$$

Note that the control speed computed by the feedback law (4.15) has to be bounded between a minimum and maximum values, i.e. $v^{\min} \leq \bar{v}^j(k) \leq v_i^{\text{free}}$, in order to prevent the speed to assume values that would be too low on highways, thus creating safety issues. Moreover, when the interface between two cells is congested, it is no more possible to control the speed that is updated according to the model dynamics described in Section 4.1.1, given by (4.12) or (4.14).

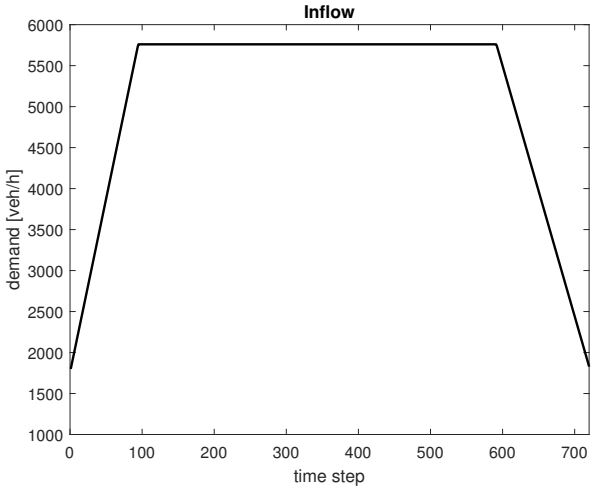

Figure 4.3: Inflow in the stretch

Simulation Results

The proposed PI feedback control is simulated considering a case study to evaluate the effectiveness of the strategy.

A stretch of freeway composed of $N = 16$ cells, each one with length $L = 0.5$ km is taken into consideration. The stretch has three lanes and no ramps. The sample time is $T = 10$ s, while the total time horizon is 2 hours that corresponds to $K = 720$ time steps.

For each cell $i = 1 \ldots, N$, the free-flow speed is ì $v_i^{\text{free}} = 100$ km/h, the congestion wave speed is equal to $w_i = 38$ km/h, the maximum value of density is $\rho_i^{max} = 360$ veh/km, $\rho_i^{cr} = 90$ veh/km while the capacity is $q_i^{max} = 6000$ veh/h.

A temporary bottleneck is modeled in order to simulate the creation of congestion. Specifically, at the beginning of the simulation time, a reduction of the capacity in cell $i = 13$ appears, to simulate the presence of a temporary physical bottleneck. During the first half of the simulation, the capacity of cell $i = 13$ is then reduced to $q_{13}^{max} = 5410$ [veh/h], while it is restored to its value of $q_{13}^{max} = 6000$ [veh/h] during the second half.

The demand of cell 0, i.e. the inflow in the highway stretch, has a trapezoidal trend that is reported in Figure 4.3.

Fig. 4.4(a) depicts the density when the control is not applied. At time step $k = 87$ the incoming flow overcomes the value of the capacity of the temporary bottleneck and congestion starts forming, and spreads for several cells upstream. In this situation, accordingly with the CTM principle, the density in the temporary

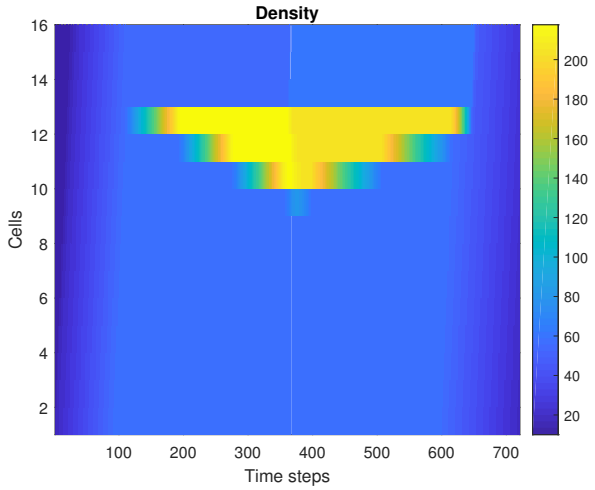

(a)

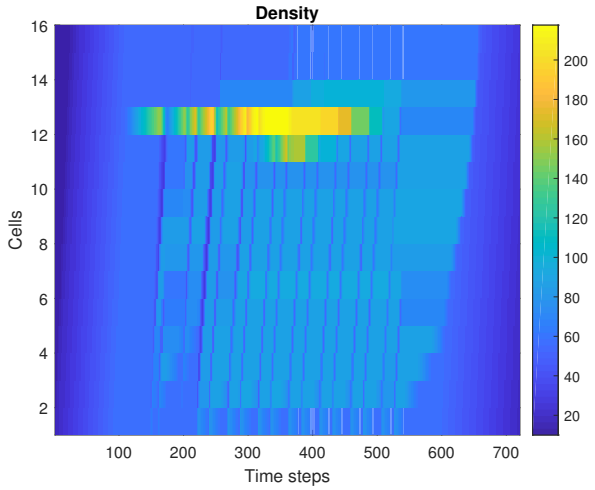

(b)

Figure 4.4: Evolution of the density in time and space in the uncontrolled case and with the moving bottleneck control.

Figure 4.5: Example of position and speed of one of the controlled moving bottleneck.

bottleneck cell $i = 13$ is kept constant at the density value $q_{13}^{max}/v_{13}^{free}$, corresponding to 54.1 veh/km, while the cell discharges a flow equal to its capacity q_{13}^{max}. At the same time, a congestion forms and propagates in the three upstream cells. At time step $k = 360$, the temporary bottleneck is cleared, since its capacity in cell $i = 13$ is restored to the maximum value, so cell $i = 13$ discharges the maximum flow and the congestion starts to dissipate. In Fig. 4.4(b) the density trend in case the decentralised feedback PI moving bottlenecks control is applied is reported. In this situation, as soon as the congestion starts to form at the physical bottleneck and the density error computed as in (4.16) becomes negative, controllers start to work. In this simulation scenario, multiple moving bottlenecks subsequently enter the stretch. Once a moving bottleneck has entered the highway, the following one enters when the previous moving bottleneck has reached at least the sixth cell. This prevents the superposition of the effects that would appear in case of the presence of two moving bottlenecks in the same cell. Moreover, at most two moving bottlenecks are present in the stretch and each moving bottleneck is seen as a formation of vehicles of length $o^j = 100$ meters. The set of cells $I^j(k)$ is composed of the two cells upstream the fixed bottleneck. As reference value for the density, the critical density is adopted while the minimum value allowed for the moving bottleneck speed is $v^{min} = 60$ km/h and the proportional gain K_P and the integral gain K_I have been selected respectively equal to 0.8 and 1.6, by applying a trial and error procedure.

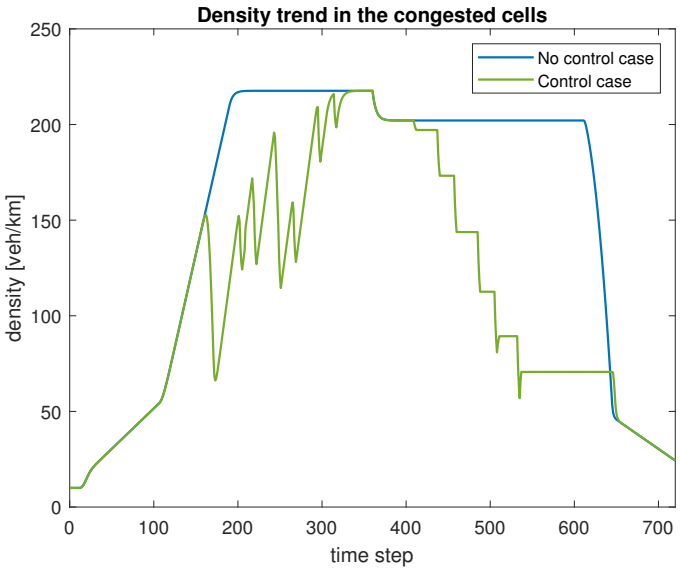

Figure 4.6: Density trend in cell $i = 12$ in the no-control case and with the application of the moving bottleneck control.

An overall number of 30 controlled moving bottlenecks enter the stretch during the simulation time. As an example, the trajectory of the first platoon entering the portion of highway is reported in Fig. 4.5. The blue line represents the position of the moving bottleneck, while the orange one is its speed. The designed feedback controller tends to properly slow down the moving bottleneck upstream the physical bottleneck reducing the capacity. This results in the creation of a controlled congestion that prevents jams to appear at the bottleneck. In this way, the density is more uniform along the highway. Moreover, the total number of cells in congestion state, i.e. the sum of the number of cells i such that $\rho_i(k) > \rho_i^{cr}$ at each time step during the overall simulation time horizon, decreases from 1079 to 857.

In Fig. 4.6, a comparison between the density in one of the cells upstream the physical bottleneck in the no-control case and in the controlled one is reported. In the absence of control action, the density in the cell is very high until the end of the simulation, while by applying the control, the congestion lasts for less time and also the density value is strongly reduced.

4.1.4 A Model Predictive Control Strategy for Travel Time Reduction

The MB-CTM and its relative control strategies have been further developed in [121], leading to a more sophisticated control scheme with more effective results. First of all, with the aim to make the simulation scenario more realistic, the capacity drop model described in Section 2.2 is here applied to the model. This results in the modification of the demand and supply function so that, in presence of active bottlenecks, the discharged flow is reduced.
Moreover, a different control action is here presented. The control variables are again the speeds of the platoons of VACS-equipped vehicles traveling on the highway. These latter, acting as moving bottlenecks, influence the neighbouring traffic.
The new approach involves the use of a MPC approach that is oriented at reducing travel times for drivers. As remarked in section 2.3, the MPC minimizes the chosen cost function over a prediction horizon in order to get an optimal control sequence. The optimization is repeated at each time step and the first sample of the sequence is applied to the system.
The formulation of the optimization problem over the finite prediction horizon of K_p time steps is as follows. At each time step k, given the current initial state $\underline{\rho}(k)$, find the optimal control sequence $\underline{u}(h), h = k...k + K_p$ minimizing the cost function J

$$J = \beta_1 T \sum_{h=k}^{k+K_p} \sum_{i=1}^{N} L_i \rho_i(k) - \beta_2 \sum_{h=k}^{k+K_p} \phi_{\bar{i}}(k) - \beta_3 \sum_{h=k}^{k+K_p} |\rho_{\bar{i}}(k) - \rho^{cr}| \tag{4.18}$$

subject to $\underline{u}^{min} \leq \underline{u}(k) \leq \underline{u}^{max}$ for $k = 1....K$.

In Eq.(4.18), the first term represents the the Total Travel Time (TTT) (see section 2.5), the second term is the outflow from the bottleneck location in cell $\bar{i}$, while the third term is defined as the density error at the bottleneck location $\bar{i}$ with respect to a reference value. Moreover, β_i, $i = 1, 2, 3$, are arbitrarily chosen weights.

The two last terms in J prevent the occurrence of the capacity drop phenomenon, since they act by maximizing the discharge flow from the bottleneck and by aiming at keeping the density below its critical value.
Following the receding horizon principle, at each iteration k the first sample of the optimal control sequence $\underline{u}(k)$ is applied to the system, while at the following iteration, based on the new available state information, a new prediction over the time horizon is done. This results in solving a nonlinear optimization problem, that

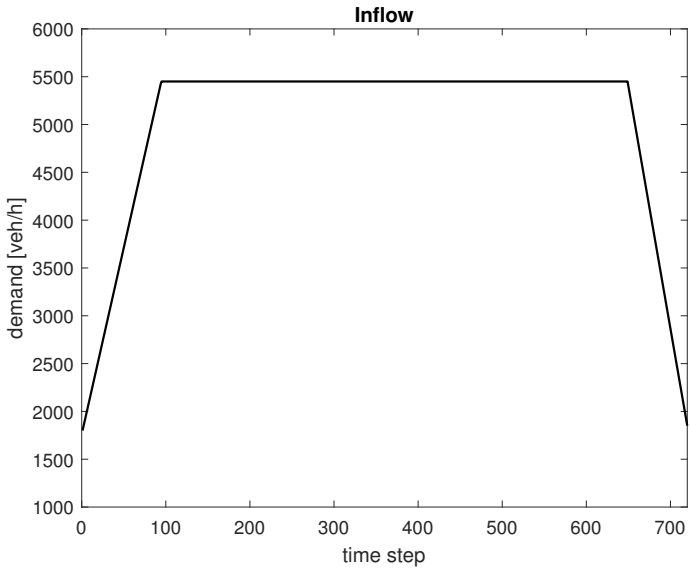

Figure 4.7: Trapezoidal traffic demand.

is here done by means of the interior-point algorithm implemented in MATLAB. Notice that, unlike the previous PI controller, the MPC approach results in the adoption of a centralised control (see Fig. 4.1).

Simulations

The MPC approach described in the previous section is here assessed in simulation. A realistic case of study consisting in a stretch of highway is simulated. It has not any intermediate on-ramps or off-ramps. The parameters adopted in the simulations are listed in Table 4.1, while the incoming traffic demand has a trapezoidal shape, as shown in Fig. 4.7. In order to create congestion, a temporary bottleneck is simulated in cell $i = 13$. It reduces the capacity to $c_{13} = 5400$ veh/km for $k < 540$, then it is restored to 6000 veh/h.

Three different situations are simulated:

- No control, no capacity drop: in this case the basic CTM is simulated. It does not account for the capacity drop phenomenon. The control is not applied yet.
- No control, capacity drop: in this situation again the control is not applied, but the capacity drop model is added.
- Control, capacity drop: in this case the complete model with the capacity

Table 4.1: Simulation parameters.

L	500 [m]
N	16
T	10 [s]
K	720
Simulation time	2 [h]
ρ_{cr}	70 [veh/km]
ρ_{jam}	320 [veh/km]
c	6000 [veh/h]
α	0.83
Bottleneck cell	13
Bottleneck capacity	5400 [veh/h]

drop model is simulated and moving bottlenecks are controlled via the MPC approach.

The trend of the density depending on time and space is depicted in Fig.4.8 where the first image is the uncontrolled case without the capacity drop model. When the arriving demand overcomes the capacity of the bottleneck cell $i = 13$, the supply function in the cell shows a lower value with respect to the demand of the previous cell. Then the flow between the two cells, given by the minimum between demand and supply, is equal to the value of the capacity of the bottleneck.

Since downstream the bottleneck location there are not congested cells, the flow leaving cell $i = 13$ is equal to its capacity, while the density value in the cell where the bottleneck is located remains equal to the critical density of the cell. A congestion forms only in the previous cell $i = 12$, and there is no capacity drop in the discharge flow.

Fig. 4.8(b) depicts the density trend when the capacity drop is modeled. Unlike the previous case, when the incoming demand overcomes the capacity of the bottleneck, the supply of the bottleneck cell is no more saturated to the capacity value and so it can accept a flow higher than its capacity, and congestion appears. As soon as the cell gets congested, the demand of cell $i = 13$ decreases according to Eq.(2.14), as explained in Section 2.2.

The discharge flow is consequently reduced and the congestion spreads for several

cells upstream. The trend of the flow leaving the bottleneck cell $i = 13$ is reported in Fig. 4.9 for both the traditional CTM, without capacity drop, and the CTM with the extension to model the capacity drop.

Fig. 4.8(c) depicts the density when the MPC control is applied. For the MPC, the prediction horizon K_p is 20 time steps, the weights in the cost function 4.18 are $\beta_1 = 0.1$, $\beta_2 = 0.1$, $\beta_3 = 0.8$ and $S^{min} = 10$. During the two hours of simulation several VACS-equipped vehicles enter the stretch and are controlled. They always keep a distance of at least one cell in order to avoid the superposition of the effects of two different controlled vehicles in the same cell. In the present simulation scenario, each platoon is composed by two vehicles. The total number of moving bottlenecks entering the stretch is 13, thus indicating that even with a limited number of controlled vehicles the proposed control can be effective. Looking at Fig.4.8(c) it is possible to notice that the controlled vehicles tend to create a jam upstream the bottleneck, thus avoiding hard congestion to form at the bottleneck. Moreover, the reduction of the congestion has another important effect in this situation where the capacity drop is captured. Specifically, reduced congestion means a reduced capacity drop effect and increased discharge flow. This can be seen in Fig. 4.9, in which the discharge flow from the bottleneck cell is depicted in the three different situations. The blue line is indeed the discharge flow from the bottleneck when there is not the capacity drop, so the flow is equal to the capacity of the bottleneck. On the other hand, the green line is the flow when the capacity drop is modeled but there is no control. The discharge flow decreases linearly with the density when the cell gets congested. The violet line, which is the flow when there is the capacity drop model but also the controller, shows that by applying the proposed solution the capacity drop is delayed and strongly reduced. This has obviously an impact on travel times. The performance of the controller are indeed evaluated also in terms of Total Travel Distance (TTD) and Mean Speed (MS) (see Section 2.5). Results are reported in Table 4.2 for the three cases. When the capacity drop effect is not considered, the TTT is equal to 824 [veh h] and it increases to 899 [veh h] when the capacity drop is instead included in the model, due to the reduced discharge flow that strongly affects the congestion formation. By applying the MPC, the TTT decreases, getting close to the uncontrolled case with no capacity drop.

About the control speeds, their profiles for two of the 13 controlled moving bottlenecks traveling in the stretch are reported in Fig. 4.10 as an example. At time step $k = 275$ a moving bottleneck enters the stretch with speed $\bar{v_1} = 82$ and then its

Table 4.2: Comparison between cost functionals.

	TTT	TTD	MS
Traditional CTM, uncontrolled	824.21	80366	97.51
CTM with capacity drop, uncontrolled	899.94	80366	89.30
CTM with capacity drop, MPC control	832.46	80102	96.22

speed is set by the controller. At $k = 291$ a second bottleneck enters the stretch and its speed trend is again given by the controller. The same is valid for each of the 13 platoons that enter the stretch during the simulation horizon, for the sake of simplicity only speeds of two of them are here depicted. The controller properly slows down the moving bottlenecks to create the needed controlled congestion.
With the adoption of the presented control action, even with a small number of controlled vehicles the capacity drop occurrence has been strongly reduced and a higher discharge flow from the bottleneck has been observed. Congestion is mitigated and travel times strongly reduced.

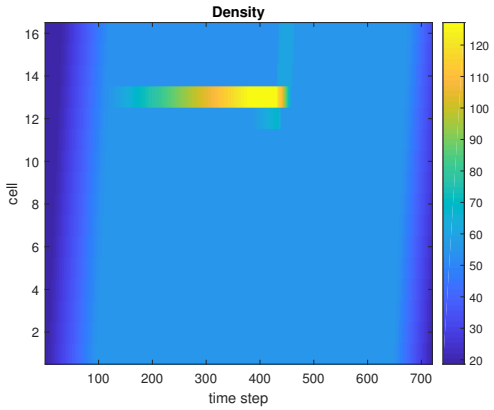

(a) No capacity drop, no control

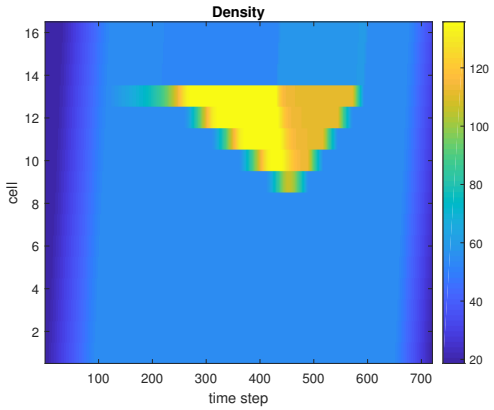

(b) Capacity drop, no control

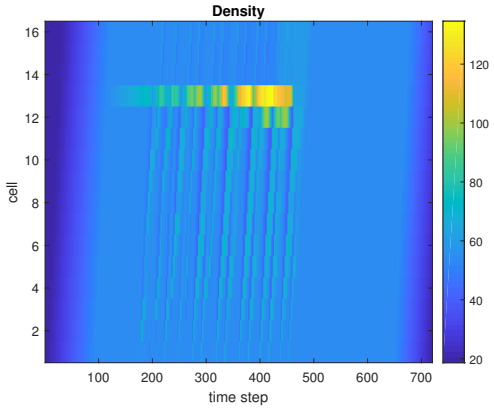

(c) Capacity drop, MPC control

Figure 4.8: Density trend in the case with traditional CTM 4.8(a), CTM with capacity drop and no control 4.8(b) and CTM with capacity drop and control 4.8(c).

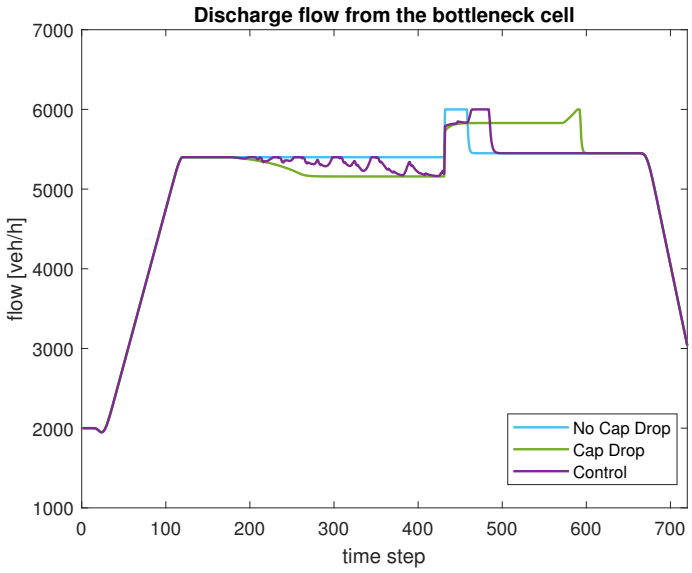

Figure 4.9: Discharge flow from the cell in which the bottleneck is located.

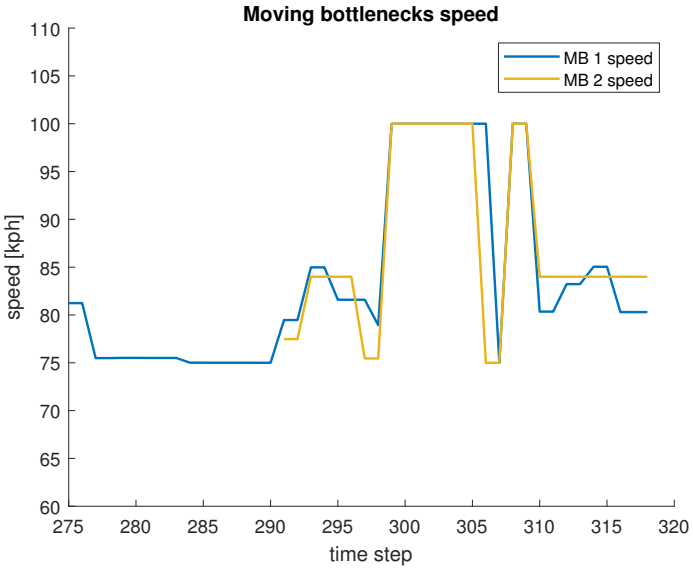

Figure 4.10: Example of the trend of the control speed for two moving bottlenecks.

4.2 A PDE-ODE Model for Platoons of CAVs

In this section a different model developed in [122] is presented. This model represents an extension of the coupled PDE-ODE model for moving bottleneck presented in Section 3.1.1, having the aim of capturing the presence of platoons of CAVs, whose length can vary in time.
Similarly to the moving bottleneck model of Section 3.1.1, the model consists of a Partial Differential Equation (PDE) for the bulk traffic flow and two Ordinary Differential Equations (ODEs) for the trajectory of the platoon. While in the moving bottleneck (MB) model one ODE was enough to describe the MB trajectory, since it was a punctual capacity restriction with no physical dimension, here one ODE describes the trajectory of the initial point of the platoon and the second describes the final point trajectory. This introduces discontinuities in the flows and a numerical methods to treat them is needed.
The literature on conservation laws having discontinuous flux functions is vast but most of the works focus only on discontinuities at fixed points in space [4], while only few researches face the issue of time dependent discontinuities, as [32, 33, 80, 110, 111, 137, 138] and, more recently, [19, 60]. Although the scalar conservation law here adopted could be assimilated to the framework reported in [19], the strong coupling of the PDE with the ODEs makes the problem more challenging. An efficient numerical strategy able to precisely capture the density discontinuities has then been developed. To this end, a conservative reconstruction strategy similar to [18, 24], requiring the knowledge of Riemann problem solutions at the flux discontinuity points, is applied.
In the following of this section, the model and the developed numerical method are presented. A control action aiming at controlling the speed and the length of the platoon is subsequently developed, showing good effectiveness in reducing traffic congestion.

4.2.1 The coupled PDE-ODE model

As in the moving bottleneck model described in Section 3.1.1, the bulk traffic flow is described by means of the LWR model. A platoon of vehicles is introduced in the model as a capacity restriction. The front-end point of the platoon is denoted as $z_d = z_d(t)$, while its back-end point is called $z_u = z_u(t)$. The platoon occupies a portion of lanes, acting as a flux constraint on the interval $[z_u(t), z_d(t)]$. A sketch of the platoon is shown in Fig. 4.11. Similarly to the model of the moving bottleneck

of Section 3.1.1, the model results in a PDE describing the traffic flow and two ODEs corresponding to the trajectory of the extremes of the platoon. The obtained coupled PDE-ODE model is

$$\partial_t \rho + \partial_x F(t,x,\rho) = 0, \qquad (t,x) \in \mathbb{R}^+ \times \mathbb{R}, \tag{4.19a}$$

$$\rho(0,x) = \rho_0(x), \qquad x \in \mathbb{R}, \tag{4.19b}$$

$$\dot{z}_u(t) = v_u(t, \rho(t, z_u(t)+)), \qquad t \in \mathbb{R}^+, \tag{4.19c}$$

$$z_u(0) = z_u^0, \tag{4.19d}$$

$$\dot{z}_d(t) = v_d(t, \rho(t, z_d(t)+)), \qquad t \in \mathbb{R}^+, \tag{4.19e}$$

$$z_d(0) = z_d^0. \tag{4.19f}$$

Above, $\rho = \rho(x,t)$ is again the conserved quantity, the traffic density, while F is the flow function, that appears to be discontinuous due to the discontinuity introduced by the platoon presence, specifically

$$F(t,x,\rho) := \begin{cases} f(\rho) & \text{if } x \notin [z_u(t), z_d(t)], \\ f_\alpha(\rho) := \alpha f(\rho/\alpha) & \text{if } x \in [z_u(t), z_d(t)]. \end{cases} \tag{4.20}$$

In (4.20), as usual $f(\rho) = \rho v(\rho)$, and a linear speed-density relationship is adopted

$$v(\rho) = V\left(1 - \frac{\rho}{R}\right)$$

Once again, the study could be easily extended to different fundamental diagrams. Above, V is the maximal speed of the flow and R is the maximal density. This latter is reduced to αR at the platoon position, where α represents the occupancy rate due to the platoon presence. The flux functions are then given by

$$f(\rho) = V\rho\left(1 - \frac{\rho}{R}\right), \tag{4.21}$$

$$f_\alpha(\rho) = V\rho\left(1 - \frac{\rho}{\alpha R}\right). \tag{4.22}$$

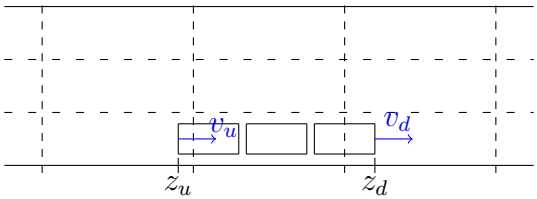

Figure 4.11: Sketch of platoon on the highway.

The initial data ρ_0 is in the form

$$\begin{aligned} &\rho_0(x) \in [0, \alpha R] \quad \text{if } x \in [z_u^0, z_d^0], \\ &\rho_0(x) \in [0, R] \qquad \text{otherwise.} \end{aligned} \tag{4.23}$$

We remark that the points of maximum of f and f_α are $\rho_{cr} = R/2$ and $\rho_{cr}^\alpha = \alpha R/2$ respectively, $f^{max} = f(\rho_{cr})$ and $f_\alpha^{max} = f_\alpha(\rho_{cr}^\alpha)$.

In 4.19, (4.19c)–(4.19e) describe the dynamic of the platoon extreme points. Their speed are given by

$$v_u(t, \rho) := \max\left\{V_u(t), -f_\alpha(\rho)/(R-\rho)\right\}, \tag{4.24}$$

$$v_d(t, \rho) := \min\left\{V_d(t), v(\rho)\right\}, \tag{4.25}$$

where $V_u(t) \in [-V, V]$ and $V_d(t) \in [0, V]$ are the maximal speeds of the upstream and downstream endpoints. Equation (4.25) accounts for the fact that the platoon cannot assume speed higher than the surrounding traffic flow.

The length of the platoon is denoted as $L(t) := z_d(t) - z_u(t)$ and it is allowed to vary depending on the number of vehicles joining the platoon and their spacing. Constraints are introduced for the length of the platoon, specifically $L_{min} \leq L(t) \leq L_{max}$, given a certain number of vehicles. The length can then vary according to

$$\dot{L}(t) = \dot{z}_d(t) - \dot{z}_u(t) = v_d(\rho(t, z_d(t)+)) - v_u(\rho(t, z_u(t)+)). \tag{4.26}$$

The downstream speed V_d is also constrained to be positive, since vehicles cannot move backwards. On the other hand, the upstream speed V_u may take negative values when additional vehicles join the platoon.

Following [80, Definition 5.1], the objective is to construct a weak entropy solutions of the system (4.19) in the following sense:

Definition 4.2.1. *A triple* $(\rho, z_u, z_d) \in \mathbf{C^0}\left(\mathbb{R}^+; \mathbf{L^1} \cap \mathbf{BV}(\mathbb{R}; [0, R])\right) \times \left(\mathbf{W^{1,\infty}}(\mathbb{R}^+; \mathbb{R})\right)^2$ *is a weak entropy solution to* (3.3)–(4.20)–(4.23) *if*

(i) $\rho(t, x) \in [0, \alpha R]$ *for a.e.* $x \in [z_u(t), z_d(t)]$ *and* $t \in \mathbb{R}^+$;

(ii) for all $\kappa \in \mathbb{R}$ *and all test functions* $\phi \in \mathbf{C_c^1}(\mathbb{R}^2; \mathbb{R}^+)$ *it holds*

$$\begin{aligned} &\int_{\mathbb{R}^+} \int_{\mathbb{R}} \Big(|\rho - \kappa| \, \partial_t \phi + \operatorname{sgn}(\rho - \kappa) \left(F(t, x, \rho) - F(t, x, \kappa) \right) \partial_x \phi \Big) \, dx \, dt \\ &\quad + \int_{\mathbb{R}} |\rho_0 - \kappa| \phi(0, x) \, dx \\ &\quad + \int_{\mathbb{R}^+} \left| F(t, z_u(t)+, \kappa) - F(t, z_u(t)-, \kappa) \right| \phi(t, z_u(t)) \, dt \\ &\quad + \int_{\mathbb{R}^+} \left| F(t, z_d(t)+, \kappa) - F(t, z_d(t)-, \kappa) \right| \phi(t, z_d(t)) \, dt \geq 0; \end{aligned}$$

(iii) z_u *and* z_d *are Carathéodory solutions of* (4.19c)–(4.19d)*, respectively* (4.19e)–(4.19f)*, i.e. for a.e.* $t \in \mathbb{R}^+$ *it holds*

$$z_u(t) = z_u^0 + \int_0^t v_u(s, \rho(s, z_u(s)+))\, ds,$$
$$z_d(t) = z_d^0 + \int_0^t v_d(s, \rho(s, z_d(s)+))\, ds.$$

Solutions to the Riemann problem

In this section the construction of the solutions to the two Riemann problems is detailed. Each Riemann problem corresponds to the discontinuities in correspondence of the upstream and downstream endpoints of the platoon, $z_u(t)$ and $z_d(t)$. Discontinuities then move with speeds V_u and V_d. For simplicity, each interface is separately studied. The solutions to these Riemann problems are needed to design the numerical scheme to accurately capture the dynamics of the platoon.

- **Downstream end-point**

  Firstly, the problem at the front-end of the platoon is detailed. The following Riemann problem appears at the downstream point of the platoon z_d:

$$\begin{cases} \partial_t \rho + \partial_x F(t,x,\rho) = 0 & x \in \mathbb{R}, t > 0, \\ \rho(0,x) = \rho_0(x) = \begin{cases} \rho_l & \text{if } x < z_d^0, \\ \rho_r & \text{if } x \geq z_d^0, \end{cases} \end{cases} \tag{4.27}$$

  where

$$F(t,x,\rho) = \begin{cases} f_\alpha(\rho) & \text{if } x \leq z_d(t), \\ f(\rho) & \text{if } x > z_d(t), \end{cases}$$

  with $z_d(t) := z_d^0 + V_d t$, $\rho_l \in [0, \alpha R]$, $\rho_r \in [0, R]$, subjected to the constraint $V_d \leq v(\rho_r)$, in order to comply with (4.25). In order to solve (4.27), the concept of supply and demand functions [52, Section 5.2.3] have to be introduced. They will be adapted into the platoon reference frame. The unique solution of the equation $f'(\rho) = V_d$ is indicated with $\rho^\sharp$, while $\rho_\alpha^\sharp$ denotes the solution of equation $f'_\alpha(\rho) = V_d$.

$$\widetilde{D}^\alpha(\rho_l) = \begin{cases} f_\alpha(\rho_l) & \text{if } \rho_l < \rho_\alpha^\sharp, \\ y_d^\alpha(\rho_l; \rho_\alpha^\sharp) & \text{if } \rho_l \geq \rho_\alpha^\sharp, \end{cases} \qquad \widetilde{S}(\rho_r) = \begin{cases} y_d(\rho_r; \rho^\sharp) & \text{if } \rho_r < \rho^\sharp, \\ f(\rho_r) & \text{if } \rho_r \geq \rho^\sharp, \end{cases}$$

where

$$y_d^\alpha(\rho;\bar\rho) = f_\alpha(\bar\rho) + V_d(\rho-\bar\rho),$$
$$y_d(\rho;\bar\rho) = f(\bar\rho) + V_d(\rho-\bar\rho),$$

indicates the straight lines having slope V_d passing respectively through $(\bar\rho, f_\alpha(\bar\rho))$ and $(\bar\rho, f(\bar\rho))$. For $\bar\rho \in [0, \alpha R]$:

$$\rho^+(\bar\rho) := \max\left\{\rho \in [0,R] \colon y_d^\alpha(\rho;\bar\rho) = f(\rho)\right\},$$
$$\rho^-(\bar\rho) := \min\left\{\rho \in [0,R] \colon y_d^\alpha(\rho;\bar\rho) = f(\rho)\right\},$$

and for $\bar\rho \in [0, R]$

$$\rho_\alpha^+(\bar\rho) := \max\left\{\rho \in [0,\alpha R] \colon y_d(\rho;\bar\rho) = f_\alpha(\rho)\right\},$$
$$\rho_\alpha^-(\bar\rho) := \min\left\{\rho \in [0,\alpha R] \colon y_d(\rho;\bar\rho) = f_\alpha(\rho)\right\}.$$

For each initial datum, several situations are possible, the different cases are here reported.

(D1) $\rho_l < \rho_\alpha^\sharp$ and $\rho_r < \rho^+(\rho_l)$.
Since in the platoon reference frame, with abuse of notation, $\widetilde{D}^\alpha(\rho_l) < \widetilde{S}(\rho_r)$, i.e.

$$y_d^\alpha(\rho;\rho_l) \le \widetilde{S}(\rho_r) + V_d(\rho-\rho_r),$$

the solution to the Riemann problem is a jump discontinuity between the values ρ_l and $\rho^-(\rho_l)$, followed then by a classical wave, a shock or a rarefaction, between $\rho^-(\rho_l)$ and ρ_r. Specifically, the left and right traces at $x = z_d(t)$ are respectively

$$\hat\rho_\alpha = \rho_l, \qquad \check\rho = \rho^-(\rho_l).$$

The solution is depicted in Figure 4.12(a), where the red line indicates the jump.

(D2) $\rho_l < \rho_\alpha^\sharp$ and $\rho_r \ge \rho^+(\rho_l)$.
In this case computing demand and supply in the platoon reference frame, one gets $\widetilde{D}^\alpha(\rho_l) \ge \widetilde{S}(\rho_r)$. The solution is then given by a shock wave between ρ_l and $\rho_\alpha^+(\rho_r)$, followed by a jump discontinuity between $\rho_\alpha^+(\rho_r)$ and ρ_r. In this case

$$\hat\rho_\alpha = \rho_\alpha^+(\rho_r), \qquad \check\rho = \rho_r,$$

as depicted in Figure 4.12(b).

(D3) $\rho_l \geq \rho_\alpha^\sharp$ and $\rho_r < \rho^+(\rho_\alpha^\sharp)$.
With these initial data, a rarefaction wave between ρ_l and $\rho_\alpha^\sharp$ and a consequent jump between $\rho_\alpha^\sharp$ and $\rho^-(\rho_\alpha^\sharp)$, followed by a shock between $\rho^-(\rho_\alpha^\sharp)$ and ρ_r form the solution, as indicated in Figure 4.12(c). Specifically

$$\hat{\rho}_\alpha = \rho_\alpha^\sharp, \qquad \check{\rho} = \rho^-(\rho_\alpha^\sharp).$$

(D4) $\rho_l \geq \rho_\alpha^\sharp$ and $\rho_r \geq \rho^+(\rho_\alpha^\sharp)$.
In this situation $\widetilde{D}^\alpha(\rho_l) \geq \widetilde{S}(\rho_r)$ and the solution is a shock or a rarefaction wave appearing between ρ_l and $\rho_\alpha^+(\rho_r)$ and a jump discontinuity between $\rho_\alpha^+(\rho_r)$ and ρ_r. Then again

$$\hat{\rho}_\alpha = \rho_\alpha^+(\rho_r), \qquad \check{\rho} = \rho_r,$$

as reported in Figure 4.12(d).

All the computed solutions ensure that the condition

$$\rho(t,x) \in [0, \alpha R] \text{ for } x < z_d(t) \quad \text{ and } \quad \rho(t,x) \in [0, R] \text{ for } x > z_d(t).$$

is satisfied.

- **Upstream end-point** Now the Riemann problem is solved in correspondence of the upstream endpoint:

$$\begin{cases} \partial_t \rho + \partial_x F(t,x,\rho) = 0 & x \in \mathbb{R}, t > 0, \\ \rho(0,x) = \rho_0(x) = \begin{cases} \rho_l & \text{if } x < z_u^0, \\ \rho_r & \text{if } x \geq z_u^0, \end{cases} \end{cases} \tag{4.28}$$

where

$$F(t,x,\rho) = \begin{cases} f(\rho) & \text{if } x < z_u(t), \\ f_\alpha(\rho) & \text{if } x \geq z_u(t), \end{cases}$$

Above, $z_u(t) := z_u^0 + V_u t$, $\rho_l \in [0, R]$ and $\rho_r \in [0, \alpha R]$. In this case the demand and supply functions are defined as

$$\widetilde{D}(\rho_l) = \begin{cases} f(\rho_l) & \text{if } \rho_l < \rho^\sharp, \\ y_u(\rho_l; \rho^\sharp) & \text{if } \rho_l \geq \rho^\sharp, \end{cases} \qquad \widetilde{S}^\alpha(\rho_r) = \begin{cases} y_u^\alpha(\rho_r; \rho_\alpha^\sharp) & \text{if } \rho_r < \rho_\alpha^\sharp, \\ f_\alpha(\rho_r) & \text{if } \rho_r \geq \rho_\alpha^\sharp, \end{cases}$$

where

$$y_u^\alpha(\rho;\bar\rho) = f_\alpha(\bar\rho) + V_u(\rho-\bar\rho),$$
$$y_u(\rho;\bar\rho) = f(\bar\rho) + V_u(\rho-\bar\rho).$$

As in the downstream case, for $\bar\rho \in [0,\alpha R]$ one defines

$$\rho^+(\bar\rho) := \max\left\{\rho\in[0,R]\colon y_u^\alpha(\rho;\bar\rho) = f(\rho)\right\},$$
$$\rho^-(\bar\rho) := \min\left\{\rho\in[0,R]\colon y_u^\alpha(\rho;\bar\rho) = f(\rho)\right\},$$

and for $\bar\rho\in[0,R]$

$$\rho_\alpha^+(\bar\rho) := \max\left\{\rho\in[0,\alpha R]\colon y_u(\rho;\bar\rho) = f_\alpha(\rho)\right\},$$
$$\rho_\alpha^-(\bar\rho) := \min\left\{\rho\in[0,\alpha R]\colon y_u(\rho;\bar\rho) = f_\alpha(\rho)\right\}.$$

The following cases are studied.

(U1) $\rho_l \le \rho^-(\rho_\alpha^\sharp)$ and $\rho_r \le \rho_\alpha^+(\rho_l)$.
Here in the moving reference frame $\widetilde{D}(\rho_l) \le \widetilde{S}_\alpha(\rho_r)$, so the solution consists in a non-classical shock between ρ_l and $\rho_\alpha^-(\rho_l)$, followed by a classical wave between $\rho_\alpha^-(\rho_l)$ and ρ_r. This is shown in Figure 4.13(a) and

$$\hat\rho = \rho_l, \qquad \check\rho_\alpha = \rho_\alpha^-(\rho_l).$$

(U2) $\rho_l \le \rho^-(\rho_\alpha^\sharp)$ and $\rho_r > \rho_\alpha^+(\rho_l)$ (this requires $\rho_\alpha^+(\rho_l) < \alpha R$ if $V_u < 0$).
Unlike the previous case, here in the moving reference frame $\widetilde{D}(\rho_l) > \widetilde{S}_\alpha(\rho_r)$. The solution is a classical shock from ρ_l to $\rho^+(\rho_r)$ followed by a non-classical shock between $\rho^+(\rho_r)$ and ρ_r, as depicted in Figure 4.13(b). For this, $\rho^+(\rho_r) \ge R$, thus $V_u \ge -f_\alpha(\rho_r)/(R-\rho_r)$ is needed and

$$\hat\rho = \rho^+(\rho_r), \qquad \check\rho_\alpha = \rho_r.$$

(U3) $\rho_l > \rho^-(\rho_\alpha^\sharp)$ and $\rho_r \le \rho_\alpha^\sharp$.
In the moving reference frame, $\widetilde{D}(\rho_l) > \widetilde{S}_\alpha(\rho_r)$, and the solution, depicted in Figure 4.13(c), is a classical wave between ρ_l and $\rho^+(\rho_\alpha^\sharp)$, followed by a non-classical jump between $\rho^+(\rho_\alpha^\sharp)$ to $\rho_\alpha^\sharp$ and a rarefaction wave from $\rho_\alpha^\sharp$ to ρ_r. For this, we need $\rho^+(\rho_\alpha^\sharp) \ge R$, thus $V_u \ge -f_\alpha(\rho_\alpha^\sharp)/(R-\rho_\alpha^\sharp)$. Therefore,

$$\hat\rho = \rho^+(\rho_\alpha^\sharp), \qquad \check\rho_\alpha = \rho_\alpha^\sharp.$$

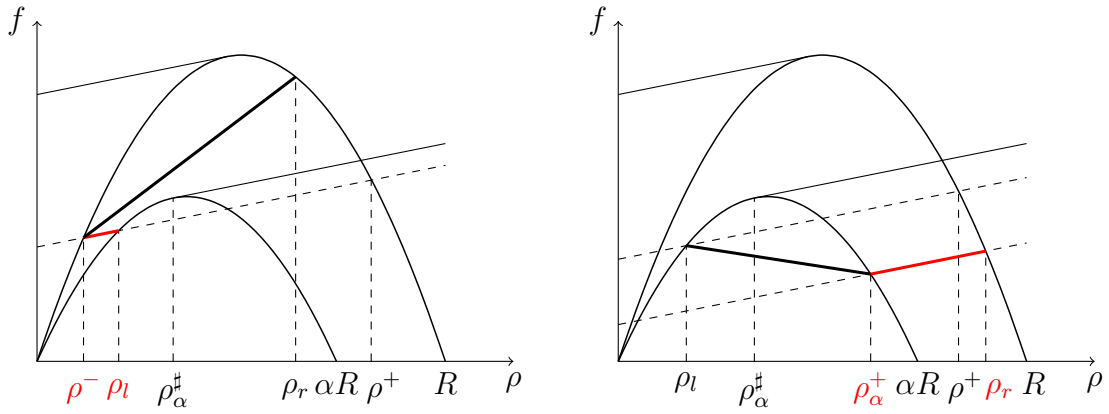

(a) Solution for $\rho_l < \rho_\alpha^\sharp$ and $\rho_r < \rho^+(\rho_l)$

(b) Solution for $\rho_l < \rho_\alpha^\sharp$ and $\rho_r \geq \rho^+(\rho_l)$

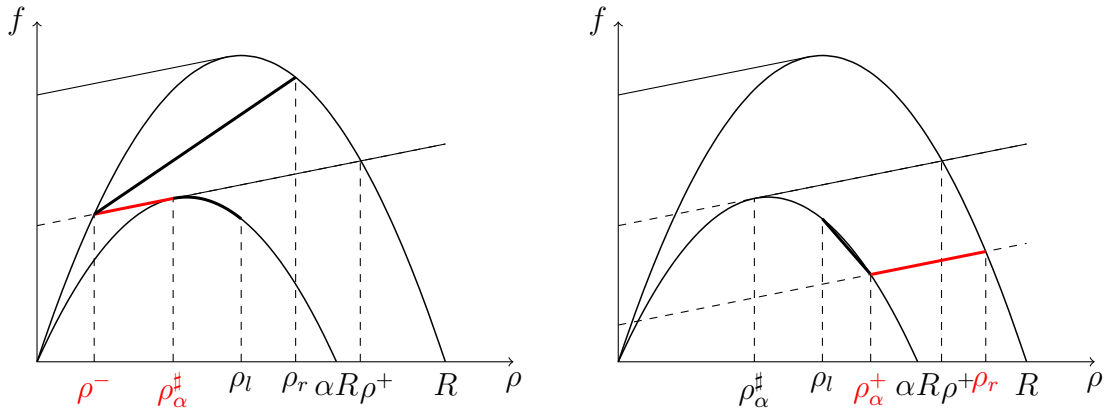

(c) Solution for $\rho_l \geq \rho_\alpha^\sharp$ and $\rho_r < \rho^+(\rho_\alpha^\sharp)$

(d) Solution for $\rho_l \geq \rho_\alpha$ and $\rho_r \geq \tilde{\rho}$

Figure 4.12: Solutions to the Riemann problem at the downstream end-point of the platoon, considering different initial data. The non-classical shock corresponding to the discontinuity in the flux is depicted in red, taken from [124]

(U4) $\rho_l > \rho^-(\rho_\alpha^\sharp)$ and $\rho_r > \rho_\alpha^\sharp$.
In the moving reference frame $\widetilde{D}(\rho_l) > \widetilde{S}_\alpha(\rho_r)$ and we get a classical wave (shock or rarefaction) between ρ_l and $\rho^+(\rho_r)$, followed by non-classical discontinuity between $\rho^+(\rho_r)$ and ρ_r, see Figure 4.13(d). Also here, we need $\rho^+(\rho_r) \geq R$, thus $V_u \geq -f_\alpha(\rho_r)/(R - \rho_r)$. We set

$$\hat{\rho} = \rho^+(\rho_r), \qquad \check{\rho}_\alpha = \rho_r.$$

As in the downstream case, here the solutions $\rho(t,x)$ satisfy the condition

$$\rho(t,x) \in [0,R] \text{ for } x < z_u(t) \quad \text{and} \quad \rho(t,x) \in [0,\alpha R] \text{ for } x > z_u(t).$$

At this point, solutions to any possible case of the Riemann solver are computed and the numerical scheme can be outlined.

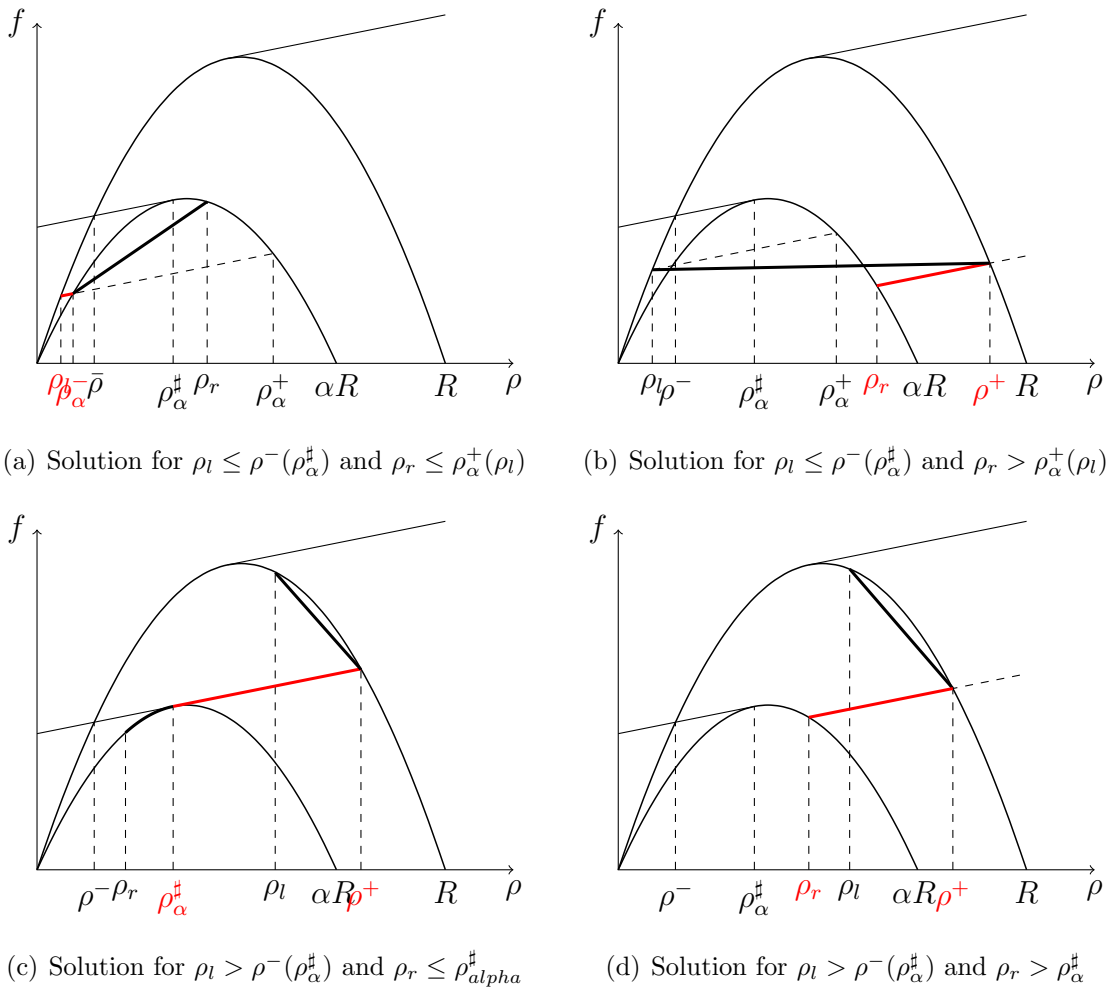

(a) Solution for $\rho_l \leq \rho^-(\rho_\alpha^\sharp)$ and $\rho_r \leq \rho_\alpha^+(\rho_l)$

(b) Solution for $\rho_l \leq \rho^-(\rho_\alpha^\sharp)$ and $\rho_r > \rho_\alpha^+(\rho_l)$

(c) Solution for $\rho_l > \rho^-(\rho_\alpha^\sharp)$ and $\rho_r \leq \rho_{alpha}^\sharp$

(d) Solution for $\rho_l > \rho^-(\rho_\alpha^\sharp)$ and $\rho_r > \rho_\alpha^\sharp$

Figure 4.13: Solutions to the Riemann problem (4.28) for different initial data. The non-classical shock corresponding to the flux discontinuity is depicted in red [124].

Similarly to the numerical scheme presented in [25] for the moving bottleneck problem, in order to approximate the solution of the conservation law (4.19a), a conservative finite volume scheme based on flux discontinuities reconstruction is here presented. First of all, the system is discretized in both time and space, with space and time steps respectively denoted as Δx and Δt. For each cell j in which the space is divided, $x_j = (j - 1/2)\Delta x$ denotes its centers and $x_{j+1/2} = j\Delta x$ its interfaces, for $j \in \mathbb{Z}$. As regards the time, $t^n = n\Delta t$, $n \in \mathbb{N}$, indicates the time mesh.

The initial datum (4.19b) is approximated by the piece-wise constant function given by its average on each discretization cell $C_j = [x_{j-1/2}, x_{j+1/2}[$, i.e.

$$\rho_j^0 = \frac{1}{\Delta x} \int_{x_{j-1/2}}^{x_{j+1/2}} \rho_0(x)dx, \qquad j \in \mathbb{Z}.$$

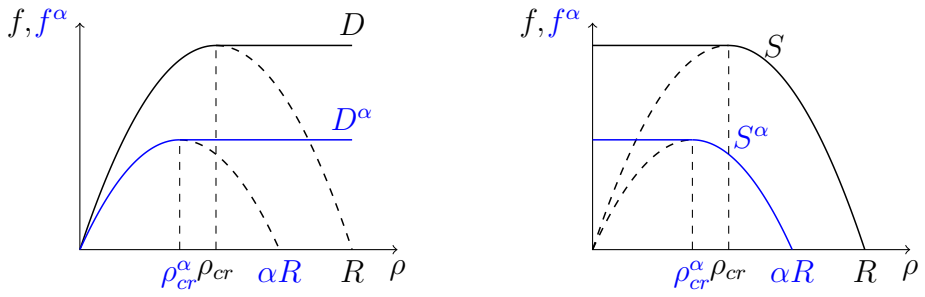

Figure 4.14: Demand and supply considering the normal flow and the reduced flow

At each time step n the density is updated as

$$\rho_j^{n+1} = \rho_j^n - \frac{\Delta t}{\Delta x}\left(F_{j+1/2}^n - F_{j-1/2}^n\right), \qquad j \in \mathbb{Z},$$

Above, $2V\Delta t \leq \Delta x$, to comply with the Courant-Friedrichs-Lewy (CFL) condition. The numerical flux $F_{j+1/2}^n$ is computed as the standard Godunov's flux [55] in the cells located away from the discontinuities locations z_u^n and z_d^n. By assuming a concave flux functions as (4.21)–(4.22), the supply-demand method [36] results to be equivalent, then, if $z_u^n \in C_{j_u}$ and $z_d^n \in C_{j_d}$ for some $j_u, j_d \in \mathbb{Z}$, the demand and the supply functions are defined as

$$D(\rho_j^n) = \begin{cases} f(\rho_j^n) & \text{if } \rho_j^n < \rho_{cr}, \\ f^{max} & \text{if } \rho_j^n \geq \rho_{cr}, \end{cases} \qquad S(\rho_j^n) = \begin{cases} f^{max} & \text{if } \rho_j^n < \rho_{cr}, \\ f(\rho_j^n) & \text{if } \rho_j^n \geq \rho_{cr}, \end{cases}$$

for $j < j_u$ or $j > j_d$, i.e. locations in which the platoon is not present. On the other hand, for $j_u < j < j_d$, the demand and supply functions are computed considering the reduced flow:

$$D^\alpha(\rho_j^n) = \begin{cases} f_\alpha(\rho_j^n) & \text{if } \rho_j^n < \rho_{cr}^\alpha, \\ f_\alpha^{max} & \text{if } \rho_j^n \geq \rho_{cr}^\alpha, \end{cases} \qquad S^\alpha(\rho_j^n) = \begin{cases} f_\alpha^{max} & \text{if } \rho_j^n < \rho_{cr}^\alpha, \\ f_\alpha(\rho_j^n) & \text{if } \rho_j^n \geq \rho_{cr}^\alpha. \end{cases}$$

Demand ans supplies are depicted in Fig. 4.14.

Therefore, the numerical fluxes $F_{j+1/2}^n$ are computed as

$$\begin{aligned} F_{j+1/2}^n &= \min\left\{D(\rho_{j-1}^n), S(\rho_j^n)\right\} && \text{for } j \leq j_u - 2 \text{ and } j \geq j_d + 1, \\ F_{j+1/2}^n &= \min\left\{D^\alpha(\rho_{j-1}^n), S^\alpha(\rho_j^n)\right\} && \text{for } j \geq j_u + 1 \text{ and } j \leq j_d - 2, \end{aligned}$$

The interfaces $x_{j_u \pm 1/2}$ and $x_{j_d \pm 1/2}$ of the cells where the discontinuities lie, need a special treatment. As before, the procedures will be separated treated for the front and the back-end of the platoon.

- **Front-end** The position of the downstream endpoint of the platoon is updated as

$$z_d^{n+1} = z_d^n + \min\{V_d^n, v(\rho_{j_d+1}^n)\}\Delta t,$$

The trajectory of the downstream endpoint could be approximated in a more detailed way following [24, Section 3.2], see also [20].

A discontinuity is expected to appear in cell C_{j_d}, motivated by presence of the flux discontinuity introduced by the presence of the platoon endpoint. This corresponds to the situation described by the Riemann problem (4.27), where $\rho_l = \rho_{j_d-1}^n$ and $\rho_r = \rho_{j_d+1}^n$. Inspired by [18, 24], the density $\rho_{j_d}^n$ in the cell C_{j_d} is replaced by a convex combination of the values $\hat{\rho}_\alpha$ and $\check{\rho}$ corresponding to ρ_l and ρ_r, computed above. More precisely, d_{j_d} is computed such that

$$\hat{\rho}_\alpha\, d_{j_d} + \check{\rho}\left(1 - d_{j_d}\right) = \rho_{j_d}^n, \qquad \text{i.e.} \qquad d_{j_d} = \frac{\rho_{j_d}^n - \check{\rho}}{\hat{\rho}_\alpha - \check{\rho}}.$$

Consequently, the reconstructed discontinuity location is at position $\bar{x}_{j_d} = x_{j_d-1/2} + d_{j_d}\Delta x$. This guarantees the conservation.

At this point, two possible scenarios may occur. In the first one, $d_{j_d} \in [0, 1]$, and reconstruction of the numerical flux at the interface $x_{j_d+1/2}$ can be easily done as

$$\Delta t F_{j_d+1/2}^n = \min\left\{\Delta t_{j_d}, \Delta t\right\} f(\check{\rho}) + \max\left\{\Delta t - \Delta t_{j_d}, 0\right\} f_\alpha(\hat{\rho}_\alpha) \tag{4.29}$$

where

$$\Delta t_{j_d} = \frac{1 - d_{j_d}}{\min\{V_d^n, v(\rho_{j_d+1}^n)\}}\,\Delta x$$

indicates the time needed by the discontinuity to reach the interface $x_{j_d+1/2}$ traveling at its speed v_d.

The numerical flux at $x = x_{j_d-1/2}$ is computed as

$$F_{j_d-1/2}^n = \min\left\{D^\alpha(\rho_{j_d-1}^n), S^\alpha(\hat{\rho}_\alpha)\right\}. \tag{4.30}$$

Figure 4.15 depicts a scheme of the reconstruction.

On the other hand, if $\rho_{j_d}^n \notin [\min\{\hat{\rho}_\alpha, \check{\rho}\}, \max\{\hat{\rho}_\alpha, \check{\rho}\}]$, then $d_{j_d} \notin [0, 1]$. Indeed, due to the approximation $\rho_l = \rho_{j_d-1}^k$ and $\rho_r = \rho_{j_d+1}^k$, the discontinuity $\bar{x}_{j_d} = x_{j_d-1/2} + d_{j_d}\Delta x$ does not in general coincide with z_d^n, the actual position of the front-end of the platoon. The traveling speed is anyway the same. In some situations it may happen that z_d^n and $\bar{x}_{j_d}$ are not located in the same cell, as depicted in Fig.4.16.

When this occurs, the following strategy is deployed

– if $\left|\rho^n_{j_d} - \hat{\rho}_\alpha\right| < \left|\rho^n_{j_d} - \check{\rho}\right|$, i.e. $d_{j_d} > 1$, we set $\hat{\rho}'_\alpha = \rho^n_{j_d}$ and $\check{\rho}' = \check{\rho}$, which corresponds to $d'_{j_d} = 1$; the corresponding numerical fluxes are then computed as

$$F^n_{j_d-1/2} = \min\left\{D^\alpha(\rho^n_{j_d-1}), S^\alpha(\rho^n_{j_d})\right\},$$
$$F^n_{j_d+1/2} = \min\left\{D^\alpha(\rho^n_{j_d}), S(\rho^n_{j_d+1})\right\};$$

– if $\left|\rho^n_{j_d} - \hat{\rho}_\alpha\right| > \left|\rho^n_{j_d} - \check{\rho}\right|$, i.e. $d_{j_d} < 0$, we take $\hat{\rho}'_\alpha = \hat{\rho}_\alpha$ and $\check{\rho}' = \rho^n_{j_d}$; the numerical fluxes are then computed as

$$F^n_{j_d-1/2} = \min\left\{D^\alpha(\rho^n_{j_d-1}), S^\alpha(\hat{\rho}_\alpha)\right\},$$
$$F^n_{j_d+1/2} = \min\left\{D(\rho^n_{j_d}), S(\rho^n_{j_d+1})\right\};$$

this accounts for the direction of propagation of the non-classical discontinuity and corresponds to (4.29)–(4.30) with $\hat{\rho}'_\alpha, \check{\rho}'$ in place of $\hat{\rho}_\alpha, \check{\rho}$.

- **Back-end** The position of the upstream endpoint of the platoon is updated as

$$z^{n+1}_u = z^n_u + V^n_u \Delta t,$$

Above, $V^n_{u,d} := \dfrac{1}{\Delta t}\int_{t^n}^{t^{n+1}} V_{u,d}(t)dt$. The same method applied to the downstream point of the platoon is here arranged for the upstream one. The cell of interest is here C_{j_u}, corresponding to the cell where the discontinuity is, and the corresponding Riemann problem is the one of Eq. (4.28).

Here $\rho_l = \rho^n_{j_u-1}$ and $\rho_r = \rho^n_{j_u+1}$ and

$$d_{j_u} = \frac{\rho^n_{j_u} - \check{\rho}_\alpha}{\hat{\rho} - \check{\rho}_\alpha},$$

where $\hat{\rho}$, $\check{\rho}_\alpha$ have been computed above.

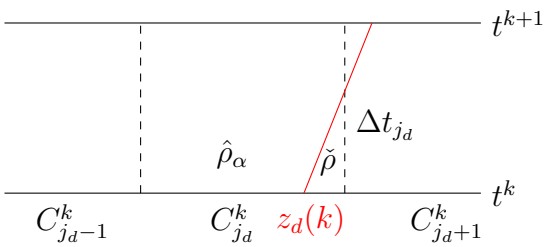

Figure 4.15: Representation of the reconstruction at the downstream endpoint discontinuity.

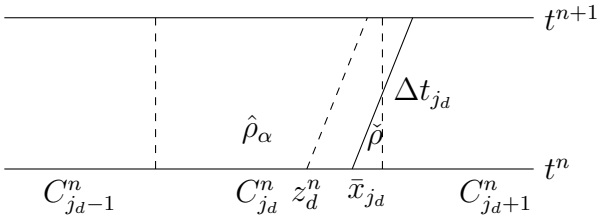

Figure 4.16: Representation of the reconstruction algorithm (4.29)–(4.30) at the downstream endpoint of the platoon.

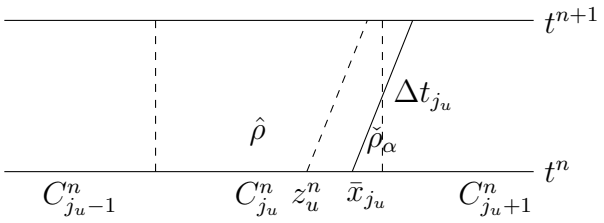

(a) Case $V^n_u \geq 0$.

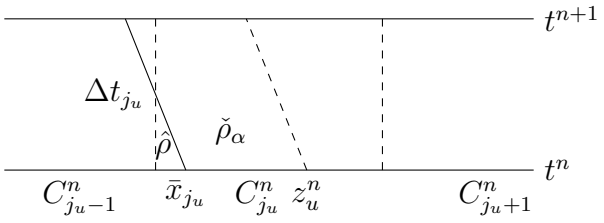

(b) Case $V^n_u < 0$.

Figure 4.17: Representation of the reconstruction algorithm at the upstream endpoint of the platoon.

If $d_{j_u} \in [0,1]$ and $V_u^n \geq 0$, the numerical flux at the interface $x_{j_u+1/2}$ is simply reconstructed as

$$\Delta t F^n_{j_u+1/2} = \min\left\{\Delta t_{j_u}, \Delta t\right\} f_\alpha(\check{\rho}_\alpha) + \max\left\{\Delta t - \Delta t_{j_u}, 0\right\} f(\hat{\rho}), \qquad (4.31)$$

where

$$\Delta t_{j_u} = \frac{1 - d_{j_u}}{V_u^n}\,\Delta x,$$

and

$$F^n_{j_u-1/2} = \min\left\{D(\rho^n_{j_u-1}), S(\hat{\rho})\right\},$$

This situation is depicted in Fig. 4.17(a)

As previously remarked, the upstream end-point of the platoon can also take negative values of the speed if vehicles join the platoon, moving its back-end backwards. When this occurs, $V_u^n < 0$ and the flux reconstruction must be done at the previous interface $x = x_{j_u-1/2}$. In this situation:

$$\Delta t F^n_{j_u-1/2} = \min\left\{\Delta t_{j_u}, \Delta t\right\} f(\hat{\rho}) + \max\left\{\Delta t - \Delta t_{j_u}, 0\right\} f_\alpha(\check{\rho}_\alpha),$$

where

$$\Delta t_{j_u} = -\frac{d_{j_u}}{V_u^n}\Delta x$$

is the time for the discontinuity to reach the interface $x_{j_u-1/2}$. In addition,

$$F^n_{j_u+1/2} = \min\left\{D^\alpha(\check{\rho}_\alpha), S^\alpha(\rho^n_{j_u+1})\right\},$$

as depicted in Figure 4.17(b).

As for the front of the platoon, it may happen that $d_{j_u} \notin [0,1]$,and the method has to be adapted as follows:

- if $\left|\rho^k_{j_u} - \hat{\rho}\right| < \left|\rho^k_{j_u} - \check{\rho}_\alpha\right|$, i.e. $d_{j_u} > 1$, we set $\hat{\rho}' = \rho^k_{j_u}$ and $\check{\rho}'_\alpha = \check{\rho}_\alpha$ and the numerical fluxes become

$$F^k_{j_u-1/2} = \min\left\{D(\rho^k_{j_u-1}), S(\rho^k_{j_u})\right\},$$
$$F^k_{j_u+1/2} = \min\left\{D(\rho^k_{j_u}), S^\alpha(\rho^k_{j_u+1})\right\};$$

- if $\left|\rho^k_{j_u} - \hat{\rho}\right| > \left|\rho^k_{j_u} - \check{\rho}_\alpha\right|$, i.e. $d_{j_u} < 0$, we take $\hat{\rho}' = \hat{\rho}$ and $\check{\rho}'_\alpha = \rho^k_{j_u}$; the numerical fluxes are then computed as

$$F^k_{j_u-1/2} = \min\left\{D(\rho^k_{j_u-1}), S(\hat{\rho})\right\},$$
$$F^k_{j_u+1/2} = \min\left\{D^\alpha(\rho^k_{j_u}), S^\alpha(\rho^k_{j_u+1})\right\}.$$

At this point the numerical fluxes between all the cells have been defined.

Simulations

In order to assess the validity of the proposed approach, the different cases are simulated. Since the aim is to assess the proposed numerical method, the front and the back end of the platoon will be first separately simulated.
For all the simulation the discretization space step is $\Delta x = 0.001$.
The front-end of the platoon is simulated as first.
In the following, the initial position of the downstream end-point of the platoon is $z_d^0 = 0.5$, the maximum speed is $V = 1$ and the maximum density $R = 1$. The occupancy parameter is $\alpha = 0.5$ and the initial speed of the point is $V_d = 0.3$, which gives $\rho_\alpha^\sharp = 0.1750$. A simulation is done for each possible type of initial data detailed in the Riemann solver in Section 4.2.1.
Case d1) The Riemann type initial datum is

$$\rho_0(x) = \begin{cases} 0.15 & \text{if } x < 0.5, \\ 0.4 & \text{if } x \geq 0.5. \end{cases}$$

The solutions $\hat{\rho}_\alpha$ and $\check{\rho}$ are computed as explained in Section 4.2.1, case **(D1)**, and $\hat{\rho}_\alpha = \rho_l = 0.15$ and $\check{\rho} = 0.1$. In Figure 4.18(a) the solution composed by a non-classical shock followed by a classical one is shown. The star represents the position of the front of the platoon.

Case d2) We consider a Riemann type initial datum

$$\rho_0(x) = \begin{cases} 0.15 & \text{if } x < 0.5, \\ 0.65 & \text{if } x \geq 0.5. \end{cases}$$

Starting from this type of initial data, $\check{\rho} = 0.65$ and $\hat{\rho}_\alpha = \rho_l = 0.29$. The solution is classical shock followed by a non-classical one, as shown in Figure 4.18(b), corresponding to the case **(D2)**.

Case d3) The initial density is now

$$\rho_0(x) = \begin{cases} 0.4 & \text{if } x < 0.5, \\ 0.5 & \text{if } x \geq 0.5. \end{cases}$$

Figure 4.18(c) reports the trend of the solution, computed as detailed in case **(D3)**. It results that $\check{\rho} = 0.1025$ and $\hat{\rho}_\alpha = \rho_\alpha^\sharp = 0.1750$ and the solution is a rarefaction wave between ρ_l and $\hat{\rho}_\alpha$, followed by a non-classical and a classical shock.

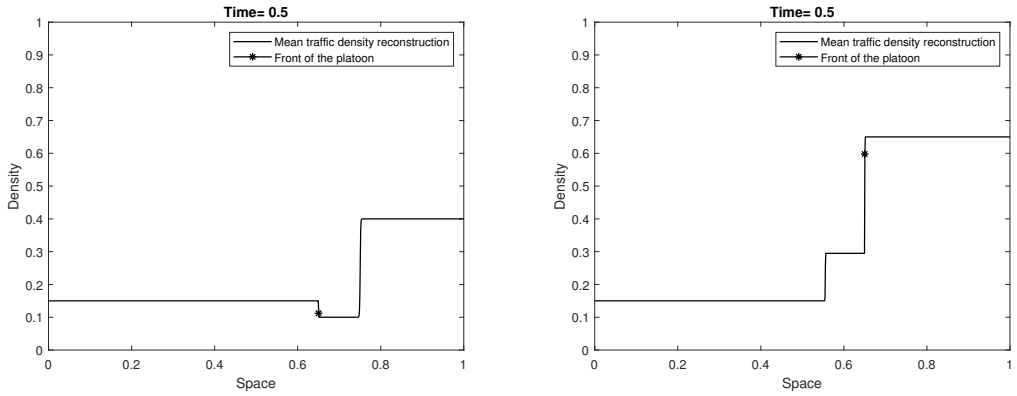

(a) case d1

(b) case d2

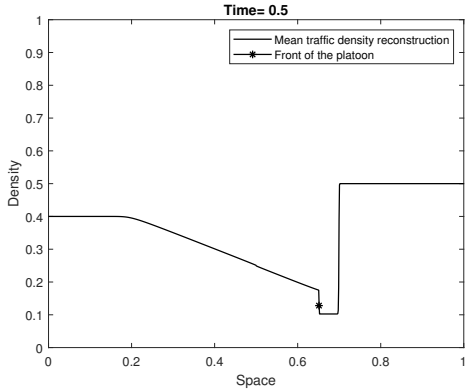

(c) case d3

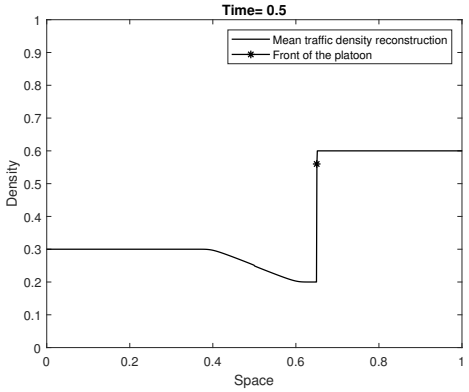

(d) case d4

Figure 4.18: Density profile at the front of the platoon at time $t = 0.5$ for the different type of initial data.

Case d4) The initial density considered in this last case is

$$\rho_0(x) = \begin{cases} 0.3 & \text{if } x < 0.5, \\ 0.6 & \text{if } x \geq 0.5. \end{cases}$$

A rarefaction wave between ρ_l and $\hat{\rho} = 0.2$ appears, and then a non-classical shock to $\check{\rho} = \rho_r$, as shown in Figure 4.18(d).

The back-end of the platoon is now simulated.
In the following, $z_u^0 = 0.5$, $V = 1$, $R = 1$, $\alpha = 0.5$, $V_u = 0.2$, corresponding to $\rho_\alpha^\sharp = 0.2$.

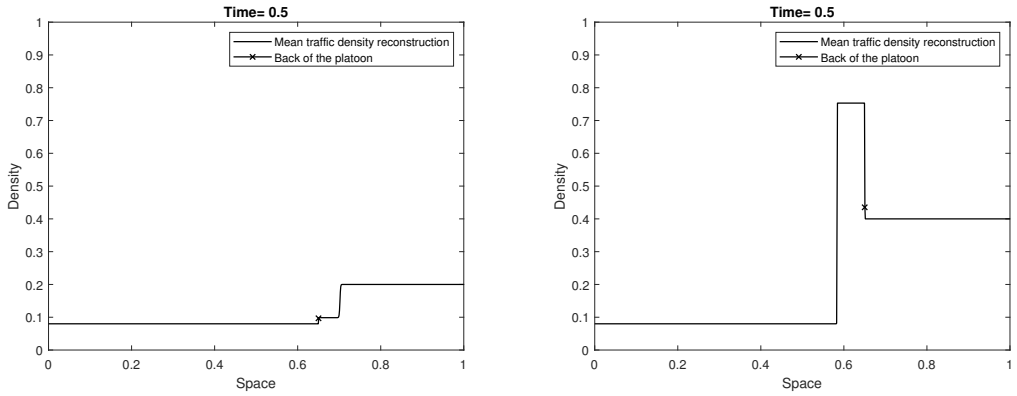

(a) case u1

(b) case u2

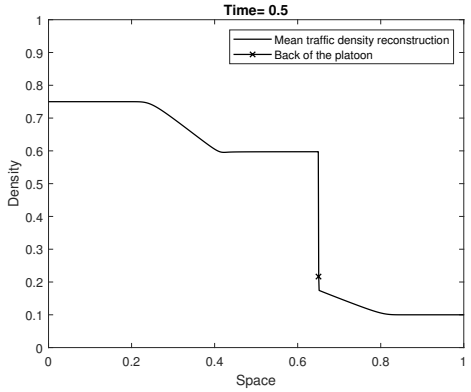

(c) case u3

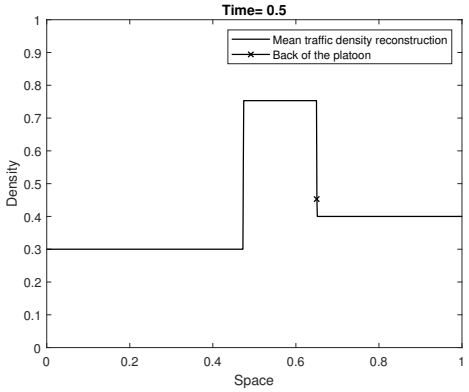

(d) case u4

Figure 4.19: Density profile at the back-end of the platoon at time $t = 0.5$ for different initial data.

Case u1) The considered Riemann type initial datum is

$$\rho_0(x) = \begin{cases} 0.08 & \text{if } x < 0.5, \\ 0.2 & \text{if } x \geq 0.5. \end{cases}$$

The solutions computed as in case **(U1)** are $\hat{\rho} = \rho_l = 0.08$ and $\check{\rho}_\alpha = 0.0942$. A non-classical shock followed by the classical one appears, as shown in Figure 4.19(a).

Case u2) The initial data is

$$\rho_0(x) = \begin{cases} 0.08 & \text{if } x < 0.5, \\ 0.4 & \text{if } x \geq 0.5. \end{cases}$$

According to case **(U2)**, $\hat{\rho} = 0.8$ and $\check{\rho}_\alpha = \rho_r = 0.4$, and the solution is reported in Figure 4.19(b).

Case u3) The initial datum now is:

$$\rho_0(x) = \begin{cases} 0.75 & \text{if } x < 0.5, \\ 0.1 & \text{if } x \geq 0.5. \end{cases}$$

The solution is depicted in Figure 4.19(c).A rarefaction wave between the value ρ_l and $\hat{\rho} = 0.6828$, followed by the non-classical shock between $\hat{\rho}$ and $\check{\rho}_\alpha = \rho_\alpha^\sharp$, and a rarefaction wave to ρ_r. Values are computed as in case **(U3)**.

Case u4)

An initial datum :

$$\rho_0(x) = \begin{cases} 0.3 & \text{if } x < 0.5, \\ 0.4 & \text{if } x \geq 0.5. \end{cases}$$

Figure 4.19(d) illustrates the solution, computed as in case **(U4)**. As expected, a shock wave between ρ_l and $\hat{\rho} = 0.8$, followed by the non-classical shock to $\check{\rho}_\alpha = \rho_r$ appears.

At this point the full platoon with its initial and final point is simulated. As an example, the following initial data is considered:

$$\rho_0(x) = \begin{cases} 0.3 & \text{if } x < 0.2, \\ 0.4 & \text{if } 0.2 \leq x < 0.5, \\ 0.5 & \text{if } 0.5 \leq x < 0.8, \\ 0.95 & \text{if } x \geq 0.8, \end{cases} \qquad z_u^0 = 0.2, \qquad z_d^0 = 0.5. \tag{4.32}$$

The initial length of the platoon is chosen equal to $L = 0.3$, the downstream point of the platoon moves with a speed $V_d = 0.3$ while the back-end point has a lower speed $V_u = 0.2$. The reduction rate α is 0.5. The back-end point of the platoon is the one of case **(U4)** (see also Case u4 in the previous simulations). A shock is then expected to appear with a value of the density equal to the computed $\hat{\rho} = 0.8$. Concerning the downstream endpoint of the platoon, the situation of case **(D3)**, in which a rarefaction wave is followed by a shock appear. At some point of the simulation the platoon reaches the downstream high density region, the front-end point of the platoon slows down adapting its speed to the downstream traffic. Since the speeds of the front-end and the back-end points of the platoon

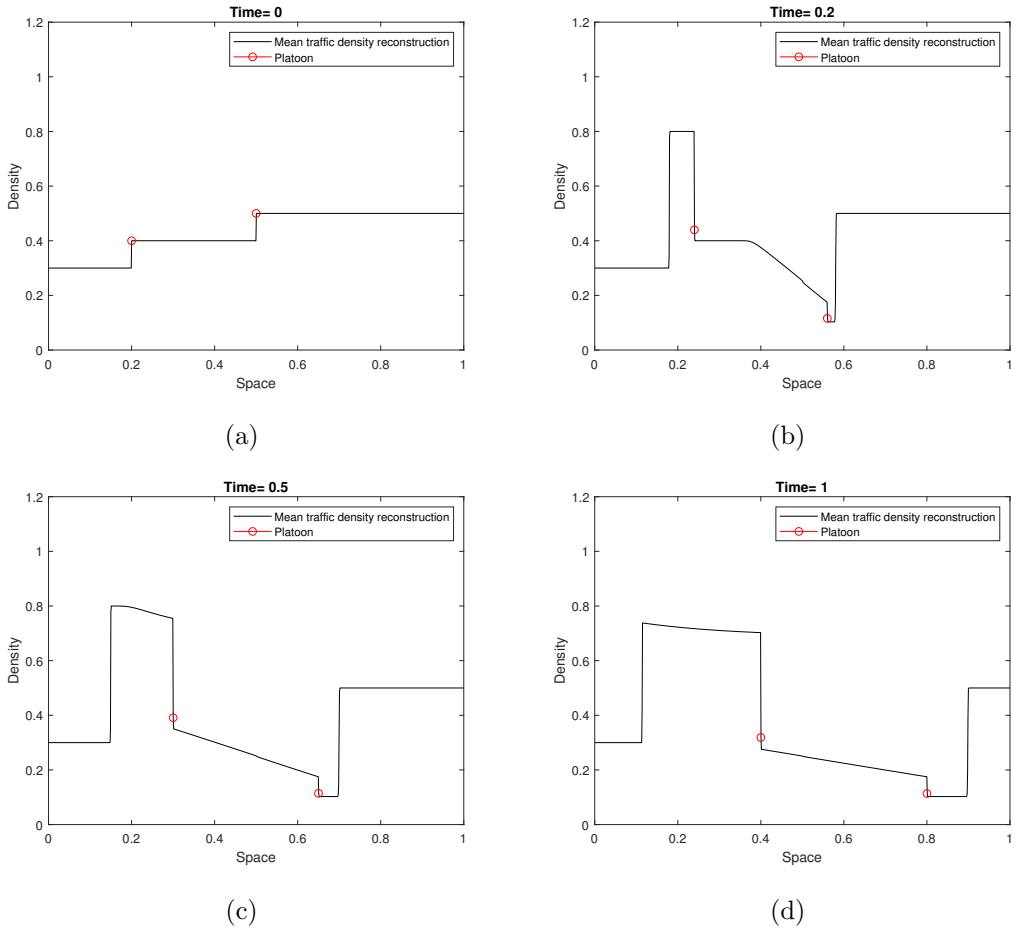

Figure 4.20: Density profile at different times corresponding to the initial condition (4.32).

are chosen to be different, the length of the platoon varies during the simulation. Figure 4.20 depicts the simulation results at different time of the simulation, while Figure 4.21 shows the space-time evolution of the solution.

4.2.2 Traffic Control via Platoons of Intelligent Vehicles for Saving Fuel Consumption in Freeway Systems

The platoon model developed and presented in Section 4.2.1 is here adopted to describe the traffic flow and a controller aiming at reducing congestion and fuel consumption is applied. This problem was solved in [122]. Specifically, the platoon is controlled in order to influence the surrounding traffic and to reduce the fuel consumption of the overall traffic flow. The approach is similar to the one adopted in section 3.1.2, with the additional degree of freedom added by considering a platoon with variable length.

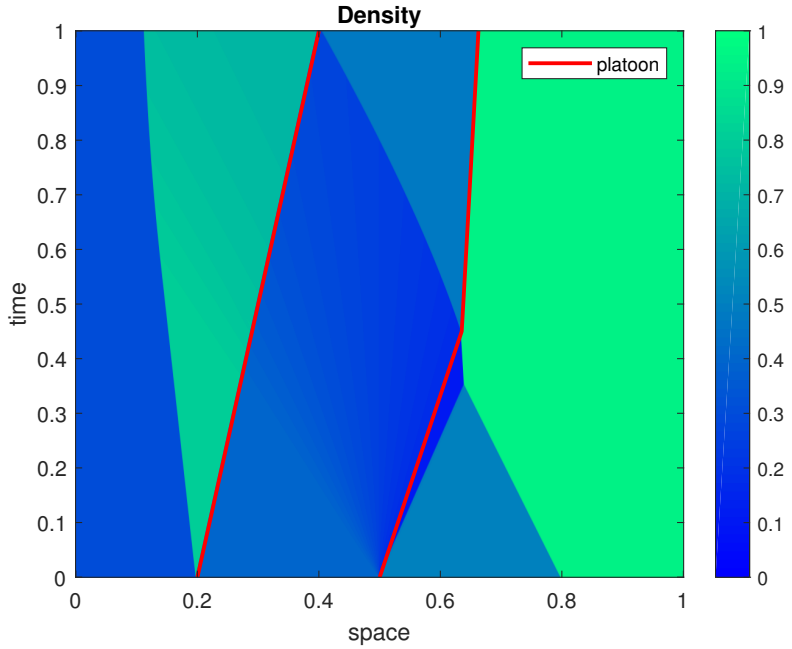

(a) Absolute density

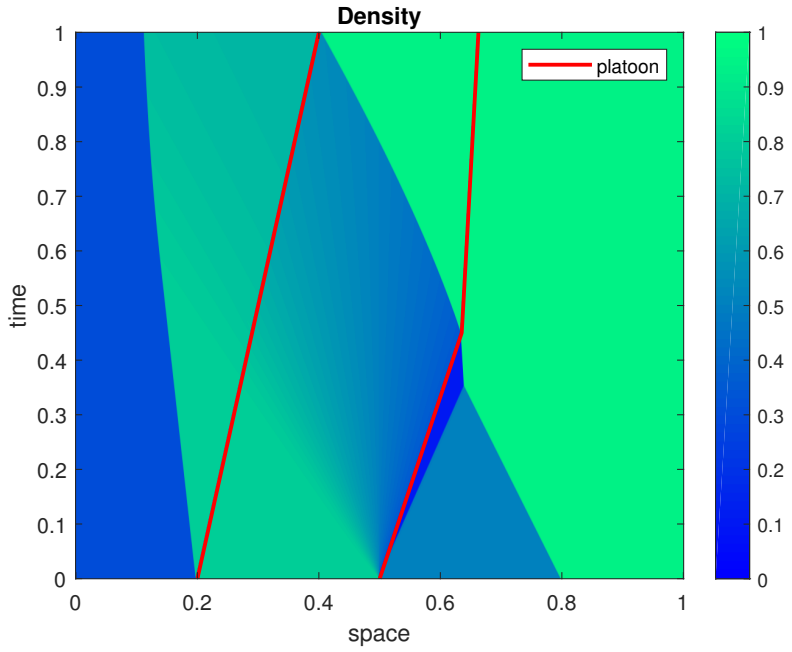

(b) Relative density

Figure 4.21: Space-time evolution of the solution to (4.19) corresponding to the initial datum (4.32): plot (a) displays the absolute density values $\rho(t, x)$ everywhere, plot (b) accounts for the relative density $\rho(t, x)/\alpha R$ at the platoon location, accounting for the reduced road capacity.

The aim is then to design a control scheme that optimizes the fuel consumption, by controlling the maximum speed of the downstream and upstream end-points of the platoon, V_d and V_u respectively. This means controlling both the speed and the length of the platoon, thanks to Eq. (4.26).
The fuel consumption of the overall traffic flow is computed by means of the model presented in [125, 128], already used in section 3.1.2. It was derived considering that variations in vehicles fuel consumption are related to their mean speed and a curve averaged on the characteristics of different cars was computed and approximated by a sixth order polynomial $K(v)$, see Eq. (3.6). The function $K(v)$ was re-parametrized in terms of density, by obtaining $\mathcal{K}(\rho)$, and the total fuel consumption was then indicated as

$$\mathcal{F}(\rho) = \rho\mathcal{K}(\rho).$$

The control problem is here again solved by means of a MPC approach, where V_d and V_u are assumed as control variables. The vector of control inputs is here indicated as $u = [V_d, V_u]$. K_p represents the number of time steps of the prediction horizon for the MPC. At each fixed time step k, given the current initial state $\underline{\rho}(k)$, the optimal control sequence $\underline{u}(h) = [\underline{V_d}(h)\, \underline{V_u}(h)]$, $h = k, \ldots, k + K_p$, minimizing the objective function is computed by solving the optimization problem over the prediction horizon. The control $\underline{u}$ is constrained to be piece-wise constant on subintervals of size $\Delta t K_p/\ell$, for some $\ell \in \mathbb{N}$ with the aim of reducing the computational complexity deriving from the non-linear problem optimization. At $t = k\Delta t$, only the first input $\underline{u}(k) = [\underline{V_d}(k)\, \underline{V_u}(k)]$ of the obtained sequence is actually applied to the real system for the time interval $[t, t + \Delta t K_p/\ell]$. At the following iteration, based on the new system information, the optimization is repeated shifting the horizon. Since the model is non-linear, the problem can be solved only numerically, by means of iterative optimization algorithms that ask at each time step to compute approximate solutions of system (4.19). At the k-th iteration, the optimal input speeds are computed as solution of the following constrained multi-variable optimization problem

$$\min_{\underline{u}} \sum_{h=k}^{k+K_p} \sum_{i=1}^{N} \mathcal{F}(\rho_i(h))\Delta x \Delta t, \tag{4.33}$$

subject to the model dynamics (4.19), (4.25), (4.24) and to the following constraints

$$L_{min} \leq L(h) \leq L_{max}, \tag{4.34a}$$

$$V_d^{min} \leq V_d(h) \leq V^{max}, \tag{4.34b}$$

$$|V_d(h) - V_u(h)| \leq c. \tag{4.34c}$$

for $h = k, ..., k + K_p$.
The first constraint (4.34a) is needed in order to limit the minimum and the maximum length that the platoon may reach. The value of L_{min} is strictly related to safety distance considerations.

The upper limit,L_{max}, has to be decided based on fuel efficiency evaluations of vehicles composing the platoon. Specifically, an excessive distancing between vehicles in the platoon would reduce the advantage for them to stay in the formation. Indeed, especially for trucks, traveling close to each other, reduces the aerodynamic drag and so the fuel consumption.

Constraint (4.34b) prevents the platoon to assume speeds that would be too low, and so dangerous, on highways. The last constraint expressed by Eq. (4.34c) limits the rate at which the platoon can change its length. Here, c is a suitable threshold to be chosen to avoid undesired accordion effects in the variation of the length of the platoon. The parameter c has to be identified based on several conditions, as the type of the highway (number of lanes, slope, etc.) and the type of vehicles traveling in the platoon, as cars, trucks etc.

Simulation Results

The control scheme presented in Section 4.2.2 is assessed in simulations to prove the validity of the approach. The simulated scenario consists in a highway stretch without any on-ramps or off-ramps. It is divided in $N = 200$ cells, each of them of length 250 $[m]$. In each segment the traffic fundamental diagram is the quadratic one, with maximum speed $V = 140$ $[km/h]$, maximum density $R = 400$ $[veh/km]$ and capacity $f^{max} = 14000$ $[veh/h]$. To comply with the CFL condition, the sampling time is $\Delta t = 5.76$ $[sec]$ and the scenario is simulated for a total time interval of one hour. The simulated platoon has initial length L=3 $[km]$ and at the beginning of the simulation is located at position $z_d(t_0) = 4$ $[km]$. Its initial speed are $v_d(t_0) = v_u(t_0) = 80$ $[km/h]$, while the capacity is reduced of a factor $\alpha = 0.6$. The arriving demand, the inflow, is equal to the capacity f^{max} for the first half of the simulation, while it is zero for the second half. As in section 3.1.2, the flow allowed to exit from the last cell of the stretch is half of the capacity, with the aim of simulating the presence of a fixed temporary bottleneck inducing congestion at the end of the highway. The prediction horizon for the MPC is 40 time steps but, in order to reduce the computational burden deriving from the solution of the non-linear optimization problem, each value of the speed is kept constant for 5 time steps. For the constraints of Eq. (4.34), the platoon minimal and maximum

allowable lengths are $L_{min} = 2$ $[km]$ and $L_{max} = 4$ $[km]$, $V_d^{min} = 40$ $[km/h]$, and $c = 30$ $[km/h]$. To solve the non-linear optimization, the `fmincon` function of the MATLAB optimization toolbox is used.

In Fig. 4.22, the spatio-temporal evolution of the density is reported, both for the case with no applied control and for the case with the application of the proposed MPC control. In the no control situation (Fig. 4.22(a)), all the vehicles travel keeping their maximum allowable speed until they reach the congestion due to the presence of the bottleneck. At this point, the speed of the flow drops down to adapt to the high density value speed. This situation causes an high fuel consumption, since vehicles travel always either at very high or very low speed, which are the worst situations in terms of fuel consumption, as highlighted by the adopted fuel consumption model.

In Fig. 4.22(b) the proposed optimal control is applied. It acts by slowing down the platoon and modifying its length in order to prevent vehicles to travel too fast towards the congestion. This prevents vehicles to abruptly brake when they reach the high congestion zone. In this way, the traffic in the surroundings of the platoon is harmonized and cars show a moderate speed that is beneficial to reduce the consumption of fuel and then the emissions.

In the last part of the simulation, the platoon enters the area with high congestion and it has to adapt its speed to the downstream traffic, that becomes no controllable anymore.

The optimal speeds computed by the controller and applied to the platoon and its consequent length are reported in Fig. 4.23.

The value of the TFC obtained with this control strategy is reported in Table 4.3. This latter shows a reduction of the 2.6% by applying the proposed approach, leading the fuel consumption of the overall traffic flow from 27629 liters to 26903 liters, that represents a saving of 726 liters of fuel. Although at a first glance this reduction could appear small, it represents a significant reduction of emissions, that is beneficial for the environment and for people health. It is important to consider that the improvement is obtained by controlling only one platoon but, considering the widespread of CAVs, scenarios with several platoons of CAVs are realistic to be considered. Moreover, this control can be applied without adding any additional infrastructure and, therefore, at low cost. Several platoons of vehicles could then be formed and controlled to increase the effectiveness of the control. Moreover, in the simulation scenario here presented individual vehicles traveling in the platoon are not specifically considered. Indeed, the original contribution of this work is

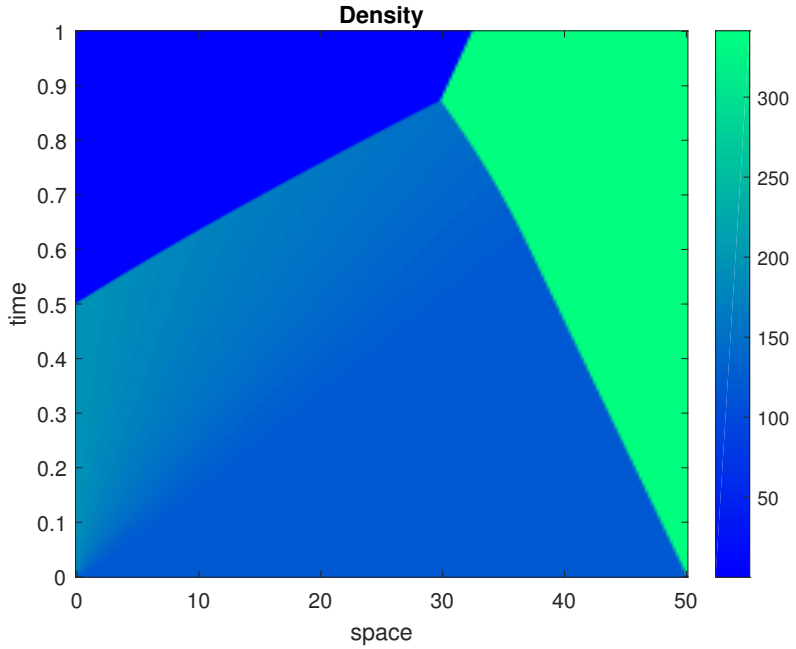

(a) No control case

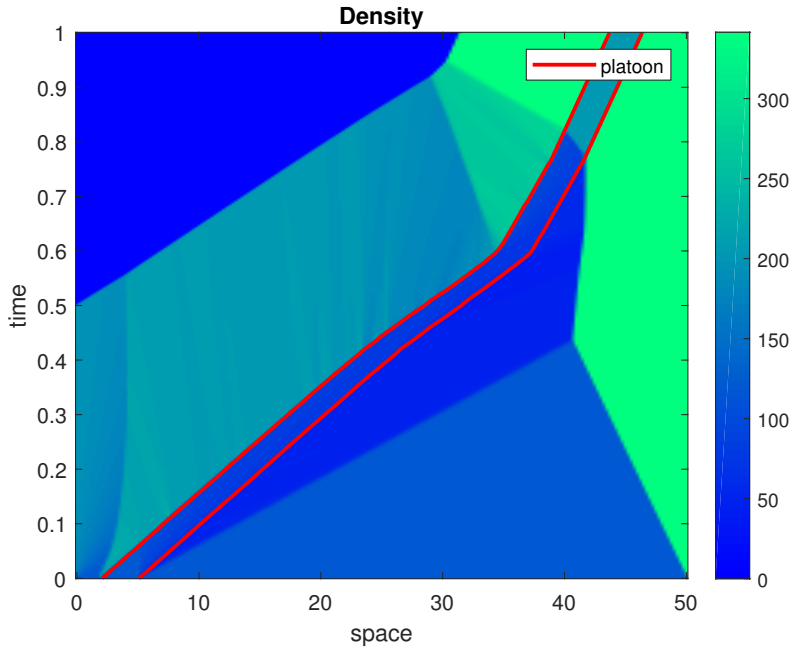

(b) Platoon length

Figure 4.22: Evolution of the density in time and space in the uncontrolled and controlled scenario.

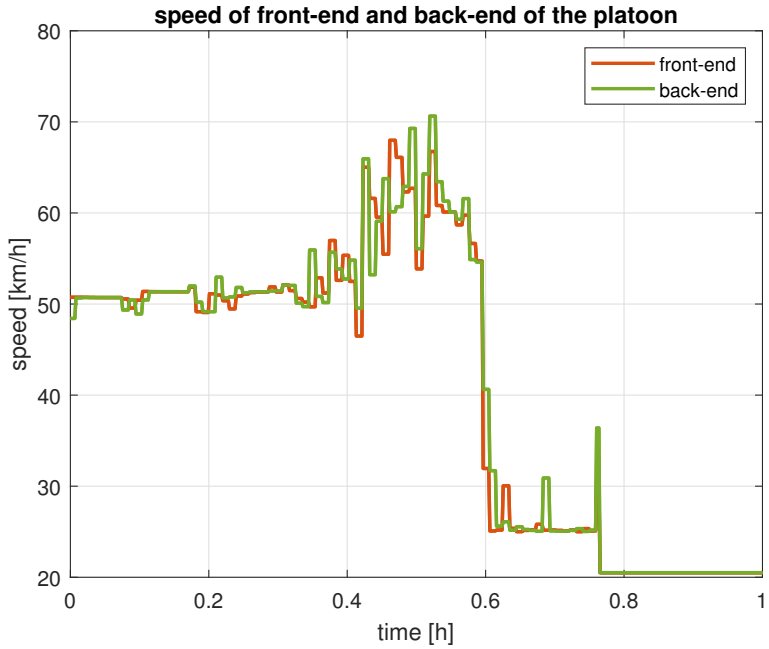

(a) Control speed

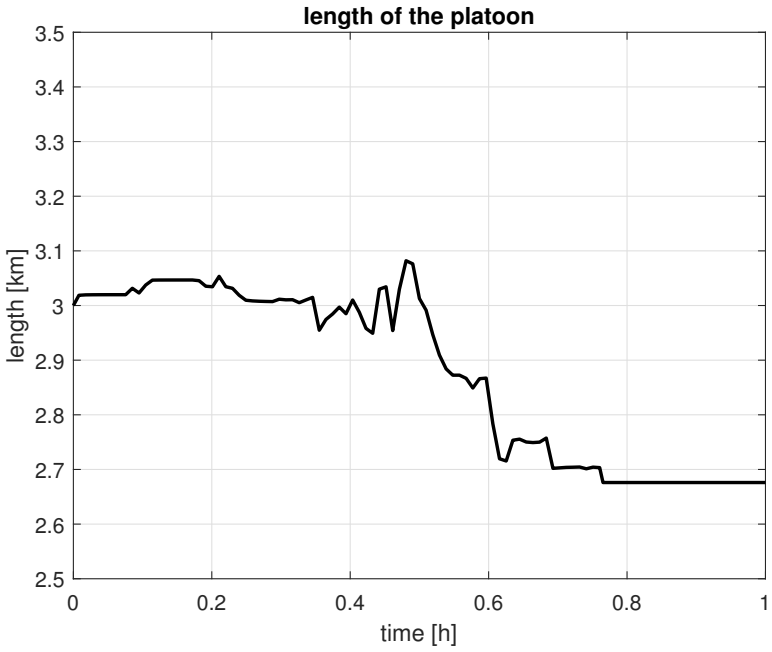

(b) Platoon length

Figure 4.23: Speed of the front-end and back-end of the platoon and length varying in time.

Table 4.3: Comparison between cost functionals.

	TFC	reduction %
No control	2.7629 e+04	0 %
MB control	2.6988 e+04	2.29 %
Platoon control	2.6903 e+04	2.63 %

related to macroscopic traffic control, while the platoon is here conceived as an actuator. The proposed control has to be considered as a two levels control. An upper level computes an optimal speed and length for the platoon, considering proper constraints, by optimizing a cost function related with the bulk traffic flow. Then a lower level will receive as inputs the optimal speed and length of the platoon and, by applying a suitable spacing policy, it adapts the platoon characteristics. Here the platoon is seen as an actuator for the macroscopic traffic control action, and to this aim also non-traditional spacing policy could be applied.

As single vehicles in the platoon are concerned, a reduction in the consumed fuel [152] can appear, since a more harmonized driving behaviour would emerge and the aerodynamics of vehicles in the platoon is improved at reduced inter-distances. In addition to this, this aspect would be more accentuated if the controlled vehicles traveling in the platoon were autonomous trucks [16], [142].

To conclude, a comparison with the control action designed in [125] and reported in Section 3.1.2 of this thesis is done. The main difference lies in the fact that the moving bottleneck model consider just a single vehicle with punctual occupancy, while here the platoon can change its length, so adding a control variable. A more effective control action is then expected to appear. The results obtained in the same simulation scenario are here compared. The trend of the density in the moving bottleneck control case is depicted in Fig. 4.24, while the fuel consumption performances are compared in Table 4.3, showing that the platoon control is more effective in reducing the fuel consumption with respect to the single vehicle control.

4.2.3 Final considerations

In this section, a PDE-ODE model describing the interaction between a platoon of vehicles and the traffic flow has been studied. The length and the speed of the platoon have been assumed as control variables in the design of a MPC aiming at reducing the fuel consumption. Simulations results have assessed the effectiveness

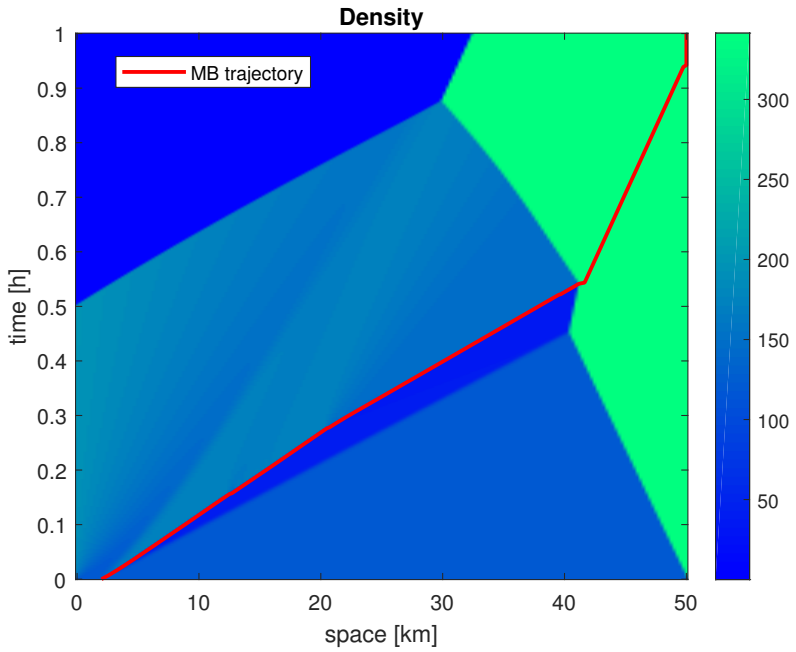

Figure 4.24: Density trend in the simple moving bottleneck control of [125]

of the control action and a comparison with the simple MB control has been done.

Chapter 5

An application of a Second Order Sliding Mode Algorithm for Ramp Metering

In this chapter the Sliding Mode Control (SMC) algorithm that has been developed in [126] to solve the ramp metering problem is presented. The sliding mode control [144, 44] is an approach that has the advantage of being a computationally light easy-to-implement solution capable to guarantee finite-time stabilization and robustness of the controlled system in front of a wide class of uncertainties.
SMC consists in a variable structure technique characterized, in its traditional version, by a bounded discontinuous input signal. This discontinuity has the drawback of being the main cause of the so-called chattering phenomenon [91], that can be disruptive for the controlled systems. Among all the possible strategies proposed to reduce such phenomenon, the idea of confining the discontinuity to the time derivative of the effective control input fed into the plant resulted an efficient solution, giving rise to the so-called Higher-Order Sliding Mode (HOSM) control algorithms, whose main aim is the chattering alleviation [10, 9, 50].

In the following, a sliding mode control approach to solve the ramp metering problem is proposed. In the literature, there are only few examples of applications of SMC to ramp-metering. In [104], a first-order traffic model is chosen to describe a stretch of highway with several on-ramps and a so-called drift algorithm is applied for the sliding mode control. The resulting control system is a coordinated Multi-Input Multi-Output (MIMO) sliding mode controller using both a first-order and a second-order algorithm. In [76], the concept of differential flatness is combined with a first-order SMC in order to keep the density close to its prescribed value by

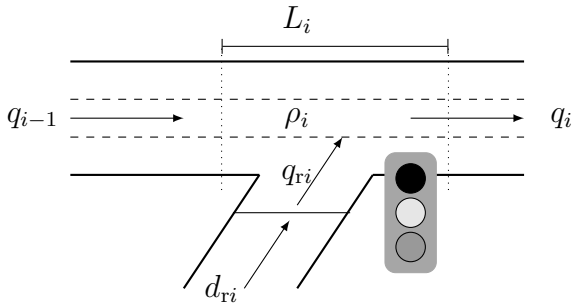

Figure 5.1: Freeway segment

modeling the traffic with the well known first-order Lighthill-Whitham-Richards (LWR) model [97][130], without taking into consideration the queue length dynamics. The same approach has then be extended by applying a Super-Twisting sliding mode approach in [42]. In [134], an integrated traffic control strategy that combines Route Guidance and RM is designed, based on the inverse control technique and Super- Twisting SMC. In [126], we introduced a Suboptimal Second-Order Sliding Mode (SSOSM) control [45] to ramp metering with the aim of minimizing the error between a chosen reference value, i.e., the critical density, and the value of the density in the vicinity of the on-ramps. The algorithm will be detailed in the following.

5.0.1 Second-order sliding mode control

To apply the sliding mode control, typically designed in the continuous time framework, a continuous version with ramps of the traditional METANET model, revised in Section 2.1, is here detailed.

As usual, a stretch of freeway divided in N cells of equal length L_i, $i = 1, \ldots, N$ is considered. A sketch of each section i is depicted in Figure 5.1. As in the classical discrete METANET, the dynamics of the density is described by the conservation law, given by the following differential equation

$$\frac{\mathrm{d}}{\mathrm{d}t}\rho_i(t) = m_{\mathrm{m}i}(t) = \frac{1}{L_i\lambda_i}\left(q_{i-1}(t) - q_i(t) + q_{\mathrm{r}i}(t)\right) \tag{5.1}$$

where $m_{\mathrm{m}i}$ denotes the density change rate, $\lambda_i \in \mathbb{N}$ is the number of lanes, while $q_{\mathrm{r}i}$ is the metered on-ramp flow.

The dynamics of the mean speed of the traffic flow in the ith cell is given by

$$\begin{aligned}\frac{\mathrm{d}}{\mathrm{d}t}v_i(t) = a_i(t) = \frac{1}{\tau}\big(V(\rho_i(t) - v_i(t)\big) + \\ + \frac{1}{L_i}v_i(t)\big(v_{i-1}(t) - v_i(t)\big) + \\ - \frac{\nu}{\tau L_i}\frac{\rho_{i+1}(t) - \rho_i(t)}{\rho_i(t) + \kappa} - \frac{\delta}{L_i\lambda_i}\frac{q_{\mathrm{r}i}v_i(t)}{\rho_i(t) + \kappa}\end{aligned} \tag{5.2}$$

where the parameters τ, ν, δ and κ have the same meaning of the traditional METANET. The steady-state speed $V(\rho_i(t))$ is

$$V(\rho_i(t)) = v_{\mathrm{f}} \exp\left(-\frac{1}{p}\left(\frac{\rho_i(t)}{\rho_{\mathrm{cr}}}\right)^p\right) \tag{5.3}$$

where p is an empirical correction factor to take into account the maximum flow, given the features of the considered cell.

For each ramp, $\omega_{\mathrm{r}i}$ denotes the number of vehicles in queue on the jth ramp. The queue model is given by

$$\frac{\mathrm{d}}{\mathrm{d}t}\omega_{\mathrm{r}i}(t) = m_{\mathrm{r}i}(t) = d_{\mathrm{r}i}(t) - q_{\mathrm{r}i}(t) \tag{5.4}$$

where $d_{\mathrm{r}i}$ is the traffic demand coming at the on-ramp. The portion of flow accessing the mainstream from the ramp depends on the traffic flow on the main segment and on the flow rate input $r_i(t) \in [r_{\min}, 1]$, where $r_i = 1$ is the case when the on-ramp is unmetered and $r_{\min} \geq 0$. More specifically, one has that

$$q_{\mathrm{r}i}(t) = r_i(t)\hat{q}_{\mathrm{r}i}(t) \tag{5.5}$$

where $\hat{q}_{\mathrm{r}i}(t) = \min\{\hat{q}_{1\mathrm{r}i}\,; \hat{q}_{2\mathrm{r}i}\}$ and

$$\hat{q}_{1\mathrm{r}j} = d_{\mathrm{r}i}(t) + \frac{\omega_{\mathrm{r}i}(t)}{T} \tag{5.6}$$

$$\hat{q}_{2\mathrm{r}i} = Q_{\mathrm{sat}} \min\left\{1\,; \frac{\rho_{\max} - \rho_i(t)}{\rho_{\max} - \rho_{\mathrm{cr}}}\right\} \tag{5.7}$$

with T being the sampling time, Q_{sat} being the on-ramp capacity under free-flow conditions and $\rho_{\max}$ being the maximum density of the mainstream segment.

5.0.2 Introduction of the canonical form for the SMC

In order to formulate the control problem at hand, it is convenient to make reference to a canonical form frequently used in the development of sliding mode control laws. The canonical form, which enables to describe the dynamics of the

tracking error in a suitable form for control design, is here presented. Consider a Single-Input-Single-Output (SISO) system affine in the control variable as follows. Let $x^i = \left[x_1^i, x_2^i, x_3^i\right]^\top = [\rho_i, v_i, \omega_{ri}]^\top \in \mathcal{X} \subset \mathbb{R}^3$ be the state vector of the ith cell, $d^i = d_r^i$ be the exogenous input on-ramps, and $u^i = r^i$ be the control variable. The output is instead σ_1^i chosen as the error between the controlled variable $x_1^i = \rho^i$ and its reference $x_1^\star = \rho^\star$ assumed to be piecewise constant. Then system (5.1)–(5.5) can be written in state-space form as follows

$$\begin{cases} \dot{x}(t) = f(x(t)) + g(x(t), d(t))u(t) \\ \sigma_1(x(t)) = x_1^i - x_1^{i\star} \end{cases} \tag{5.8}$$

where $x \in \mathcal{X}$ is the state vector, with initial conditions $x(t_0) = x_0$, t_0 being the initial time instant and $u \in \mathcal{U} \subset \mathbb{R}$ is the control input such that $\mathcal{U} := [-\alpha, \alpha]$ with $\alpha > 0$, while $f(x(t)) : \mathcal{X} \to \mathbb{R}^n$ and $b(x(t)) : \mathcal{X} \to \mathbb{R}^n$ are uncertain functions of class $\mathrm{C}^1(\mathcal{X})$. The uncertain nature of these functions is due to the fact that modeling uncertainties related to the traffic demand are assumed to be present. The output function $\sigma_1(x(t)) : \mathcal{X} \to \mathbb{R}$ plays the role of the so-called "sliding variable". The following input constraint holds

$$0 \leq r_{\min} \leq u^i \leq 1 \,. \tag{5.9}$$

The scalar input, belonging to the set $[r_{\min}, 1]$, can be mapped into a new input $\tilde{u}^i$ taking value in the set $[-\bar{u}, \bar{u}]$, with $\bar{u} > 0$ by applying the following transformation

$$u^i = \frac{(1 - r_{\min})(\tilde{u}^i - \bar{u})}{2\bar{u}} + 1 \,. \tag{5.10}$$

Furthermore, the following assumptions hold.

Assumption 1. *System* (5.8) *has an uniform and time invariant relative degree equal to 1.* □

By virtue of Assumption 1, exploiting (5.10) the following first-order dynamics can be defined

$$\dot{\sigma}_1^i = f_1(x^{i-1}, x^i) + g_1(x^i, d^i)\tilde{u}^i \tag{5.11}$$

where σ_1^i is the ith *sliding variable*, while

$$f_1(x^{i-1}, x^i) = \frac{1}{L\lambda^i}\left(x_1^{i-1}x_2^{i-1} - x_1^i x_2^i + w_1^i + \frac{1 + r_{\min}}{2}\hat{q}_{\mathrm{r}}^i\right) \tag{5.12}$$

$$g_1(x^i, d^i) = \frac{1 - r_{\min}}{2\bar{u}L\lambda^i}\hat{q}_{\mathrm{r}}^i \,. \tag{5.13}$$

Above, w_1^i is the uncertainty on the traffic demand of the mainstream, while $\hat{q}_{\mathrm{r}}^i$ is as in (5.7) with an additional disturbance, i.e.,

$$\hat{q}_{1\mathrm{r}}^i(t) = d^i(t) + w_2^i(t) + \frac{x_3^i(t)}{T}\,, \tag{5.14}$$

where w_2^i is the uncertainty due to the flow coming at the ramps.

Moreover, the following condition holds.

Assumption 2 (Boundedness of the vector field)**.** *There exist positive constants F, $G_{\min}$ and $G_{\max}$ such that the following inequalities hold,*

$$\left| f_1(x^{i-1}, x^i) \right| \leq F \tag{5.15}$$

$$0 < G_{\min} \leq g_1(x^i, d^i) \leq G_{\max}\,, \tag{5.16}$$

$\forall\, i \in \mathcal{C}$.

Following the standard sliding mode approach, the control law could be designed as a discontinuous control law. Another option is to design it as the output of an integrator having in input the discontinuous signal, i.e., $w(t) = \dot{u}(t)$. This second strategy is called Higher-Order Sliding Mode (HOSM).

5.0.3 Auxiliary system

With the aim to design a Second-Order Sliding Mode (SOSM) control, letting $\sigma = [\sigma_1,\, \dot{\sigma}_1]^\top = [\sigma_1,\, \sigma_2]^\top$ be the vector of the sliding variable and its time derivative, the relative degree of system (5.8) is artificially increased to 2 [11].

The system (5.1)-(5.7), with the degree artificially increased to 2, becomes:

$$\begin{cases} \dot{\sigma_1}(t) = \sigma_2 \\ \dot{\sigma_2}(t) = \frac{1}{L_i \lambda_i} \left(\dot{q}_{i-1}(t) - \dot{q}_i(t) + \dot{q}_{\mathrm{r}i}(t) \right) \end{cases} \tag{5.17}$$

where $\dot{q}_{\mathrm{r}i}$ explicitly depends on the input $r_i(t)$, since $q_{\mathrm{r}i}(t) = r_i(t)\hat{q}_{\mathrm{r}i}(t)$ from (5.5).

By adopting the canonical notation introduced for the SMC in Section 5.0.2, letting $\tilde{\mu}^i(t) = \dot{\tilde{u}}^i(t)$ be an auxiliary control input, the system with the additional integral dynamics is

$$\begin{cases} \dot{\sigma}_1^i = \sigma_2^i \\ \dot{\sigma}_2^i = h_1(x^{i-1}, x^i, \tilde{u}^i) + g_1(x^i, d^i)\tilde{\mu}^i \end{cases} \tag{5.18}$$

where the augmented vector of the sliding variable and its derivative is $\sigma^i = \left[\sigma_1^i, \sigma_2^i\right]^\top$, while the drift term becomes

$$h_1(x^{i-1}, x^i, \tilde{u}^i) = \tfrac{\mathrm{d}}{\mathrm{d}t} f_1(x^{i-1}, x^i) + \left(\tfrac{\mathrm{d}}{\mathrm{d}t} g_1(x^i, d^i)\right) \tilde{u}^i \,, \tag{5.19}$$

and g_1 is as in (5.13). Furthermore, the following assumption holds.

Assumption 3 (Boundedness of the auxiliary drift term)**.** *There exists a positive constants H such that the following inequality holds,*

$$\left| h_1(x^{i-1}, x^i, \tilde{u}^i) \right| \leq H, \quad \forall\, i \in \mathcal{C} \,. \tag{5.20}$$

Note that Assumption 2 and 3 mean that uncertainties affecting the systems are bounded, that is reasonable due to the nature of the involved variables.

5.0.4 The SSOMC algorithm

Given these preliminaries, a discontinuous finite-time SMC law, generically indicated as ψ is defined

$$\tilde{\mu}^i := \psi(\sigma_1^i, \sigma_2^i), \quad \forall\, i \in \mathcal{R} \,, \tag{5.21}$$

such that there exists $\sigma_1^i(t) \equiv 0$, $\forall\, t \geq \bar{t}$, in spite of the uncertainties, with $\bar{t} \geq t_0$ being the so-called *reaching time*. The presented second order sliding mode control law is a SSOSM control [11]. Starting from the Bang-Bang principle [6], if bounded uncertain terms are present, it is possible to generate a "suboptimal" state trajectory with respect to that obtained with the Bang-Bang minimum time optimal control law. Specifically, computing the local minimum or maximum of the sliding variable, referred to as $\sigma_{1i\,\max}$, instead of its first time derivative, the SSOSM control law can be defined as

$$\psi(t) = -\eta_i \cdot \overline{\alpha}_i \operatorname{sgn}\left(\sigma_{1i}(t) - \frac{1}{2}\sigma_{1i\,\max}(t)\right) \tag{5.22}$$

where $\psi = \dot{r}_i$ in our case, while $\eta_i = \eta^*$ and $\overline{\alpha}_i$ are chosen such that

$$\overline{\alpha}_i > \max\left(\frac{\beta_i}{\eta^* \gamma_i}, \frac{4\beta_i}{3\gamma_i - \eta^* \varepsilon_i}\right) \tag{5.23}$$

$$\eta^* \in (0, 1] \cap \left(0, \frac{3\gamma_i}{\varepsilon_i}\right) . \tag{5.24}$$

As for the stability analysis, according to [11], one can prove that, under sufficient conditions (5.23) and (5.24), the control law (5.22) implies a contraction property of the extreme values of the sliding variable in time, so that the sliding variable and its first time derivative are steered to zero in a finite time t_r.

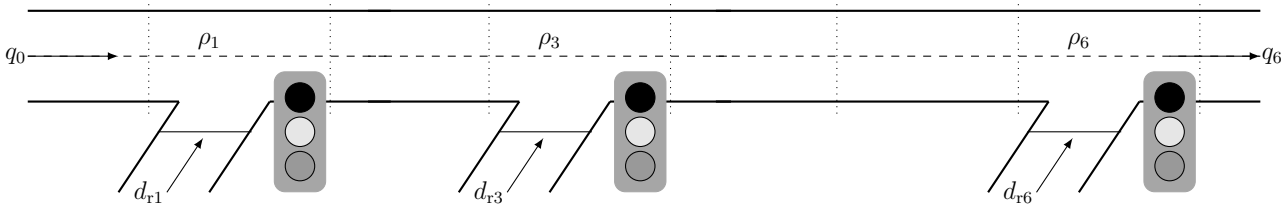

Figure 5.2: Sketch of the considered highway portion

5.0.5 Extension to the classical SSOSM control

The performance of the proposed algorithm is increased through two modifications. Firstly, a saturation strategy is introduced to take into account the limit of the on-ramp flow r_i. Indeed, since the ramp signal r_i is constrained to assume values between $r_{\min}$ and 1, while $\overline{\alpha}_i$ has to be set according (5.23), it is needed to modify the proposed control (5.22) in order to take into account these bounds. Inspired by [45], the SSOSM control law is modified adding an additional law depending on the sign of the input signal $r_i(t)$. More specifically, the control law (5.22) becomes

$$\psi(t) \quad = \quad \begin{cases} -\eta_i \cdot \overline{\alpha}_i \operatorname{sgn}\left(\sigma_{1i}(t) - \mu\sigma_{1i\max}(t)\right) & r_{\min} < r_i(t) < 1 \\ -\overline{\alpha}_i \operatorname{sgn}\left(r_i(t)\right) & \text{otherwise}, \end{cases} \tag{5.25}$$

where $\mu \in \left[\frac{1}{2}, \bar{\mu}\right]$ and $\bar{\mu}(t) = \frac{\sigma_{1i}(t)}{\sigma_{1i\max}(t)}$, $\forall\, t \in \mathcal{T} := \{t_k\}$, $k \in \mathbb{N}$ and $\mathcal{T}$ being the sequence of the time instants t_k when the control law switches.

The second mechanism that is considered is the introduction of a supervisor with the aim to avoid that ramps are blocked for too long periods. The supervision mechanism is introduced as follows: if the flow rate input $r_i(t) = r_{\min}$ for a time interval greater than cT, $c \in \mathbb{N}$, then set $r_i > r_{\min}$; if instead $r_i(t) = 1$ for less than $\frac{cT}{2}$, maintain $r_i = 1$ up to $\frac{cT}{2}$. This mechanism has the aim to avoid the generation of long queues on the ramps, thus avoiding too high waiting time.

5.0.6 Simulation results

The proposed SMC has been assessed in simulation. To this aim we have considered a stretch of highway composed by $N = 7$ cells with $M = 3$ ramps located in the first, third and sixth cell. The sketch of the highway is depicted in Figure 5.2.

The inflow to the highway, both from the mainstream and from the on-ramps, has a trapezoidal shape as depicted in Figure 5.3. The parameters adopted for the model in the simulations are reported in Table 5.1.

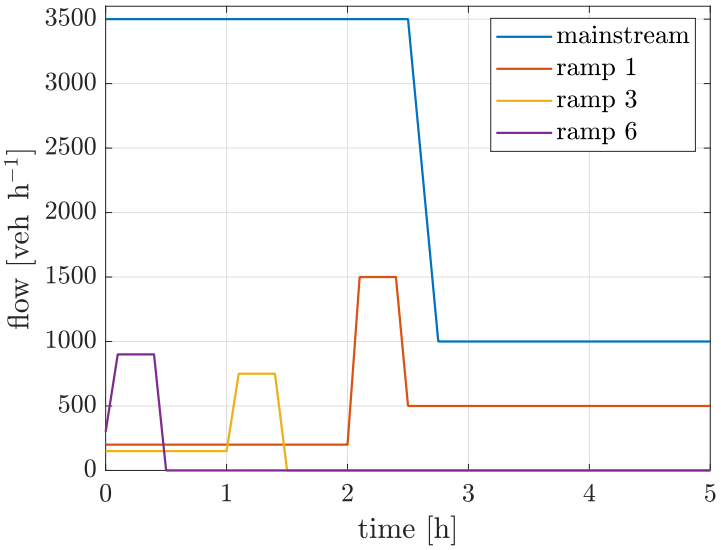

Figure 5.3: Inflow to the highway

Table 5.1: Simulation parameters

N	7
M	3
t_f	5 h
ρ_cr	33.5 veh/km/lane
ρ_max	180 veh/km/lane
v_f	102 km/h
p	1.867
τ	0.005 h
T	0.0028 h
ν	60 km^2/h
κ	40 veh/km/lane
δ	0.0122
L_i	1 km
λ_i	2 lane
$\overline{\alpha}_i$	10
η_i	0.9
c	4
r_min	0

Figure 5.4(a) shows the trend of the density along the stretch of highway when the ramp metering control is not applied yet. Looking at the incoming demand, the inflow of the on-ramp of the cell 6 shows a peak at the beginning of the simulation time. The sum of the ramp demand and the mainstream inflow overcomes the value of the capacity and this causes the formation of congestion that starting from cell 6 propagates for several cells upstream. The same scenario occurs around the first hour of simulation when a peak of demand appears at ramp 3 and again at 2 hours of the simulation when a severe congestion is caused by the peak of demand coming from the first ramp. In the scenario without control, the access of vehicles from ramps is not regulated, so all the incoming cars can enter the highway and vehicles do not wait at ramps forming queue.

The scenario with the developed SSOSM algorithm where the reference value is chosen equal to the critical density, has been simulated. The correspondent trend of the density in time and space in this controlled case is depicted in Figure 5.4(b). By applying the ramp metering control, the congestion in the mainstream is completely solved. The control variables r_1, r_3 and r_6, metering rates of the three controlled ramps, are reported in Figure 5.5. As previously remarked, the control variable r_i is the metering rate, that represents the portion of incoming flow allowed to access the highway from the on-ramp.

The first control action that is activated is the one regulating the access to ramp 6. According to its incoming demand, depicted in Figure 5.3, a peak of flow appears at the beginning of the simulation time. The controller reacts by applying a strong reduction of the metering rate for the whole duration of the demand peak. A similar situation appears in the other two ramps when their traffic demands show a strong increase, causing a congestion. Figure 5.6 reports the trend of the sliding variables, i.e., the difference between the reference value and the density respectively appearing downstream each ramp. It is possible to see that the control action successfully steers the error to zero when the traffic demand coming from the ramp is high, so that the density value is very close to the one of the reference. An error high but negative appears when there is not enough incoming demand to let the density increase up to the reference value but, as highlighted before, this behavior does not represent a problem in the traffic control since a free-flow condition holds.

The drawback that occurs by controlling the on-ramps inflows is obviously the formation of queues at the ramps. Their trends are depicted in Figure 5.7.

The control effectiveness is evaluated considering the value assumed by the TTS, that is the time spent by all the drivers on the highway both in the mainstream

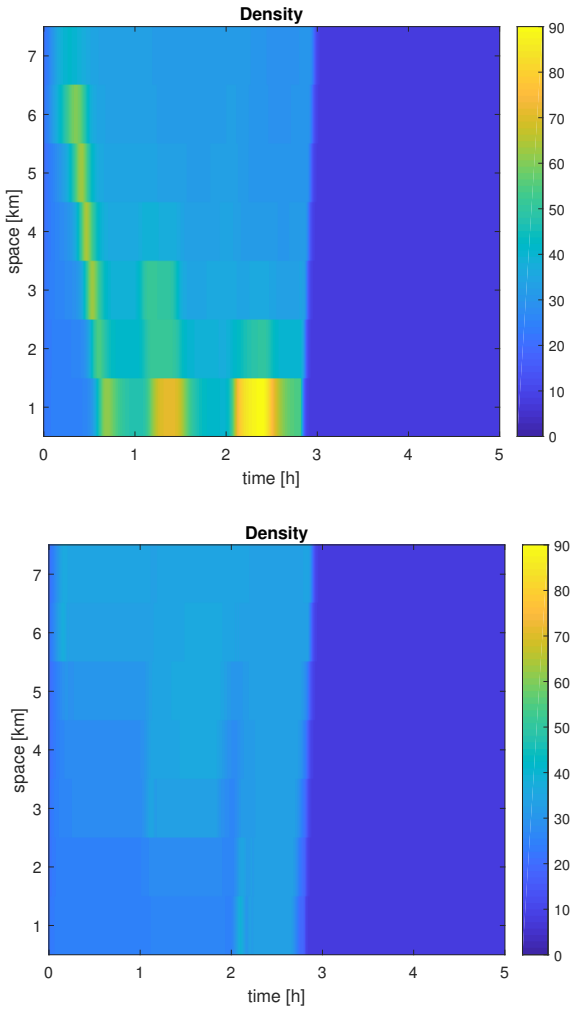

(b)

Figure 5.4: Density trend in the uncontrolled and controlled case

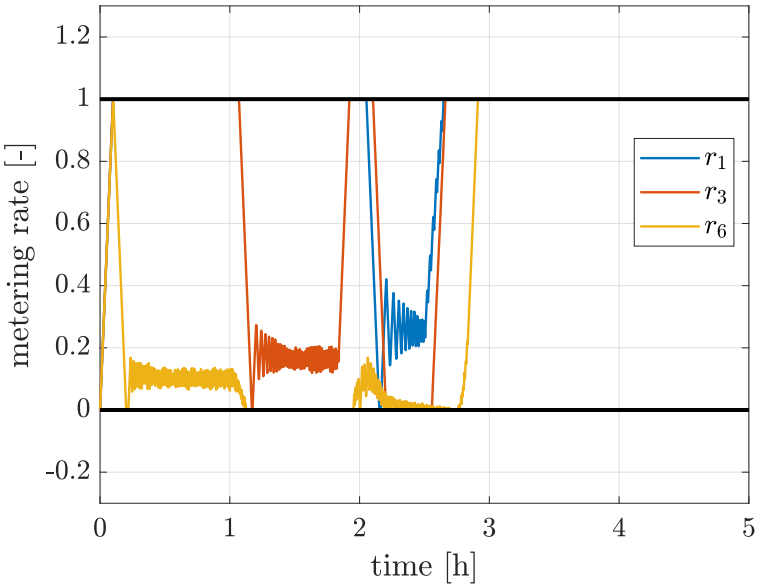

Figure 5.5: Controlled metering rate for the three ramps

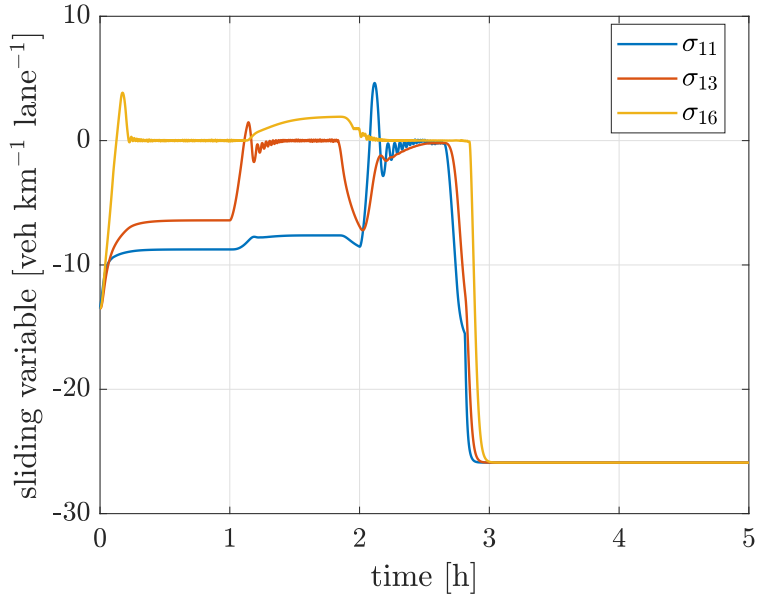

Figure 5.6: Trend of the sliding variables

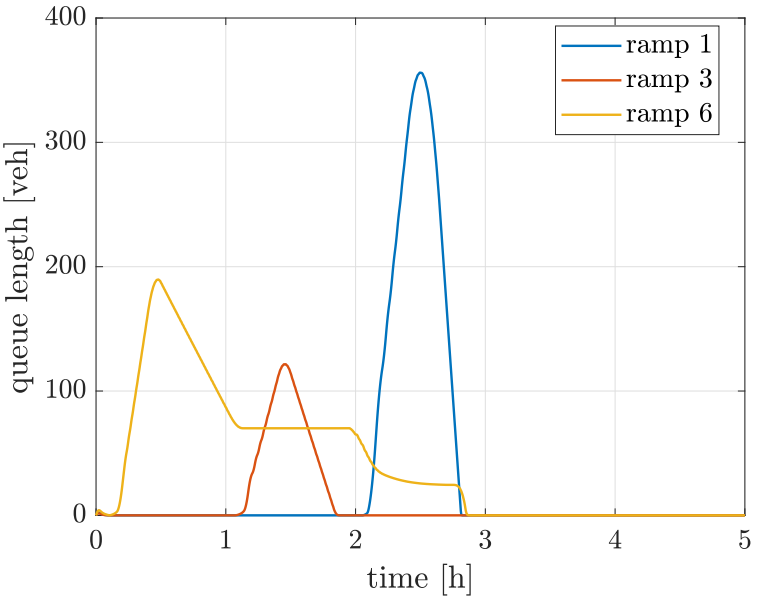

Figure 5.7: Queue length at the ramps

Table 5.2: Performance indexes

Strategy	TTT	TWT	TTS	RMSE
Unmetered	1769	311	2080	26.33
ALINEA	1689	337.9	2027	20.99
FOSM	1690	323.5	2014	20.94
SSOSM	1453	396	1849	18.02

and waiting at the queue. In order to quantitatively verify the performance of the present proposal with respect to already exixting algorithms, the SSOSM control algorithm is compared with a First-Order Sliding Mode (FOSM) control algorithm, with the ALINEA strategy and with the unmetered case. The achieved results are reported in Table 5.2, in terms of TTT, TWT, TTS (see Section 2.5),and Root Mean Square Error (RMSE) of the density. The TTS presents a strong reduction of thea 11.1% by applying the proposed SSOSM with respect to the uncontrolled case, given by an expected increase of the TWT due to the ramps closure, balanced by a strong reduction of the TTT. The latter results outperform the improvements that are achieved via the traditional ALINEA strategy. The FOSM algorithm succeeds as well in reducing the TTS with respect to the unmetered case (3.2%) but its performance is lower than the proposed SSOSM. Moreover, the latter outperforms

all the other strategies in terms of RMSE.

5.0.7 A Hierarchical MPC and Sliding Mode Based Two-Level Control for Freeway Traffic Systems with Partial Demand Information

In the present section, the SSOSM algorithm is adopted to design a more sophisticated control scheme capable to solve an optimal RM problem, while being robust in front of disturbances acting on the system. The approach has been presented in [46]. Differently from other works published in the literature, the control problem to solve is made more challenging and realistic due to the introduction uncertainties and disturbances acting on the system. Note that the considered uncertainty is physically reasonable due to the uncertain nature of the traffic. In this perspective, the proposal consists of a hierarchical control architecture based on the combined use of MPC and SMC. Specifically, an high-level controller is based on the use of a MPC as supervisor, that supplies the reference value for the density based on an ideal model of the traffic system. On the other hand, a low-level controller implements a decentralized SSOSM algorithm to track the reference provided by the high-level controller. In this way, the real control input is generated and fed into the real traffic system. This proposal introduces the need for the two loops to run at different rates. Specifically, due to its nature the MPC runs at low frequency, while the SSOSM control needs a frequency sufficiently high to enforce the sliding mode, while fulfilling the sampling constraint of the actuators, as the traffic lights. The combination of MPC and SMC is a solution that proved to be effective, as remarked in survey [74], or in [75] and [73] where it was applied to microgrids and robot manipulators.
As previously remarked, in the proposed control scheme, the lower level controller is represented by the sliding mode algorithm proposed in Section 5.0.4. The higher level controller is instead a MPC generating the reference signal, that will be here detailed.

The higher level MPC

By virtue of the fact that the lower level sliding mode local controllers ensure robustness to the controlled system, the upper level based on MPC can rely on a nominal model representing the real system with reduced uncertainties. Moreover, in order to apply the MPC, the continuous dynamics (5.8) is discretized, and the

output is chosen equal to the cell density $y_2 = x_1^i$, thus leading to a discrete model in the form

$$\begin{cases} x_{k+1} = \hat{f}(x_k^{i+1}, x_k^i, x_k^{i+1}) + \hat{g}(x_k^i, d_k^i)u_k^i \\ y_{2_k} = x_{1_k}^i \end{cases} \qquad \forall\, i \in \mathcal{C}\ , \tag{5.26}$$

with $k \in \mathcal{N}$ and $x_k = x(t_k)$ meaning the variable x at the sampling instant $t_k = kT$, while $\hat{f}$ and $\hat{g}$ are the nominal (that is without disturbances w_1^i and w_2^i) counterparts corresponding to functions f and g in (5.8). The MPC is based on the solution of the so-called Finite-Horizon Optimal Control Problem (FHOCP). It consists in minimizing, at any time step t_k, a suitably defined cost function with respect to the control sequence $\mathbf{u}^i_{[t_k, t_{k+N_\mathrm{p}-1}|t_k]} := [u_0^i(t_k),\, u_1^i(t_k), \ldots, u_{N_\mathrm{p}-1}^i(t_k)]$, where $N_\mathrm{p} \geq 1$ is the prediction horizon.

The aim of the control scheme is to reduce travel times for drivers. Specifically, considering the travel times definition presented in 2.5, the cost function to minimize with respect to $\mathbf{u}_{[t_k, t_{k+N_\mathrm{p}-1}|t_k]}$ is given by

$$J(x^i(t_k), N_\mathrm{p}) = T \sum_{p=0}^{N_\mathrm{p}-1} \left(\sum_{i=1}^{N} L x_1^i(t_{k+p}) \lambda^i + \sum_{j=1}^{M} x_3^{[j]}(t_{k+p}) \right)\ . \tag{5.27}$$

representing the Total Time Spent (TTS). Furthermore, the cost function is subject to the hard constraint represented by the dynamics (5.26) and the inequality constraint on the input given in (5.9).

Then, given $\mathbf{u}^{\star i}_{[t_k, t_{k+N_\mathrm{p}-1}|t_k]} := [u_0^{\star i}(t_k),\, u_1^{\star i}(t_k), \ldots, u_{N_\mathrm{p}-1}^{\star i}(t_k)]$, the optimal sequence generated from the solution of the FHOCP, according to the Receding Horizon strategy, the applied piecewise-constant high-level control law is the following

$$u_{\mathrm{HL}}^{\star i}(t) = u_0^{\star i}(t_k), \quad t \in [t_k,\, t_{k+1})\ , \tag{5.28}$$

where $t_{k+1} - t_k = T$ is the MPC time step, and $u_0^\star(t_k)$ the first value at t_k of the optimal control sequence for the ith cell.

Case of Study

In order to assess the validity of the proposed two levels controller a scenario is simulated, as depicted in Figure 5.9.

A stretch of highway divided in $N = 7$ cells, each of them with length $L = 1$ km, has been considered. Two on-ramps are present in cells 4 and 6.
As previously remarked, the proposal is a multi-rate control scheme, that requires

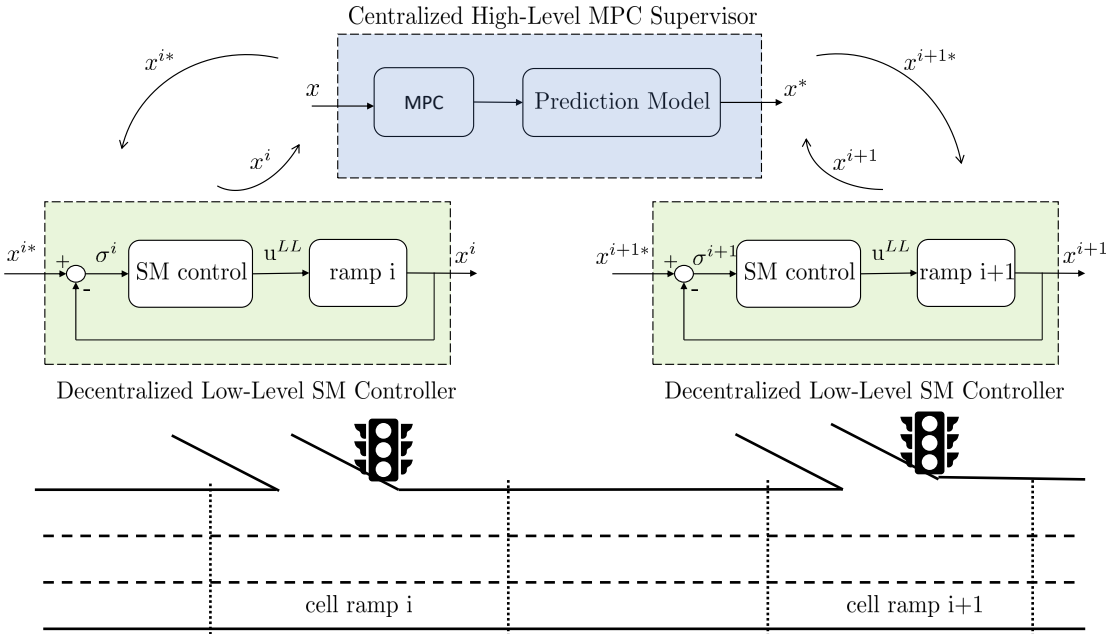

Figure 5.8: Scheme of the multi-level hierarchical control

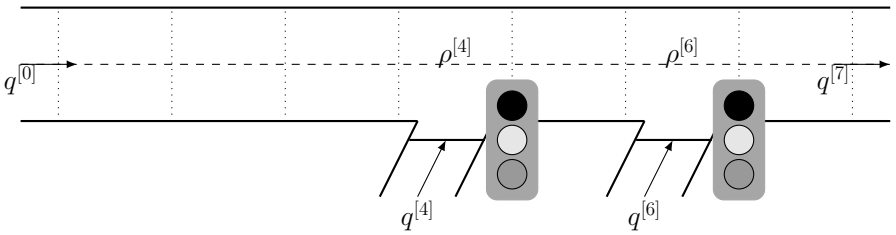

Figure 5.9: Sketch of the considered highway portion

the numerical implementation of the FHOCP and a time discretization such that the input constraints can be verified only at the integration time step. Following the results in [103], an integration step $\tau_{\mathrm{i}} = 1$ second is chosen, while the MPC time step is $T = 30$ seconds. This choice still guarantees the convergence properties of the control system.

The minimum value of the input is chosen as $r_{\min} = 0$, to indicate the case in which the ramp can be completely closed. The external inflow is depicted in Figure 5.10. This profile is given by a trapezoidal shape plus a random unpredictable disturbance, whose amplitude is chosen as a percentage of the maximum value of the nominal demand. The critical density is ρ_{cr}= 33.5 veh/km per lane, the maximum density is given by $\rho_{\max}$ =180 veh/km per lane and the flow speed is v_{f} 102 km/h. The METANET speed model parameters are c=1.867, τ is 0.005 hours, ν=60km^2/h, κ=40 veh/km per lane and δ=0.0122.

Three different scenarios are simulated in order to make a comparison:

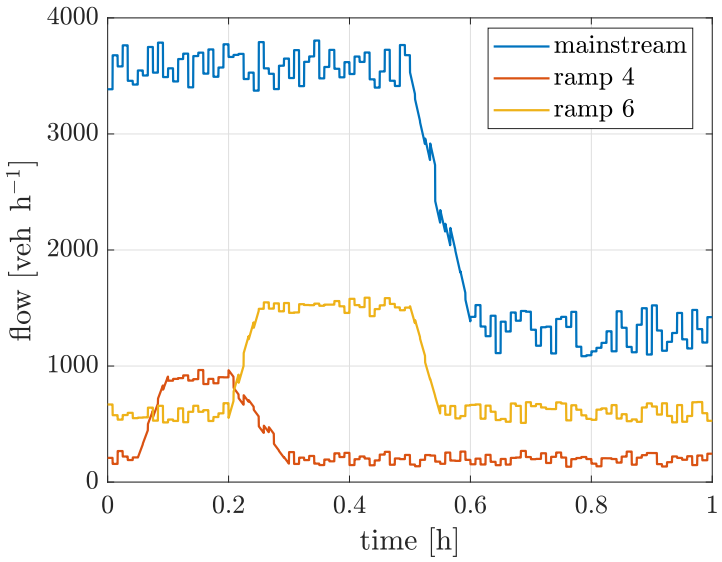

Figure 5.10: Example of incoming traffic demand both on the mainstream and on-ramps, with an overlapped disturbance having amplitude equal to 10% of the nominal demand.

S1) Umetered case: no control is applied to the ramp and then the whole incoming ramp demand is allowed to access the mainstream. Queues at the ramps obviously do not form. The TWT is zero, or can be very close to zero in the case in which the congestion in cells downstream a ramp is so severe that vehicles arriving from ramps cannot accede.

S2) MPC standalone: in this situation a genuine MPC is applied, without the lower level SM. The prediction is done by adopting the nominal model of the system with a prediction horizon equal to $N_\mathrm{p} = 30$ time steps. The optimal input is then applied to the real system using a zero-order-hold mechanism, which converts the signal sampled each T seconds into a signal at the integration step τ_i.

S3) High level MPC with local SSOSM control: this is the proposed control scheme. The high-level MPC supervisor produces the reference density signals to be tracked by applying the saturated SSOSM control algorithm, locally acting on the controlled cells. The prediction horizon is chosen again equal to $N_\mathrm{p} = 30$.

MPC standalone in presence of uncertainties

Before discussing the results achieved by adopting the two levels control scheme, the effect of disturbances acting on the demand on a genuine MPC is evaluated. As

reference case study, an MPC standalone is directly applied to on-ramps in nominal conditions, assuming that a perfect knowledge of the traffic demand is available. Different simulations have been done by increasing the disturbance on the traffic demand with amplitude variation, namely $\Delta w_{\%}$, from 10% to 25% of the nominal demand. All the cases are then compared in terms of TTT, TWT and TTS, as reported in Table 5.3. The high nonlinearity of the system under control strongly

Table 5.3: Travel times by applying only the MPC with increasing disturbances acting on the system

$\Delta w_{\%}$	TTT	TWT	TTS	$\Delta TTT_{\%}^{\text{S2n}}$	$\Delta TWT_{\%}^{\text{S2n}}$	$\Delta TTS_{\%}^{\text{S2n}}$
0	318.85	176.10	494.95	–	–	–
10	341.93	209.48	551.42	7.24	18.95	11.41
15	357.53	248.15	605.68	12.13	40.91	22.37
20	428.10	269	697.35	34.27	52.75	40.89
25	427.10	315.34	742.52	33.95	79.07	50.02

influences the TTS, but it is still possible to observe that the percentage variation with respect to the MPC in nominal condition (namely, $\Delta TTT_{\%}^{\text{S2n}}$, $\Delta TWT_{\%}^{\text{S2n}}$, and $\Delta TTS_{\%}^{\text{S2n}}$) considerably increases, the higher is the disturbance amplitude. These results are illustrated in Figure 5.11, where it is evident the increase of travel times compared to a baseline nominal MPC scenario. These results introduces the need for the adoption of two levels control schemes, aiming at increasing the robustness of the control action.

Two levels controllers: Simulation Results

The results obtained by means of the proposed two-levels scheme, indicated as scenario S3, are here discussed. The amplitude of the considered disturbance acting on the inflow is equal to 10% of the nominal demand. Moreover, the unmetered case (scenario S1) is also simulated to make a comparison.

The trend of the density in time and space is shown in Figure 5.12 for all the simulated scenarios. Figure 5.12(a) depicts the trend in the umetered situation, without any control. In correspondence of the two ramps in cell 4 and 6, a congestion forms and spreads for several cells upstream, reaching also the first cell of the considered stretch. High values of density, up to 70 veh/km/lane occur along the stretch, thus indicating the presence of a severe congestion. The TTS in

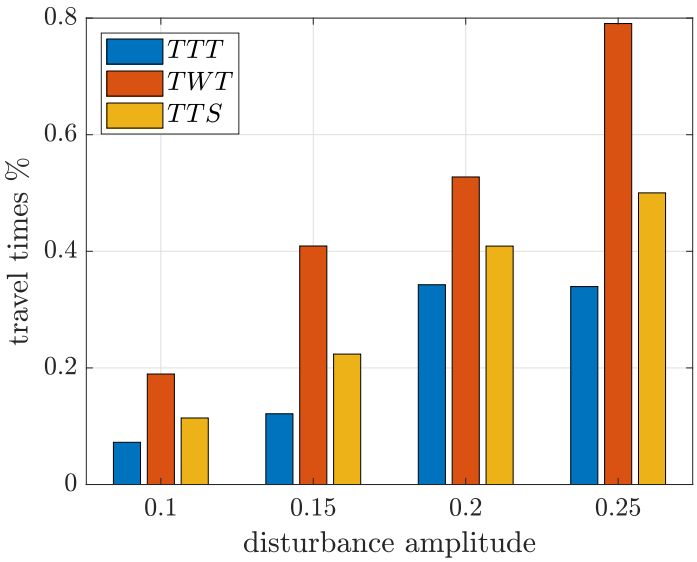

Figure 5.11: Percentage of growth in travel times with increasing disturbances when the MPC standalone is used

this case, as reported in Table 5.4 reaches the value of 569 veh/h. Figure 5.12(b) depicts the density trend when the MPC standalone is adopted. On the other hand, the effect on the density of the complete hierarchical two levels controller is shown in Figure 5.12(c). In this case, congestion appears strongly reduced, with results that are better than in the case of the MPC standalone. This demonstrates the effectiveness of the SSOSM control to reduce the uncertainty level affecting the system. Travel times in the different scenarios are reported in Table 5.4. A scenario has been simulated also with an increased disturbance amplitude equal to 25% of the nominal demand is reported for further assessing the proposal, and the percentage variation with respect to the unmetered case (namely, $\Delta TTS^{\mathrm{S1}}_{\%}$) is computed.

The reference density signals generated by the MPC supervisor are depicted in Figure 5.13 for cells 4 and 6. The trend of the sliding variable for both the ramps is instead reported in Fig. 5.14, in which it is important to notice that they are steered to zero in a finite time. The abrupt variations of the disturbed demand causes the sliding mode to be lost sometimes, but it is always recovered in a finite-time. The presence of some oscillations is instead mainly due to the multi-rate nature of the scheme in which the error between the continuous-time system and its discretized model slightly propagates over time. This does not have a strong negative impact on the performance of the proposed scheme. The optimal control inputs $r^{\star 4}$, $r^{\star 6}$ computed by the MPC supervisor, solving the FHOCP, are

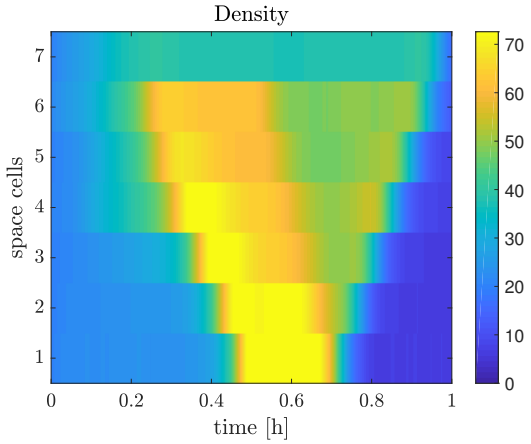

(a) umetered (S1)

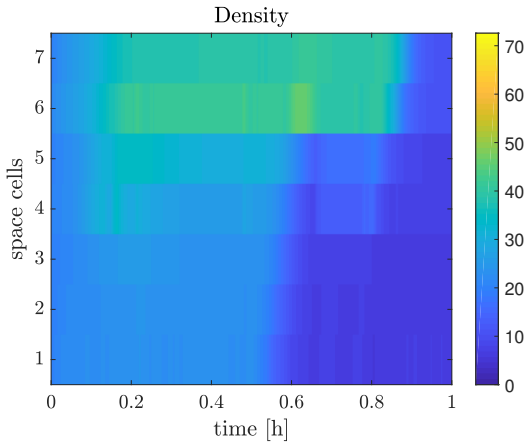

(b) MPC (S2)

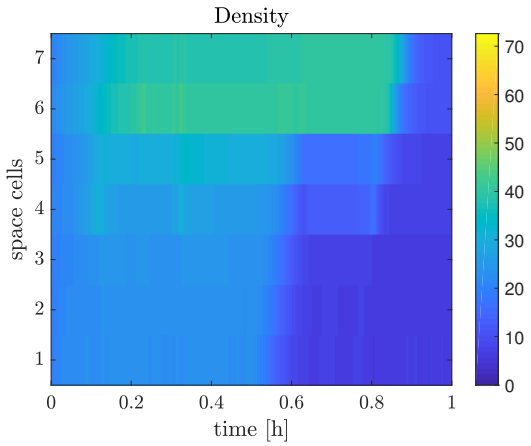

(c) MPC/SSOSM (S3)

Figure 5.12: Density trend in the three considered scenarios. (a) unmetered case (S1). (b) MPC standalone (S2). (c) high level MPC with local SSOSM control (S3)

Table 5.4: Performance indexes

$\Delta w_{\%}$	Scenario	TTT	TWT	TTS	$\Delta TTS^{S1}_{\%}$
10	S1	566	3	569	-
	S2	321	175	496	12.8%
	S3	317	175	492	13.5%
25	S1	543	1	544	-
	S2	315	157	472	13.2%
	S3	311	157	468	13.7%

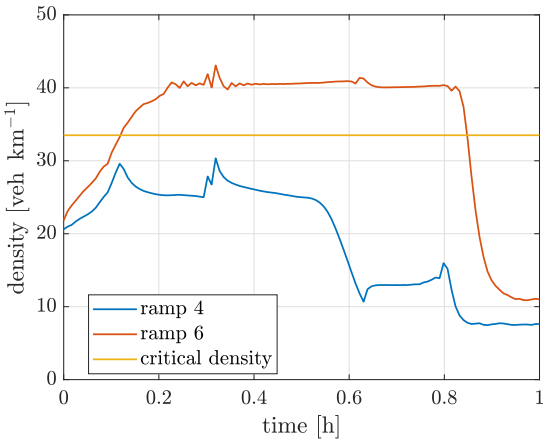

Figure 5.13: Reference signals genereted by the MPC control

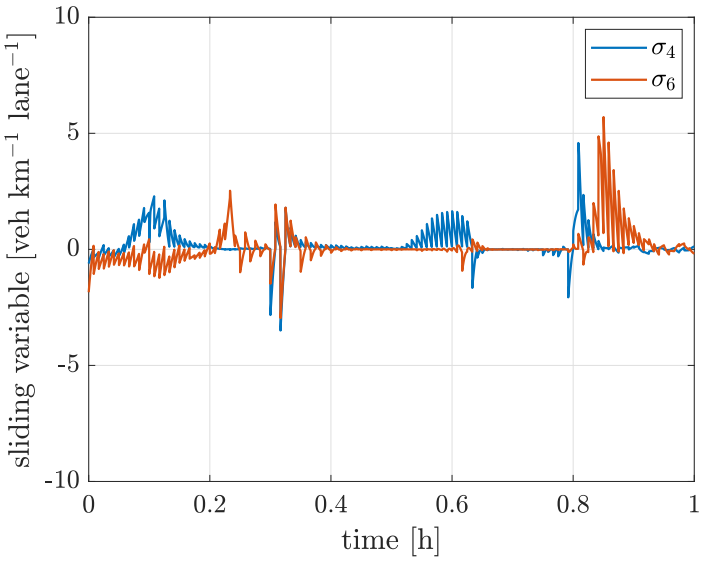

Figure 5.14: Sliding variables

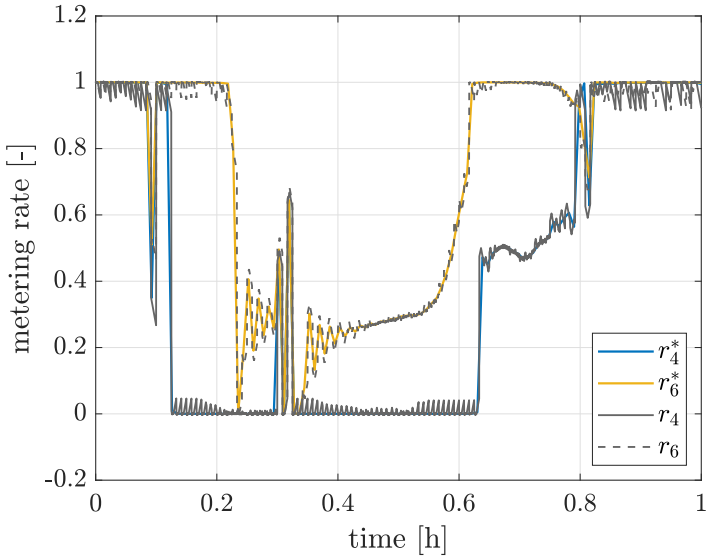

Figure 5.15: Control inputs computed by the controller

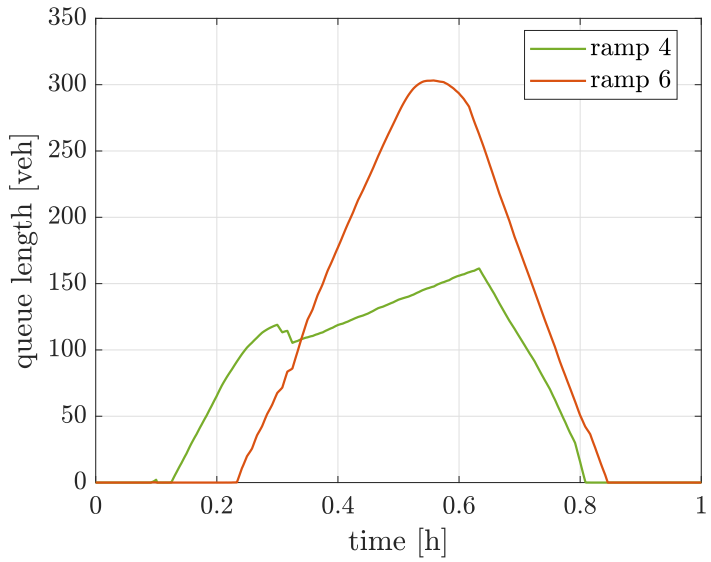

Figure 5.16: Traffic queues forming at the on-ramps 4 and 6

illustrated in Figure 5.15.
Figure 5.15 depicts the trend of the optimal input computed by the MPC and the input generated by the SM algorithm. It is worth noting that the local SSOSM controllers do not only reject the uncertainties affecting the system, but, following the reference provided by the MPC supervisor, generate control inputs which reproduce the optimal ones achieved by solving the FHOCP at high level.
Looking at the time evolution of the control signals, the first peak of the demand depicted in Figure 5.10 occurs in cell 4, thus letting the MPC provide a density reference such that the corresponding SSOSM input closes ramp 4. The same happens for ramp 6 when the second peak of demand arrives. The signals are then modulated in order to avoid, at the same time, too high congestion on the highway and too long queues at the ramps, reported in Figure 5.16.

Final considerations

The proposed hierarchical two-level MPC with SSOSM control, adopted to solve a ramp metering problem for traffic systems characterized by partial demand information, has proven to be effective to reduce the level of uncertainty of the controlled system, while maximizing the traffic throughput. The proposal outperforms the other compared cases in terms of improvements of total travel times.

Conclusion

In this chapter final considerations and some possible future works are considered.

The central theme of this dissertation is the possibility of exploiting new technologies implemented on vehicles, as connectivity and automation features, to regulate traffic control. Specifically, throughout the thesis, the use of smart vehicles as actuators for traffic control actions is investigated. The central question is if also in scenarios with low penetration rates of connected ans automated vehicles, a small number of actuated vehicles is sufficient to influence the traffic.

Unlike the majority of the works present in the literature, the problem is faced in a macroscopic framework, to reduce the computational complexity that characterizes microscopic approaches.

To overcome the first-order macroscopic model problem of not being able to capture the capacity drop phenomenon, a capacity drop modelling approach has been investigated and it is applied to most of the presented models, making them more realistic.

Several approaches have been investigated to describe flows with smart vehicles. The technique that is mainly adopted in the thesis is the representation of connected and automated vehicles as they were moving bottleneck with a their own motion law different from the rest of the traffic flow. Each single moving bottleneck is individually controlled to influence the traffic in its neighborhood.

The problem was first explored in the framework of PDE traffic models, leading to a PDE-ODE model describing the interaction between the macroscopic flow and the moving bottleneck, whose trajectory is described by the ODE. A speed control is then applied to the moving bottleneck to optimize the fuel consumption of the overall traffic flow, showing that even with only one controlled vehicle, benefits are brought to the traffic flow.

A second field of research has focused on the modelling of CAVs by means of multi-class flow modelling, leading to the development of a multi-class CTM model

for mixed human-driven and CAVs flow. A centralized decision maker computing the optimal speed to be communicated to the CAVs class has been developed and benefits are visible for the overall traffic flow, leading to a reduction of travel times. A lot of attention has recently been paid to platooning, especially for trucks, looking at the energy efficiency that derives from reducing the aerodynamic drag between trucks and then decreasing the fuel consumption. However, the impact of platooning on the traffic flow is not yet well understood. A part of this dissertation is devoted to study the interaction between platoons and the surrounding traffic, leading to the development of two different modelling approaches. Moreover, the length and the speed of the platoon become the control variables in control schemes aiming at improving traffic conditions and demonstrating that platoons could be even beneficial for traffic.

There are several possible future developments that could be explored. The presented models and the control strategies, derived in a macroscopic framework, could be tested by means of micro-simulators in order to validate them.
Additionally, platooning related aspects have not been central in the dissertation, that mainly focused on the impact of platoons on the bulk traffic flow. Platoons have been assumed as simple actuators for the macroscopic traffic control action without focusing on their internal spacing-policy, that will be further investigated.

Bibliography

[1] Mohamed Abdel-Aty, Ryan J. Cunningham, Vikash V. Gayah, and Liang Hsia. "Dynamic Variable Speed Limit Strategies for Real-Time Crash Risk Reduction on Freeways". In: *Transportation Research Record: Journal of the Transportation Research Board* 2078.1 (Jan. 2008), pp. 108–116.

[2] A. Alam, B. Besselink, V. Turri, J. MåRtensson, and K. H. Johansson. "Heavy-Duty Vehicle Platooning for Sustainable Freight Transportation: A Cooperative Method to Enhance Safety and Efficiency". In: *IEEE Control Systems Magazine* 35.6 (2015), pp. 34–56.

[3] Joel A E Andersson, Joris Gillis, Greg Horn, James B Rawlings, and Moritz Diehl. "CasADi – A software framework for nonlinear optimization and optimal control". In: *Mathematical Programming Computation* (2018).

[4] Boris Andreianov, Kenneth Hvistendahl Karlsen, and Nils Henrik Risebro. "A theory of L^1-dissipative solvers for scalar conservation laws with discontinuous flux". In: *Arch. Ration. Mech. Anal.* 201.1 (2011), pp. 27–86.

[5] Armin Askari, Daniel Albarnaz Farias, Alex A. Kurzhanskiy, and Pravin Varaiya. "Effect of adaptive and cooperative adaptive cruise control on throughput of signalized arterials". In: *2017 IEEE Intelligent Vehicles Symposium (IV)*. IEEE, June 2017, pp. 1287–1292.

[6] M. Athans and P. L. Falb. *Optimal Control*. New York: McGraw Hill, 1966.

[7] SBD Automotive. *Connected Cars global forecast*. Tech. rep. 2018.

[8] Matthew Barth and Kanok Boriboonsomsin. "Traffic Congestion and Greenhouse Gases - ACCESS Magazine". In: *Access Magazine* 1(35) (2009), pp. 2–9.

[9] G. Bartolini, A. Ferrara, A. Levant, and E. Usai. "On Second Order Sliding Mode Controllers". In: *Variable Structure Systems, Sliding Mode and*

Nonlinear Control. Ed. by K. D. Young and Ü. Özgüner. Lecture Notes in Control and Information. London: Springer-Verlag, 1999, pp. 329–350.

[10] G. Bartolini, A. Ferrara, and E. Usai. "Chattering avoidance by second-order sliding mode control". In: *IEEE Transactions on Automatic Control* 43.2 (Feb. 1998), pp. 241–246.

[11] G. Bartolini, A. Ferrara, and E. Usai. "Chattering avoidance by second-order sliding mode control". In: *IEEE Transactions on Automatic Control* 43.2 (Feb. 1998), pp. 241–246.

[12] Nikolaos Bekiaris-Liberis, Claudio Roncoli, and Markos Papageorgiou. "Highway Traffic State Estimation With Mixed Connected and Conventional Vehicles". In: *IEEE Transactions on Intelligent Transportation Systems* 17.12 (Dec. 2016), pp. 3484–3497.

[13] Sylvie Benzoni-Gavage and Rinaldo M. Colombo. "An n-populations model for traffic flow". In: *European Journal of Applied Mathematics* 14.5 (2003), pp. 587–612.

[14] I. Berry. "The effects of driving style and vehicle performance on the real-world fuel consumption of U.S.light-duty vehicles." In: *MIT MS Thesis* (2010).

[15] Robert L. Bertini, Steven Boice, and Klaus Bogenberger. "Dynamics of Variable Speed Limit System Surrounding Bottleneck on German Autobahn". In: *Transportation Research Record* 1978.1 (2006), pp. 149–159.

[16] Anirudh Kishore Bhoopalam, Niels Agatz, and Rob Zuidwijk. "Planning of truck platoons: A literature review and directions for future research". In: *Transportation Research Part B: Methodological* 107 (2018), pp. 212–228.

[17] Christophe Bonnet and Hans Fritz. "Fuel Consumption Reduction in a Platoon: Experimental Results with two Electronically Coupled Trucks at Close Spacing". In: Aug. 2000.

[18] Benjamin Boutin, Christophe Chalons, Frédéric Lagoutière, and Philippe G. LeFloch. "Convergent and conservative schemes for nonclassical solutions based on kinetic relations. I". In: *Interfaces Free Bound.* 10.3 (2008), pp. 399–421.

[19] Alberto Bressan, Graziano Guerra, and Wen Shen. "Vanishing viscosity solutions for conservation laws with regulated flux". In: *J. Differential Equations* 266.1 (2019), pp. 312–351.

[20] Gabriella Bretti and Benedetto Piccoli. “A tracking algorithm for car paths on road networks”. In: *SIAM J. Appl. Dyn. Syst.* 7.2 (2008), pp. 510–531.

[21] Eduardo F. Camacho and Carlos Bordons Alba. *Model Predictive Control*. Ed. by Springer Advanced Textbooks in Control and Signal Processing. 2007.

[22] Rodrigo C. Carlson, Ioannis Papamichail, Markos Papageorgiou, and Albert Messmer. “Optimal Motorway Traffic Flow Control Involving Variable Speed Limits and Ramp Metering”. In: *Transportation Science* 44.2 (2010), pp. 238–253.

[23] O.M.J. Carsten and F.N. Tate. “Intelligent speed adaptation: accident savings and cost–benefit analysis”. In: *Accident Analysis and Prevention* 37.3 (2005), pp. 407–416.

[24] C. Chalons, M. L. Delle Monache, and P. Goatin. “A conservative scheme for non-classical solutions to a strongly coupled PDE-ODE problem”. In: *Interfaces Free Bound.* 19.4 (2017), pp. 553–570.

[25] C. Chalons, Maria Laura Delle Monache, and Paola Goatin. “A conservative scheme for non-classical solutions to a strongly coupled PDE-ODE problem”. Interfaces and Free Boundaries, European Mathematical Society, to appear. 2014.

[26] Gang-Len Chang, Sung Yoon Park, and Jawad Paracha. “Intelligent Transportation System Field Demonstration: Integration of Variable Speed Limit Control and Travel Time Estimation for a Recurrently Congested Highway”. In: *Transportation Research Record* 2243.1 (2011), pp. 55–66.

[27] Danjue Chen and Soyoung Ahn. “Variable speed limit control for severe non-recurrent freeway bottlenecks”. In: *Transportation Research Part C: Emerging Technologies* 51 (2015), pp. 210–230.

[28] Danjue Chen, Soyoung Ahn, and Andreas Hegyi. “Variable speed limit control for steady and oscillatory queues at fixed freeway bottlenecks”. In: *Transportation Research Part B: Methodological* 70 (2014), pp. 340–358.

[29] Koohong Chung, Jittichai Rudjanakanoknad, Michael J. Cassidy, Koohong Chung, Jittichai Rudjanakanoknad, and Michael J. Cassidy. *Transportation research Part B, Methodological.* Vol. 41. 1. Elsevier Science, 2007, pp. 82–95.

[30] M. Cicic and K. H. Johansson. “Energy-optimal platoon catch-up in moving bottleneck framework”. In: *2019 18th European Control Conference (ECC).* 2019, pp. 3674–3679.

[31] Mladen Cicic and Karl Henrik Johansson. “Traffic regulation via individually controlled automated vehicles: a cell transmission model approach”. In: *2018 21st International Conference on Intelligent Transportation Systems (ITSC)*. IEEE, Nov. 2018, pp. 766–771.

[32] G. M. Coclite, K. H. Karlsen, S. Mishra, and N. H. Risebro. “Convergence of vanishing viscosity approximations of 2×2 triangular systems of multi-dimensional conservation laws”. In: *Boll. Unione Mat. Ital. (9)* 2.1 (2009), pp. 275–284.

[33] Giuseppe Maria Coclite and Nils Henrik Risebro. “Conservation laws with time dependent discontinuous coefficients”. In: *SIAM J. Math. Anal.* 36.4 (2005), pp. 1293–1309.

[34] R. Courant, K. Friedrichs, and H. Lewy. “On the Partial Difference Equations of Mathematical Physics”. In: *IBM Journal of Research and Development* 11.2 (1967), pp. 215–234.

[35] S. Cui, B. Seibold, R. Stern, and D. B. Work. “Stabilizing traffic flow via a single autonomous vehicle: Possibilities and limitations”. In: *2017 IEEE Intelligent Vehicles Symposium (IV)*. 2017, pp. 1336–1341.

[36] Carlos F. Daganzo. “The cell transmission model: A dynamic representation of highway traffic consistent with the hydrodynamic theory”. In: *Transportation Research Part B: Methodological* 28.4 (Aug. 1994), pp. 269–287.

[37] M L Delle Monache and P Goatin. “Scalar conservation laws with moving constraints arising in traffic flow modeling: An existence result”. In: *Journal of Differentials Equations* 257 (2014), pp. 4015–4029.

[38] Maria Laura Delle Monache and Paola Goatin. “A front tracking method for a strongly coupled PDE-ODE system with moving density constraints in traffic flow”. In: *Discrete and Continuous Dynamical Systems - Series S* 7.3 (June 2014), pp. 435–447.

[39] Christina Diakaki, Markos Papageorgiou, Ioannis Papamichail, and Ioannis Nikolos. “Overview and analysis of Vehicle Automation and Communication Systems from a motorway traffic management perspective”. In: *Transportation Research Part A: Policy and Practice* 75 (May 2015), pp. 147–165.

[40] Vinayak V. Dixit, Sai Chand, and Divya J. Nair. “Autonomous Vehicles: Disengagements, Accidents and Reaction Times”. In: *PLOS ONE* 11.12 (Dec. 2016), pp. 1–14.

[41] Wooseok Do, Omid M Rouhani, and Luis Miranda-Moreno. "Simulation-Based Connected and Automated Vehicle Models on Highway Sections: A Literature Review". In: *Journal of Advanced Transportation* 2019 (2019). Ed. by Claudio Roncoli, p. 9343705.

[42] Vesela Dryankova, Hassane Abouäissa, and Daniel Jolly. "High order sliding mode control for real-time ramp metering". In: *2011 International Conference on Communications, Computing and Control Applications (CCCA)*. Mar. 2011, pp. 1–6.

[43] A Ferrara, S Sacone, and S Siri. "Event-triggered model predictive schemes for freeway traffic control". In: *Transportation Research Part C: Emerging Technologies* 58 (2015), pp. 554–567.

[44] A. Ferrara, G. P. Incremona, and M. Cucuzzella. *Advanced and Optimization Based Sliding Mode Control: Theory and Applications*. Philadelphia, PA: Society for Industrial and Applied Mathematics, 2019.

[45] A. Ferrara and M. Rubagotti. "A Suboptimal Second Order Sliding Mode Controller for Systems With Saturating Actuators". In: *IEEE Transactions on Automatic Control* 54.5 (May 2009), pp. 1082–1087.

[46] Antonella Ferrara, Gian Paolo Incremona, and Giulia Piacentini. "A Hierarchical MPC and Sliding Mode Based Two-Level Control for Freeway Traffic Systems with Partial Demand Information". In: *Provisionally accepted to the European Control Journal*. 2021.

[47] Antonella Ferrara, Alberto Nai Oleari, Simona Sacone, and Silvia Siri. "Freeways as Systems of Systems: A Distributed Model Predictive Control Scheme". In: *IEEE Systems Journal* 9.1 (Mar. 2015), pp. 312–323.

[48] Antonella Ferrara, Simona Sacone, and Silvia Siri. "A switched ramp-metering controller for freeway traffic systems". In: *Proceedings of the 5th IFAC Conference on Analysis and Design of Hybrid Systems, Atlanta, USA* 48.27 (2015), pp. 105–110.

[49] Antonella Ferrara, Simona Sacone, and Silvia Siri. "An Overview of Traffic Control Schemes for Freeway Systems". In: *Freeway Traffic Modelling and Control*. Springer, Cham, 2018. Chap. 8, pp. 193–234.

[50] L. Fridman and A. Levant. "Higher-Order Sliding Modes". In: *Sliding Mode Control in Engineering*. Control Engineering Series. New York Basel: CRC Press, 2002. Chap. 3, pp. 1–51.

[51] Bernhard Friedrich. “The Effect of Autonomous Vehicles on Traffic”. In: *Autonomous Driving*. Berlin, Heidelberg: Springer Berlin Heidelberg, 2016, pp. 317–334.

[52] Mauro Garavello and Benedetto Piccoli. *Traffic flow on networks*. Vol. 1. AIMS Series on Applied Mathematics. Conservation laws models. American Institute of Mathematical Sciences (AIMS), Springfield, MO, 2006, pp. xvi+243.

[53] Denos C. Gazis, Robert Herman, and Richard W. Rothery. “Nonlinear Follow-The-Leader Models of Traffic Flow”. In: *Operations Research* 9.4 (1961), pp. 545–567.

[54] P.G. Gipps. “A behavioural car-following model for computer simulation”. In: *Transportation Research Part B: Methodological* 15.2 (1981), pp. 105–111.

[55] S. K. Godunov. “A difference method for numerical calculation of discontinuous solutions of the equations of hydrodynamics”. In: *Mat. Sb. (N.S.)* 47 (89) (1959), pp. 271–306.

[56] Phil Goodwin. *The economic costs of road traffic congestion*. Tech. rep. discovery.ucl.ac.uk, 2004.

[57] Paweł Gora, Christos Katrakazas, Arkadiusz Drabicki, Faqhrul Islam, and Piotr Ostaszewski. “Microscopic traffic simulation models for connected and automated vehicles (CAVs) - State-of-the-art”. In: *Procedia Computer Science*. Vol. 170. Elsevier B.V., Jan. 2020, pp. 474–481.

[58] Ian Greenwood and Christopher R. Bennett. “The effects of traffic congestion on fuel consumption”. In: *Road and Transport Research* 5.2 (1996), pp. 18–32.

[59] Ellen Grumert, Xiaoliang Ma, and Andreas Tapani. “Analysis of a cooperative variable speed limit system using microscopic traffic simulation”. In: *Transportation Research Part C: Emerging Technologies* 52 (Mar. 2015), pp. 173–186.

[60] Graziano Guerra and Wen Shen. “Backward Euler Approximations for Conservation Laws with Discontinuous Flux”. In: *arXiv e-prints*, arXiv:1803.00493 (Mar. 2018), arXiv:1803.00493. arXiv: `1803.00493 [math.AP]`.

[61] Md. Hadiuzzaman, Tony Z. Qiu, and Xiao-Yun Lu. “Variable Speed Limit Control Design for Relieving Congestion Caused by Active Bottlenecks”. In: *Journal of Transportation Engineering* 139.4 (Apr. 2013), pp. 358–370.

[62] Yu Han, Andreas Hegyi, Yufei Yuan, Serge Hoogendoorn, Markos Papageorgiou, and Claudio Roncoli. "Resolving freeway jam waves by discrete first-order model-based predictive control of variable speed limits". In: *Transportation Research Part C: Emerging Technologies* 77 (Apr. 2017), pp. 405–420.

[63] Ilse M. Harms and Karel A. Brookhuis. "Dynamic traffic management on a familiar road: Failing to detect changes in variable speed limits". In: *Transportation Research Part F: Traffic Psychology and Behaviour* 38 (Apr. 2016), pp. 37–46.

[64] A. Hegyi, B. De Schutter, and J. Heelendoorn. "MPC-based optimal coordination of variable speed limits to suppress shock waves in freeway traffic". In: *Proceedings of the 2003 American Control Conference, 2003.* Vol. 5. 2003, 4083–4088 vol.5.

[65] Andreas Hegyi, Bart De Schutter, and Hans Hellendoorn. "Model predictive control for optimal coordination of ramp metering and variable speed limits". In: *Transportation Research Part C: Emerging Technologies* 13.3 (June 2005), pp. 185–209.

[66] Bernd Heid, Christian Huth, Sebastian Kempf, and Geng Wu. *Ready for inspection: The automotive aftermarket in 2030.* Tech. rep. McKinsey&Company, 2018.

[67] Bruce Hellinga and Michael Mandelzys. "Impact of Driver Compliance on the Safety and Operational Impacts of Freeway Variable Speed Limit Systems". In: *Journal of Transportation Engineering* 137.4 (Apr. 2011), pp. 260–268.

[68] Dwight A. Hennessy and David L. Wiesenthal. "The relationship between traffic congestion, driver stress and direct versus indirect coping behaviours". In: *Ergonomics* 40.3 (1997), pp. 348–361.

[69] Dwight A. Hennessy and David L. Wiesenthal. "Traffic congestion, driver stress, and driver aggression". In: *Aggressive Behavior* 25.6 (1999), pp. 409–423.

[70] Sebastian van de Hoef, Karl Henrik Johansson, and Dimos V Dimarogonas. "Fuel-efficient en route formation of truck platoons". In: *IEEE Transactions on Intelligent Transportation Systems* 19.1 (2017), pp. 102–112.

[71] Serge P. Hoogendoorn and Piet H.L. Bovy. “Continuum modeling of multi-class traffic flow”. In: *Transportation Research Part B: Methodological* 34.2 (Feb. 2000), pp. 123–146.

[72] A. Ibrahim, M. Cicic, D. Goswami, T. Basten, and K. H. Johansson. “Control of Platooned Vehicles in Presence of Traffic Shock Waves”. In: *2019 IEEE Intelligent Transportation Systems Conference (ITSC)*. 2019, pp. 1727–1734.

[73] Gian Paolo Incremona, Michele Cucuzzella, Antonella Ferrara, and Lalo Magni. “Model predictive control and sliding mode control for current sharing in microgrids”. In: *Proc. 56th Annual Conference on Decision and Control*. Melbourne, Australia, Dec. 2017, pp. 2661–2666.

[74] Gian Paolo Incremona, Antonella Ferrara, and Lalo Magni. “Hierarchical Model Predictive/Sliding Mode Control of Nonlinear Constrained Uncertain Systems”. In: *IFAC-PapersOnLine* 48.23 (2015). 5th IFAC Conference on Nonlinear Model Predictive Control NMPC 2015, pp. 102–109.

[75] Gian Paolo Incremona, Antonella Ferrara, and Lalo Magni. “MPC for robot manipulators with integral sliding modes generation”. In: *IEEE/ASME Transactions on Mechatronics* 22.3 (June 2017), pp. 1299–1307.

[76] Violina Iordanova, Hassane Abouäissa, and Daniel Jolly. “Sliding Mode Control and Flatness-Based Concept for Real-Time Ramp Metering”. In: *Proceedings of the 17th World Congress The International Federation of Automatic Control, Seoul, Korea*. 2008.

[77] *J3016: Taxonomy and Definitions for Terms Related to On-Road Motor Vehicle Automated Driving Systems*. Tech. rep. SAE International, 2014, p. 12.

[78] Felipe Jiménez, José Eugenio Naranjo, José Javier Anaya, Fernando García, Aurelio Ponz, and José María Armingol. “Advanced Driver Assistance System for Road Environments to Improve Safety and Efficiency”. In: *Transportation Research Procedia*. Vol. 14. Elsevier B.V., Jan. 2016, pp. 2245–2254.

[79] Li Jin, Mladen Cicic, Saurabh Amin, and Karl H. Johansson. “Modeling Impact of Vehicle Platooning on Highway Congestion: A Fluid Queuing Approach”. In: *21st ACM International Conference on Hybrid Systems: Computation and Control (HSCC)*. 2018.

[80] K. H. Karlsen and J. D. Towers. "Convergence of the Lax-Friedrichs scheme and stability for conservation laws with a discontinous space-time dependent flux". In: *Chinese Ann. Math. Ser. B* 25.3 (2004), pp. 287–318.

[81] Boris S Kerner and Sergey L Klenov. "A theory of traffic congestion at moving bottlenecks". In: *Journal of Physics A: Mathematical and Theoretical* 43.42 (Sept. 2010), p. 425101.

[82] B Khondaker and L Kattan. "Variable speed limit: An overview". In: *Transportation Letters The International Journal of Transportation Research* (2015).

[83] Maria Kontorinaki, Anastasia Spiliopoulou, Claudio Roncoli, and Markos Papageorgiou. "First-order traffic flow models incorporating capacity drop: Overview and real-data validation". In: *Transportation Research Part B: Methodological* 106 (Dec. 2017), pp. 52–75.

[84] A. Kotsialos and M. Papageorgiou. "Nonlinear Optimal Control Applied to Coordinated Ramp Metering". In: *IEEE Transactions on Control Systems Technology* 12.6 (Nov. 2004), pp. 920–933.

[85] Apostolos Kotsialos, Markos Papageorgiou, and Frans Middelham. "Local and optimal coordinated ramp metering for freeway networks". In: *Journal of Intelligent Transportation Systems: Technology, Planning, and Operations* 9.4 (Oct. 2005), pp. 187–203.

[86] Eil Kwon, Daniel Brannan, Kahled Shouman, Cassandra Isackson, and Bernie Arseneau. "Development and Field Evaluation of Variable Advisory Speed Limit System for Work Zones". In: *Transportation Research Record: Journal of the Transportation Research Board* 2015.1 (Jan. 2007), pp. 12–18.

[87] J. Lebacque, J. Lesort, and F. Giorgi. "Introducing Buses into First-Order Macroscopic Traffic Flow Models". In: *Transportation Research Record: Journal of the Transportation Research Board* (2014).

[88] Jean-Patrick Lebacque. "The Godunov scheme and what it means for first order traffic flow models". In: *Transportation and traffic theory. Proceedings of the 13th international symposium on transportation and traffic theory, Lyon, France, 24-26 JULY 1996.* 1996.

[89] Jean-Patrick Lebacque, Jean-Baptiste Lesort, and Florence Giorgi. "Introducing buses into first-order macroscopic traffic flow models". In: *Transportation Research Record* 1644.1 (1998), pp. 70–79.

[90] Chris Lee, Bruce Hellinga, and Kaan Ozbay. "Quantifying effects of ramp metering on freeway safety". In: *Accident Analysis and Prevention* 38.2 (Mar. 2006), pp. 279–288.

[91] A. Levant. "Chattering Analysis". In: *IEEE Transactions on Automatic Control* 55.6 (June 2010), pp. 1380–1389.

[92] Michael W. Levin and Stephen D. Boyles. "A multiclass cell transmission model for shared human and autonomous vehicle roads". In: *Transportation Research Part C: Emerging Technologies* 62 (Jan. 2016), pp. 103–116.

[93] Jonathan I. Levy, Jonathan J. Buonocore, and Katherine Von Stackelberg. "Evaluation of the public health impacts of traffic congestion: A health risk assessment". In: *Environmental Health: A Global Access Science Source* 9.1 (Oct. 2010), pp. 1–12.

[94] Zhibin Li, Ye Li, Pan Liu, Wei Wang, and Chengcheng Xu. "Development of a variable speed limit strategy to reduce secondary collision risks during inclement weathers". In: *Accident Analysis and Prevention* 72 (2014), pp. 134–145.

[95] K Liang, J Mårtensson, and K H Johansson. "Experiments on platoon formation of heavy trucks in traffic". In: *2016 IEEE 19th International Conference on Intelligent Transportation Systems (ITSC)*. 2016, pp. 1813–1819.

[96] M. J. Lighthill and G. B. Whitham. "On Kinematic Waves. II. A Theory of Traffic Flow on Long Crowded Roads". In: *Prc. Roy. Soc. London Ser A* 229 (1955), pp. 317–346.

[97] Michael J. Lighthill and Gerald B. Whitham. "On Kinematic Waves. II. A Theory of Traffic Flow on Long Crowded Roads". In: *Proceedings of the Royal Society of London. Series A.* 229 (1955), pp. 317–346.

[98] Pei Wei Lin, Kyeong Pyo Kang, and Gang Len Chang. "Exploring the effectiveness of variable speed limit controls on highway work-zone operations". In: *Journal of Intelligent Transportation Systems: Technology, Planning, and Operations* 8.3 (Jan. 2004), pp. 155–168.

[99] B. Liu, D. Ghosal, C. Chuah, and H. M. Zhang. "Reducing Greenhouse Effects via Fuel Consumption-Aware Variable Speed Limit (FC-VSL)". In: *IEEE Transactions on Vehicular Technology* 61.1 (2012), pp. 111–122.

[100] S. Liu, H. Hellendoorn, and B. De Schutter. "Model predictive control for freeway networks based on multi-class traffic flow and emission models". In: *IEEE Transactions on Intelligent Transportation Systems* 18.2 (Feb. 2017), pp. 306–320.

[101] Xiao-Yun Lu, Pravin Varaiya, Roberto Horowitz, Dongyan Su, and Steven E. Shladover. "Novel Freeway Traffic Control with Variable Speed Limit and Coordinated Ramp Metering". In: *Transportation Research Record: Journal of the Transportation Research Board* 2229.1 (Jan. 2011), pp. 55–65.

[102] L. Magni and R. Scattolini. *Advanced and multivariable control*. Ed. by Pitagora. 2014.

[103] L. Magni and R. Scattolini. "Model predictive control of continuous-time nonlinear systems with piecewise constant control". In: *IEEE Transactions on Automatic Control* 49.6 (June 2004), pp. 900–906.

[104] S. Mammar, S. Mammar, and M. Netto. "Coordinated Ramp Metering Via Second Order Sliding Mode Control". In: *2006 IEEE Intelligent Transportation Systems Conference*. IEEE, 2006, pp. 261–266.

[105] *McKinsey's Connected Car Consumer Survey*. Tech. rep. McKinsey&Company, 2014.

[106] Eduardo R. Müller, Rodrigo C. Carlson, and Werner Kraus. "Cooperative Mainstream Traffic Flow Control on Freeways". In: *IFAC-PapersOnLine* 49.32 (Jan. 2016), pp. 89–94.

[107] Juan Carlos Muñoz and Carlos F. Daganzo. "Moving Bottlenecks: A Theory Grounded on Experimental Observation". In: *Transportation and Traffic Theory in the 21st Century*. Elsevier, 2002, pp. 441–461.

[108] Ioannis A Ntousakis, Ioannis K Nikolos, and Markos Papageorgiou. "On Microscopic Modelling of Adaptive Cruise Control Systems". In: *Transportation Research Procedia*. Vol. 6. 0. Corsica, France, 2015, pp. 111–127.

[109] Hui Ou and Tie-Qiao Tang. "Impacts of moving bottlenecks on traffic flow". In: *Physica A: Statistical Mechanics and its Applications* 500 (2018), pp. 131–138.

[110] E. Yu. Panov. "Erratum to: Existence and strong pre-compactness properties for entropy solutions of a first-order quasilinear equation with discontinuous flux [MR2592291]". In: *Arch. Ration. Mech. Anal.* 196.3 (2010), pp. 1077–1078.

[111] E. Yu. Panov. “Existence and strong pre-compactness properties for entropy solutions of a first-order quasilinear equation with discontinuous flux”. In: *Arch. Ration. Mech. Anal.* 195.2 (2010), pp. 643–673.

[112] M. Papageorgiou, C. Diakaki, V. Dinopoulou, A. Kotsialos, and Yibing Wang. “Review of road traffic control strategies”. In: *Proceedings of the IEEE* 91.12 (Dec. 2003), pp. 2043–2067.

[113] M. Papageorgiou, H. Hadj-Salem, and J.-M. Blosseville. “ALINEA: A local feedback control law for on-ramp metering”. In: *Transportation Research Record* 1320 (1991), pp. 58–64.

[114] M. Papageorgiou, H. Hadj-Salem, and F. Middelham. “ALINEA Local Ramp Metering: Summary of Field Results”. In: *Transportation Research Record: Journal of the Transportation Research Board* 1603.1 (Jan. 1997), pp. 90–98.

[115] M. Papageorgiou and A. Kotsialos. “Freeway ramp metering: an overview”. In: *IEEE Transactions on Intelligent Transportation Systems* 3.4 (Dec. 2002), pp. 271–281.

[116] Markos Papageorgiou, Jean-Marc Blosseville, and Habib Hadj-Salem. “Modelling and real-time control of traffic flow on the southern part of Boulevard Peripherique in Paris: Part I: Modelling”. In: *Transportation Research Part A: General* 24.5 (Sept. 1990), pp. 345–359.

[117] Markos Papageorgiou and Ioannis Papamichail. “Overview of traffic signal operation policies for ramp metering”. In: *Transportation Research Record* 2047 (2008), pp. 28–36.

[118] Ioannis Papamichail, Katerina Kampitaki, Markos Papageorgiou, and Albert Messmer. “Integrated Ramp Metering and Variable Speed Limit Control of Motorway Traffic Flow”. In: *IFAC Proceedings Volumes* 41.2 (2008). 17th IFAC World Congress, pp. 14084–14089.

[119] Cecilia Pasquale, Simona Sacone, Silvia Siri, and Antonella Ferrara. “New Micro-Macro METANET Model for Platoon Control in Freeway Traffic Networks”. In: *Proceedings of The 21st IEEE International Conference on Intelligent Transportation Systems, Maui, Hawaii, USA, November 4-7*. 2018.

[120] Jeff Patten, Brian McAuliffe, William Mayda, and Bernard Tanguay. *Review of Aerodynamic Drag Reduction Devices for Heavy Trucks and Buses*. Tech. rep. National Research Council Canada - Centre for Surface Transportation Technology, 2012.

[121] G. Piacentini, A. Ferrara, I. Papamichail, and M. Papageorgiou. "Highway Traffic Control with Moving Bottlenecks of Connected and Automated Vehicles for Travel Time Reduction". In: *Proceedings of the 58th Conference on Decision and Control (CDC)*. 2019, pp. 3140–3145.

[122] G. Piacentini, P. Goatin, and A. Ferrara. "Traffic Control Via Platoons of Intelligent Vehicles for Saving Fuel Consumption in Freeway Systems". In: *IEEE Control Systems Letters* 5.2 (2021), pp. 593–598.

[123] Giulia Piacentini, Mladen Cicic, Antonella Ferrara, and Karl Henrik Johansson. "VACS equipped vehicles for congestion dissipation in multi-class CTM framework". In: *Proceedings of the 18th European Control Conference (ECC)*. 2019, pp. 2203–2208.

[124] Giulia Piacentini, Paola Goatin, and Antonella Ferrara. "A Macroscopic Model for Platooning in Highway Traffic". In: *SIAM Journal on Applied Mathematics* 80.1 (Jan. 2020), pp. 639–656.

[125] Giulia Piacentini, Paola Goatin, and Antonella Ferrara. "Traffic control via moving bottleneck of coordinated vehicles". In: *Proceedings of the 15th IFAC Symposium on Control in Transportation Systems (CTS)* 51.9 (Jan. 2018), pp. 13–18.

[126] Giulia Piacentini, Gian Paolo Incremona, and Antonella Ferrara. "Freeway Traffic Control via Second-Order Sliding Modes Generation". In: *Proc. European Control Conference*. Saint Pittsburgh, Russia, May 2020, pp. 1–6.

[127] Giulia Piacentini, Cecilia Pasquale, Simona Sacone, Silvia Siri, and Antonella Ferrara. "Multiple Moving Bottlenecks for Traffic Control in Freeway Systems". In: *Proceedings of the 18th European Control Conference (ECC)*. Napoli, Italy, 2019.

[128] R. A. Ramadan and B. Seibold. "Traffic Flow Control and Fuel Consumption Reduction via Moving Bottlenecks". Preprint, https://arxiv.org/pdf/1702.07995.pdf. 2017.

[129] P.I. Richards. "Shockwaves on the highway". In: *Operations Research* 4 (1956), pp. 42–51.

[130] Paul. I. Richards. "Shockwaves on the highway". In: *Operations Research* 4 (1956), pp. 42–51.

[131] Claudio Roncoli, Markos Papageorgiou, and Ioannis Papamichail. "Motorway Traffic Flow Optimisation in Presence of Vehicle Automation and Communication Systems". In: 2015, pp. 1–16.

[132] Claudio Roncoli, Markos Papageorgiou, and Ioannis Papamichail. "Traffic flow optimisation in presence of vehicle automation and communication systems – Part II: Optimal control for multi-lane motorways". In: *Transportation Research Part C: Emerging Technologies* 57 (Aug. 2015), pp. 260–275.

[133] Claudio Roncoli, Ioannis Papamichail, and Markos Papageorgiou. "Model Predictive Control for Motorway Traffic with Mixed Manual and VACS-equipped Vehicles". In: *Transportation Research Procedia* 10 (Jan. 2015), pp. 452–461.

[134] Bhawna Sharma and Pushkin Kachroo. "Robust Hybrid Feedback Control Design for Ramp Metering using Sliding Mode Control". In: *International Journal of Advanced Research in Computer Science* 4.9 ().

[135] Raphael E. Stern, Shumo Cui, Maria Laura Delle Monache, Rahul Bhadani, Matt Bunting, Miles Churchill, Nathaniel Hamilton, R'mani Haulcy, Hannah Pohlmann, Fangyu Wu, Benedetto Piccoli, Benjamin Seibold, Jonathan Sprinkle, and Daniel B. Work. "Dissipation of stop-and-go waves via control of autonomous vehicles: Field experiments". In: *Transportation Research Part C: Emerging Technologies* 89 (Apr. 2018), pp. 205–221. arXiv: 1705.01693.

[136] Alireza Talebpour and Hani S. Mahmassani. "Influence of connected and autonomous vehicles on traffic flow stability and throughput". In: *Transportation Research Part C: Emerging Technologies* 71 (Oct. 2016), pp. 143–163.

[137] John D. Towers. "Convergence of the Godunov scheme for a scalar conservation law with time and space discontinuities". In: *J. Hyperbolic Differ. Equ.* 15.2 (2018), pp. 175–190.

[138] John D. Towers. "Convergence via OSLC of the Godunov scheme for a scalar conservation law with time and space flux discontinuities". In: *Numer. Math.* 139.4 (2018), pp. 939–969.

[139] Martin Treiber. *How Much does Traffic Congestion Increase Fuel Consumption and Emissions? Applying a Fuel Consumption Model to the NGSIM Trajectory Data car-following models with fluctuations View project Trans-*

portmetrica A Special Issue Call for Papers: Connected and Au. Tech. rep. 2007.

[140] Martin Treiber, Ansgar Hennecke, and Dirk Helbing. "Congested traffic states in empirical observations and microscopic simulations". In: *Physical Review E* 62.2 (Aug. 2000), pp. 1805–1824.

[141] Martin Treiber, Arne Kesting, and Dirk Helbing. "Understanding widely scattered traffic flows, the capacity drop, and platoons as effects of variance-driven time gaps". In: *Phys. Rev. E* 74 (1 July 2006), p. 016123.

[142] S. Tsugawa, S. Kato, and K. Aoki. "An automated truck platoon for energy saving". In: Institute of Electrical and Electronics Engineers (IEEE), Dec. 2011, pp. 4109–4114.

[143] V. Turri, B. Besselink, and K. H. Johansson. "Cooperative Look-Ahead Control for Fuel-Efficient and Safe Heavy-Duty Vehicle Platooning". In: *IEEE Transactions on Control Systems Technology* 25.1 (2017), pp. 12–28.

[144] Vadim Utkin, Jürgen Guldner, and Jingxin Shi. *Sliding Mode Control in Electro-Mechanical Systems, Second Edition*. Vol. 31. Automation and Control Engineering. CRC Press, 2009.

[145] Sven Vlassenroot, Steven Broekx, Johan De Mol, Luc Int Panis, Tom Brijs, and Geert Wets. "Driving with intelligent speed adaptation: Final results of the Belgian ISA-trial". In: *Transportation Research Part A: Policy and Practice* 41.3 (2007), pp. 267–279.

[146] M. Wang, W. Daamen, S.P. Hoogendoorn, and B. Van Arem. "Connected variable speed limits control and vehicle acceleration control to resolve moving jams". In: *94th Annual Meeting Transportation Research Board, Washington, USA, 11-15 January 2015; Authors version* (2015).

[147] Dominik Wee, Matthias Kässer, Michele Bertoncello, Kersten Heineke, Gregor Eckhard, Julian Hölz, Florian Florian Saupe, and Thibaut Thibaut Müller. *Competing for the connected customer: Perspectives on the opportunities created by car connectivity and automation*. Tech. rep. McKinsey&Company, 2015.

[148] G.C.K Wong and S.C Wong. "A multi-class traffic flow model – an extension of LWR model with heterogeneous drivers". In: *Transportation Research Part A: Policy and Practice* 36.9 (Oct. 2002), pp. 827–841.

[149] Matthew Wright, Gabriel Gomes, Roberto Horowitz, and Alex A. Kurzhanskiy. “A new model for multi-commodity macroscopic modeling of complex traffic networks”. In: (Sept. 2015). arXiv: 1509.04995.

[150] Yibing Wang and M. Papageorgiou. “Local Ramp Metering in the Case of Distant Downstream Bottlenecks”. In: *2006 IEEE Intelligent Transportation Systems Conference*. 2006, pp. 426–431.

[151] M. Zambelli and A. Ferrara. “Robustified Distributed Model Predictive Control for Coherence and Energy Efficiency-Aware Platooning”. In: *2019 American Control Conference (ACC)*. July 2019, pp. 527–532.

[152] Jin Zhao, Rongchen Zhao, Guangwei Wang, and Xiangnan Zhang. “Analysis of fuel economy of autonomous vehicle platoon”. In: *ICTE 2013 - Proceedings of the 4th International Conference on Transportation Engineering*. 2013, pp. 980–986.